AD-A132 670 STUDY TO SYNTHESIZE AND INTERPRET DATA FROM SEVERAL SATELLITES AND GROUND..(U) RICE UNIV HOUSTON TX DEPT OF SPACE PHYSICS AND ASTRONOMY R A WOLF 03 MAY 83 1/1

UNCLASSIFIED AFGL-TR-83-0128 F19628-80-C-0009 NL

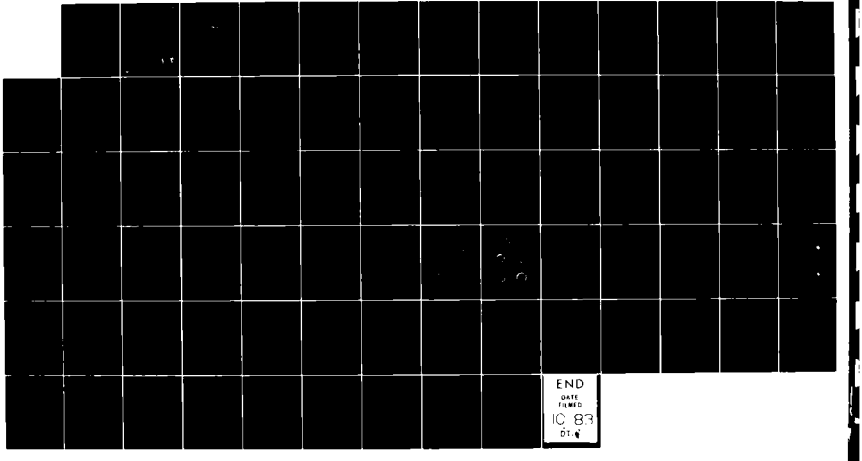

END
DATE FILMED
10 83
DTIC

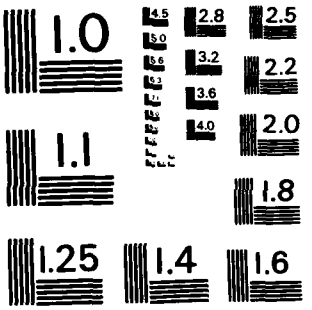

AD-A133 629

AFOSR-TR-83-0128

ABILITY TO SYNTHESIZE AND INTERPRET DATA FROM GEOSYNCHRONOUS SATELLITES AND GROUND MAGNETOMETERS

W. A. WOLF

Department of Space Physics and Astronomy
Rice University
P.O. Box 1892
Houston, TX 77251

Final Report
1 January 1980 - 31 December 1982

1 May 1983

This report has been reviewed by the ESD Public Affairs Office (PA) and is releasable to the National Technical Information Service (NTIS).

"This technical report has been reviewed and is approved for publication"

WILLIAM J. BURKE
Contract Manager

Plasma Physics Division Branch
Space Physics Division

FOR THE COMMANDER

Space Physics Division

Qualified requestors may obtain additional copies from the Defense Technical Information Center. All others should apply to the National Technical Information Service.

If your address has changed, or if you wish to be removed from the mailing list, or if the addressee is no longer employed by your organization, please notify AFGL/[illegible], Hanscom AFB, MA 01731. This will assist us in maintaining a current mailing list.

Do not return copies of this report unless contractual obligations or notices on a specific document require that it be returned.

SECURITY CLASSIFICATION OF THIS PAGE (When Data Entered)

REPORT DOCUMENTATION PAGE

READ INSTRUCTIONS BEFORE COMPLETING FORM

1. REPORT NUMBER: AFGL-TR-83-0128	2. GOVT ACCESSION NO.: AD-A132 670
3. RECIPIENT'S CATALOG NUMBER:	
4. TITLE (and Subtitle): Study to Synthesize and Interpret Data from Several Satellites and Ground Magnetometers	5. TYPE OF REPORT & PERIOD COVERED: Final Report 1/1/80-12/31/82
	6. PERFORMING ORG. REPORT NUMBER:
7. AUTHOR(s): R. A. Wolf	8. CONTRACT OR GRANT NUMBER(s): F19628-80-C-0009
9. PERFORMING ORGANIZATION NAME AND ADDRESS: Department of Space Physics and Astronomy, Rice University, P.O. Box 1892, Houston, TX 77251	10. PROGRAM ELEMENT, PROJECT, TASK AREA & WORK UNIT NUMBERS: 61102F, 2311G2CC
11. CONTROLLING OFFICE NAME AND ADDRESS: U.S. Air Force Geophysics Laboratory, Hanscom AFB, Massachusetts 01731, Contract Monitor: Dr. William J. Burke/PHG	12. REPORT DATE: May 3, 1983
	13. NUMBER OF PAGES: 75
14. MONITORING AGENCY NAME & ADDRESS (if different from Controlling Office)	15. SECURITY CLASS. (of this report): unclassified
	15a. DECLASSIFICATION DOWNGRADING SCHEDULE:

16. DISTRIBUTION STATEMENT (of this Report)
Approved for public release; distribution unlimited

17. DISTRIBUTION STATEMENT (of the abstract entered in Block 20, if different from Report)

18. SUPPLEMENTARY NOTES

19. KEY WORDS (Continue on reverse side if necessary and identify by block number)
magnetosphere, ionosphere, convection, magnetic storm

20. ABSTRACT (Continue on reverse side if necessary and identify by block number)

The objective of the work has been to study convective plasma motion in the Earth's magnetosphere-ionosphere system during magnetic storms and substorms. Using the Rice Convection Model, multiple simulations have been performed for several well-observed events. Model predictions have been compared with observational data, and the computer model has been improved in several respects. The work included the following six projects.

1. Extension to higher latitude. The region covered by the Rice Convection Model was extended to higher ionospheric latitudes, to the high-latitude

DD FORM 1 JAN 73 1473 EDITION OF 1 NOV 65 IS OBSOLETE

unclassified
SECURITY CLASSIFICATION OF THIS PAGE (When Data Entered)

edge of the auroral zone. Detailed analysis of currents and electric fields in this region was carried out for the substorm event of September 19, 1976. This extension of the model allows predictions of global current systems and global Joule heating of the upper atmosphere.

2. Magnetospheric current systems. Using the time-dependent global current distributions computed for the September 19, 1976 substorm, many "theoretical magnetograms" were computed and compared with observations. One result of this analysis was a new interpretation of a classic observational feature of a substorm and of the early main phase of a magnetic storm, namely that the horizontal magnetic field at low latitude is depressed more on the dusk side than on the dawn side.

3. Simulation of the July 29, 1977 magnetic storm. A simulation was run for the magnetic storm of July 29, 1977, which involved a dramatic compression of the magnetosphere. The total ring current predicted by the simulation agreed well with the observed Dst index. We thus concluded that the magnetospheric compression (as calculated from observed solar-wind ρv^2) and the increased polar-cap potential drop (as estimated from solar-wind $\underline{B}$), when fed into the model, produced a realistic storm-time ring current. The simulation also provided new insight into the effect of a magnetospheric compression on the inner plasma sheet, Birkeland currents, and low-latitude electric field. Comparisons were made with various data from the S3-3 spacecraft.

4. Test of the KRM algorithm. Results from the Rice Convection Model for the September 19, 1976 event were used to test the KRM algorithm for deducing ionospheric currents and electric fields from global ground-magnetometer data. Theoretical magnetograms from our simulation of the September 19, 1976 substorm were fed into the KRM algorithm, along with our conductivity model. Currents and electric fields computed from the KRM algorithm were then compared with the parent distributions from the Rice Convection Model. The test verified the accuracy of the KRM algorithm for deducing auroral-zone currents and electric fields, given an accurate conductivity model.

5. Generation of region-1 currents. We have quantitatively investigated the possibility that substantial nightside region-1 Birkeland currents connect to gradient/curvature drift currents in the plasma sheet and not to open field lines or boundary layers. It appears that region-1 currents, which connect the ionosphere to the "generator" of the magnetosphere-driven ionospheric currents, can connect to the slow-flow region of the plasma sheet, providing that there is a local-time sector in the plasma sheet that contains plasma-depleted flux tubes, i.e., plasma sheet flux tubes that contain less plasma than the surrounding flux tubes. Analytic stability analyses and computer runs with the Rice Convection Model suggest that these channels could exist and generate significant region-1 current.

6. Simulation of the March 22, 1979 magnetic storm. The magnetic storm of March 22, 1979, provides an exceptionally good basis for study of ring-current injection. Extensive data are available from the solar wind (IMP-J and ISEE-3), the plasma sheet (ISEE-1 and 2) and the geosynchronous-orbit region (SCATHA and GEOS-2). Many simulations of this event have been carried out, to determine physical cause-and-effect relationships and also to test and improve numerical accuracy. Results of three computer experiments indicate that strong convection and compression of the magnetosphere both play major roles in formation of the ring current. We find that increasing ionospheric conductivity by a factor of 2 increases the strength of the ring current, but by less than a factor of 2. Decreasing the density in the outer plasma sheet by a factor of 2, but keeping temperature the same, reduces the maximum strength of the ring current, but by less than a factor of 2. Increasing the temperature in the outer plasma sheet, but decreasing the density to keep pressure constant, decreases ring current strength.

TABLE OF CONTENTS

I. INTRODUCTION

The scientific objective of this study has been achievement of better understanding of the dynamics of convection in the inner magnetosphere and ionosphere, through further development and application of the Rice Convection Model, and comparison with observations.

The Rice Convection Model, which has been developed over a period of years [Wolf, 1970; Jaggi and Wolf, 1973; Harel and Wolf, 1976; Harel et al., 1981a], forms the computational basis for this study. Given certain input information (potential distribution at the polar-cap boundary, ionospheric-conductivity model, magnetic-field model, plasma sheet distribution function at the outer boundary of the model, initial magnetospheric plasma distribution), it computes ionospheric and magnetospheric electric fields, flow velocities, and currents, and also magnetospheric plasma distributions. The modeling region usually is arranged to extend to a geocentric distance just slightly less than the subsolar-magnetopause standoff distance. Discussions of the formulation of the model are given by Harel et al. [1981a] and Wolf et al. [1982]. The basic program was developed before the present contract.

Work under contract F19628-80-C-009 has been in the following general areas:

1. Application of the model to new events and to different physical situations.
2. Checking model predictions against much more — and different kinds of — observational data.
3. Doing computer experiments, varying assumptions and boundary conditions to determine the physical cause-and-effect relations that govern the ionosphere-magnetosphere system.
4. Extension of the model and addition of new physics.
5. Programming improvements to make the model easier to run, and refinement of the numerical method to improve accuracy and efficiency.

There are still several relevant physical processes that are not included in the model (parallel electric fields, neutral winds, charge exchange, injection of ions from the ionosphere). We have taken the attitude that we should first thoroughly understand the behavior of the model with the physics already included, before adding complicating effects. We feel that we are close to understanding the physical behavior of the system, with the physics that is

now included in the model.

Section II presents some key results from different aspects of the work.

II. DESCRIPTION OF WORK

A. Extension of the Model to Higher Ionospheric Latitude

(References: Karty, 1981; Karty et al., 1982)

Uncertainties about the detailed physics governing solar-wind/magnetosphere coupling amd magnetotail dynamics have prevented us from including the magnetopause boundary layer, the tail lobe and the outermost part of the plasma sheet in the self-consistent modeling scheme. In other words, we have excluded, from the self-consistent simulations, the part of the magnetosphere that serves as the generator for magnetospheric convection. Part of the auroral ionosphere has also been excluded, namely, the polar cap and the part of the ionosphere that corresponds to the region 1 Birkeland currents, which connect the ionosphere to the generator of the magnetospheric-convection system. The effect of the generating currents on inner-magnetospheric convection has been represented by a boundary condition.

Exclusion of the high-latitude part of the auroral zone from the modeling region proved awkward in several respects. Most of the westward electrojet flows in the high-latitude part of the auroral zone. Neglecting the high-latitude ionospheric currents consequently precluded any serious comparisons between theoretical and observed ground-magnetometer data. It also precluded accurate calculation of global Joule heating.

Janice Karty has addressed these problems by adding a conducting band, in the ionosphere, at the poleward edge of the main modeling region. This conducting band, typically 2-6° wide, represents ionospheric latitudes between the equatorward edge of the region-1 currents and the poleward edge of the auroral zone. Ionospheric conductivity and Birkeland-current density are assumed independent of latitude within the band. The polar cap (poleward of the band) was assumed to have zero conductivity.

Numerical calculations were carried out for the September 19, 1976 substorm event. Figure 1 shows a current distribution near the peak of the model substorm, including both the main model calculation and the high-latitude

band. Note the classic current pattern with well developed eastward and westward electrojets. Figure 2 shows Joule heating per unit ψ for the poleward band, the main modeling region and both regions together, for a time near the peak of the substorm. (The angle ψ essentially represents local time.) Note that Joule heating rates in the two regions tend to have peaks at quite different local times, so that the total Joule heating rate per unit local time depends only fairly weakly on local time. Figure 3 shows total Joule heating rates in the two regions, as functions of universal time through the event. Note that the high-latitude band makes an important contribution to the global Joule heating rate. Note also that the total time-integrated Joule heating through the substorm event is about three times the change in ring current.

B. Magnetospheric Current Systems

(Reference: Chen et al., 1982)

Before the initiation of this contract, C.-K. Chen and collaborators at Rice developed a program that performs a Biot-Savart integration over the complete model current system, thus deducing values for the magnetic perturbations $\Delta\underset{\sim}{B}$ at desired points on the Earth's surface. Many comparisons were made between theoretical and observed magnetograms for the event of September 19, 1976.

The theoretical-magnetogram machinery developed earlier was applied, under the present contract, to further study of currents in the magnetosphere and ionosphere that are driven by magnetospheric convection. The most important result of this study has been a modification of the traditional picture of the currents that flow between magnetosphere and ionosphere in a substorm, and their connection to observed ground magnetic variations.

The pattern of mid- and low-latitude magnetic disturbances is conveniently represented in terms of a two-current loop picture as shown in Figure 4a [e.g., Kamide and Fukushima, 1972; Crooker and McPherron, 1972; Crooker and Siscoe, 1971; Clauer and McPherron, 1980]. One current loop, which represents diversion of some westward tail current through the westward electrojet during a substorm [Atkinson, 1967; McPherron et al., 1973], "explains" the substorm enhancement of the westward electrojet and the positive ΔH observed at mid-latitudes near midnight in a substorm. The other current, which represents a

westward partial ring current centered near dusk connected by Birkeland currents to an eastward electrojet [e.g., Cummings and Dessler, 1967], "explains" the eastward electrojet and also the well-known dawn-dusk asymmetry in low-latitude ΔH that exists in a substorm period, or, more strongly, in the main phase of a geomagnetic storm.

The classical two-current-loop picture of Figure 4a must contain a strong element of truth, because it is based on well-established observations, but it is not immediately clear how it relates to the observation-based picture of Birkeland currents, which comes directly from TRIAD observations (e.g., Figure 13b of Iijima and Potemra [1978]). This pattern is basically the same in quiet times, substorms, and storms, except, of course, that the pattern intensifies greatly and expands equatorward in times of high activity. The solid curve in Figure 4a might be thought to correspond to the poleward set of Birkeland currents in the TRIAD observations (the region 1 currents). However, the dashed curve current in Figure 4a is about 90° out of phase with the observed region 2 currents.

In the computer simulations of the September 19, 1976, event, the complex model current system, with its thousands of current carrying wires and ribbons, represents the real three-dimensional current system more realistically than any simple picture. In fact, the computer simulation results are in good agreement with both the ground observations that motivated Figure 4a and with TRIAD results. Our model eastward and westward electrojets are realistic; and mid-latitude stations near midnight show positive ΔB_x during the substorm, a low-latitude station at local dusk sees a substantially greater southward deviation than a similar station at dawn [Chen et al., 1982].

With regard to the relationship between the solid-curve loop in Figure 4a and region-1 Birkeland currents, our computer-model current patterns (e.g., Figure 1) indicate that region 1 Birkeland currents connect to each other partly by dawn-to-dusk flowing electrojet currents; however, most of the region 1 Birkeland current connects to meridional Pedersen currents, which in turn connect to region 2 Birkeland currents.

The connection between the dawn-dusk asymmetry in low-latitude ΔH and the dashed loop in Figure 4a is subtle. On the basis of our model results, we conclude the following:

1. Region 2 currents connect to the inner plasma sheet and ring current region. However, the dashed current loop in Figure 4a does not accurately reflect the total region 2 current, which, in both model and observations, flows outward from the earth on the dawnside, inward toward the earth on the duskside.

2. The middle panels of Figure 5 show that the dawn-dusk asymmetry is due primarily to Birkeland currents (two-thirds of the asymmetry); the asymmetry in ring-current-induced ΔB_x is much smaller, as was originally pointed out by Fukushima and Kamide [1973].

3. Horizontal ionospheric currents contribute one-third of the asymmetry. Siscoe [1979] raised the possibility that horizontal ionospheric currents, particularly overhead Hall currents, are responsible for the asymmetry, but the effect of overhead Hall currents on ΔB_x is relatively small in our model. The asymmetry produced by the horizontal ionospheric currents, as indicated in the second panel of Figure 5, is due to the auroral electrojets.

4. Although the actual dawn-dusk asymmetry is mainly a Birkeland-current effect, it should not be visualized as an effect of region 2 Birkeland current alone. The bottom panel of Figure 5 shows that region 1 and region 2 currents generally make opposing contributions. It is more accurate to visualize the asymmetry as being due to a net Birkeland current, which, according to Figure 6a, is downward on the dawnside and dayside, upward on the duskside and nightside. This net Birkeland current, a combination of region 1 and region 2, feeds the electrojets, which, as shown in Figure 6b, flow away from a region centered near 1100 LT, toward a region centered near 2200 LT. The theoretical necessity for downward currents on the dayside, upward at night, was pointed out by Hughes and Rostoker [1977, 1979], and they have also found some evidence for this in ground magnetograms. The TRIAD data do not clearly suggest net Birkeland current flow in this sense.

If we try to represent the complex model substorm current system schematically in terms of a small number of current loops, we arrive at a picture like Figure 4b. The solid loop in Figure 4a remains the same. However, the dawn-dusk asymmetry in low-latitude ΔB is caused not by a dusk side partial ring current loop, but by net downward day side Birkeland currents and net upward night side Birkeland currents. These currents connect partly to the inner magnetospheric ring current, partly to the outer magnetosphere, the

boundary layers and the outer plasma sheet. The thin solid lines in Figure 4b correspond to the dominant current system measured by low-altitude satellites — downward region 1 currents on the dawn side connecting to equatorward ionospheric currents and then to upward region 2 currents. This current flows westward as the westward inner magnetospheric ring and plasma sheet current to the dusk side where region 2 currents flow downward connecting to poleward ionospheric Pedersen currents and finally to upward region 1 currents. This current system has only modest ground magnetic signature, but carries more current than the other two loops.

We should mention that Crooker and Siscoe [1981] have recently discussed the relationship between the asymmetry in low-latitude ΔH and region 1/region 2 Birkeland currents, in terms of a clever analytic argument; they deduce ground magnetic disturbances by applications of Fukushima's theorem and equivalent currents. Their results and conclusions, derived by quite different calculational methods and by using different approximations, are very consistent with ours.

We should also comment that Kamide et al. [1981] have derived an average low-latitude disturbance pattern, using horizontal and Birkeland currents derived from high-latitude magnetograms. Their computed disturbances exhibit a dawn-dusk asymmetry that has the same sense as ours.

C. Analysis of the Magnetic Storm of July 29, 1977

(Reference: Wolf et al., 1982)

The second event that we chose to computer simulate was the magnetic storm of July 29, 1977, an event which involved a major compression of the magnetosphere (the magnetopause came inside geosynchronous orbit), and development of a moderate ring current. (Dst dropped to about -100 γ.) Our major objectives in modeling the event were to determine whether our model could produce a realistic storm-time ring current and to study the effect of a magnetospheric compression on convection.

Figure 7 shows theoretical electric-potential patterns at four times early in the event of July 29, 1977. Before the sudden commencement at 0030 UT, the inner edge of the plasma sheet efficiently shielded the low-L region from the convection electric field (Figure 7a). In the sudden commencement,

the magnetosphere was compressed, and the inner edge of the plasma sheet was significantly distorted, destroying the shielding (Figure 7b). The result was a large dawn-to-dusk electric field across the inner magnetosphere. On the nightside, this westward electric field forced the plasma sheet much closer to the earth, helping to form the storm time ring current. An hour after the sudden commencement (0130 UT), shielding had not yet re-asserted itself strongly (Figure 7c). However, shielding was nearly complete 2.75 hours later (0415 UT) (Figure 7d); by this time plasma sheet plasma had moved in to $\lesssim 4\ R_E$ on the nightside.

Figure 8 shows computed Birkeland-current patterns for a similar series of times. The sudden commencement caused a major but temporary disruption in the normal pattern of Birkeland current. Specifically, note that the field-aligned currents thirty minutes after the sudden commencement (Figure 8c) do not correspond to the normal Iijima-Potemra pattern shown in Figure 8a.

Figure 9 illustrates the basic physical effect of the sudden commencement on the ring current inner edge, the partial ring currents, and the magnetospheric electric field. The compression moves the ring-current inner edge antisunward, changes the configuration of partial ring current, and causes a strong dawn-to-dusk electric field near the Earth. Over the period of an hour or so, the configuration changes to regain the normal shielded condition. Meanwhile, the Birkeland-current and electric-field configuration is disturbed.

Our simulation of the July 29, 1977 event was our first effort at simulating the injection of a storm-time ring current. The way in which one species of particles moves in to form part of the ring current is shown in Figure 10. Fennell et al. [1982] have compared our predicted inner edge locations with observations, and found generally good agreement.

As was mentioned earlier, one of our major objectives in this run was to determine whether magnetospheric convection, including effects of shielding, could be sufficient by itself to inject enough plasma sheet plasma close to the earth to result in a full storm time main phase ring current.

A "yes" answer to this question is apparently provided by Figure 11, which compares the observed Dst with our theoretical values. The theoretical values were computed by integrating the Biot-Savart law over our model ring

current using the program described by Chen et al. [1982], and then correcting for changes in Chapman-Ferraro currents using the model of Voigt [1981]. Relative to a reference "quiet" state of the magnetosphere, the Chapman-Ferraro currents result in a positive contribution to Dst when the magnetosphere is compressed. The changes in Chapman-Ferraro currents occurred at 0030 UT (sudden commencement) and 0430 UT (partial re-expansion).

Predicted and observed Dst values agree remarkably well. On this first try, the model correctly predicted the time development of total ring current strength (as measured by Dst), using as essential time-dependent input the following parameters: interplanetary magnetic field (used to estimate polar-boundary potential drop); solar wind density and velocity (used to estimate standoff distance); and AL index (used to scale the conductivity model). Since vB_{south} or ε correlate extremely well with AE or AL [e.g., Garrett et al., 1974; Akasofu, 1980; or Murayama et al. ,1980], we could equally well have run our theoretical model using only solar-wind data as time-dependent input.

The agreement between observed and predicted Dst does not prove that the ring current is formed by simple earthward convection of plasma sheet plasma. It does, however, suggest that this simple process would be sufficient to produce a storm-time main-phase ring current, even if there were no more complicated processes operating (further energization of previously injected ring current plasma [Lyons and Williams, 1980] or injection of ionospheric ions directly into the ring current region [e.g., McIlwain, 1976; Shelley et al., 1976]).

D. Test of the KRM Algorithm

(Reference: Wolf and Kamide, 1983)

Recently, computational algorithms have been developed for routine, automated calculation, from ground magnetograms, of global distributions of ionospheric electric fields, horizontal ionospheric currents, and vertical or magnetic field-aligned currents [Mishin et al., 1980; Kamide et al., 1981]. These calculations required that the divergence of current be zero, neglecting neutral-wind effects, by means of the equation

$$\nabla_h \cdot (\underline{\Sigma} \cdot \nabla_h V) = j_\parallel \qquad (1)$$

where $\underline{\Sigma}$ is a tensor representing height-integrated ionospheric conductivity, V is the electrostatic potential in the rest frame of the solid Earth, $j_\parallel$ is the density of upward Birkeland current, and ∇_h is a horizontal gradient operator. Electric-potential and Birkeland-current distributions were then adjusted to fit the ground magnetometer data. By utilizing equation (1) and an assumed conductivity model, it has been shown that such advanced techniques seem to have the potential for providing observation-based, high-time-resolution pictures of the global ionospheric current and electric-field patterns for interesting events; see recent reviews by Rees [1982], Kamide [1982], and Greenwald [1983].

We have carried out a blind test to determine whether the KRM algorithm can deduce overhead current patterns, given ground magnetic perturbations and an accurate conductivity model. R. A. Wolf prepared a conductivity subroutine which would, for either of the two chosen universal times during the September 19, 1976 substorm and any specified geomagnetic latitude and magnetic local time, calculate exactly the conductivity values that were used in the computer simulation of the event.

From the electric fields and conductivities specified by the Rice Convection Model, Wolf ran the "theoretical magnetogram" program of Chen et al. [1982] to calculate $\Delta\underline{B}$'s for each of 96 points on the earth's surface. Ground currents are not included in the $\Delta\underline{B}$ calculation. The 96 points were chosen to have 16 different latitudes and 6 magnetic local times (00, 04, 08, 12, 16, 20). Magnetic latitudes range from about 26° to 80°, with spacing that ranges from about 2° at high latitudes to about 5° at low latitudes.

Wolf sent Kamide the following items: 1. a conductivity program, set up to calculate conductivities for each of the two chosen times, 2. locations of the 96 "ground stations," and 3. $\Delta\underline{B}$ values for each of the 96 "ground stations" and each of the two chosen times. Kamide was not then given any additional information concerning the current or electric field distributions that produced the $\Delta\underline{B}$'s or concerning the substorm times.

Kamide then applied the KRM algorithm to this 96-station ensemble, using the two horizontal components of $\Delta\underline{B}$ from the data sent from Rice.

Once Kamide had completed computations of $\underset{\sim}{j}$ and $\underset{\sim}{E}$, plots of these vectors were prepared both at NOAA and at Rice, and were exchanged simultaneously by mail. These plots are shown in Figures 12 and 13.

Figure 12 compares ionospheric current distributions computed by the KRM algorithm from "theoretical magnetograms" with the Rice-model ionospheric current distributions that formed the parent distribution for the "theoretical magnetograms." Note that overall agreement is remarkably good for the two cases, indicating that the KRM scheme was successful in deducing the overall current pattern. Note also that the KRM algorithm tended to smooth out the sharp latitudinal variations in the current density.

Figure 13 compares horizontal flow velocities $\underset{\sim}{E} \times \underset{\sim}{B}/B^2$ computed by the KRM algorithm with the original Rice-model flow velocities. Again, there is very good agreement with regard to overall flow patterns at high latitudes. Note, however, that the KRM algorithm implies large flow velocities on the nightside below 65° latitude, whereas the Rice source-model has very small flow velocities there. The reason for this discrepancy is clear. The KRM algorithm neglects ring currents and considers Birkeland currents to flow on straight, vertical magnetic field lines. On the nightside at subauroral latitudes, where the ionospheric conductivity is low, the ring current makes a major contribution to the ground $\Delta\underset{\sim}{B}$ [Chen et al., 1982]. Also, $\Delta\underset{\sim}{B}$ is affected by Birkeland currents flowing at high altitudes (> 1 R_E), where field-line curvature is important [Fukushima and Kamide, 1973]. Some of the $\Delta\underset{\sim}{B}$ that is due to ring current and high-altitude Birkeland current is interpreted, by the KRM algorithm, as being due to overhead currents. Since the conductivity is so low, significant densities of overhead current correspond to large electric fields, as shown on the right side of Figure 13 for 60-65° latitude at night.

Figure 14 shows the same electric-field comparison as Figure 13, but this time expressed in terms of equipotential patterns. Again, agreement is very good at high latitudes, with drastic discrepancies at low latitudes at night. Total point-to-point potential drops are also in good agreement for high latitudes. For example, consider the polar-cap potential drop, specifically, the total potential drop across curve H. The values deduced from the "theoretical magnetograms" by the KRM algorithm agree with those from the Rice source-model within 10%.

The blind test was successful in the sense that there was overall agreement between electric fields and currents calculated by the RCM and KRM schemes. There were some detailed discrepancies, but those seem attributable to known differences between the computational schemes employed in the two models. The blind test thus has verified that the KRM algorithm does what it was mainly designed to do, specifically to deduce the large-scale pattern of high-latitude horizontal ionospheric electric fields and currents from ground magnetograms and a suitable conductivity model. It is important to note, however, that the algorithm should not be used at subauroral latitudes; particularly on the nightside, the algorithm produced too strong electric fields and flow velocities. This test naturally cannot give any indication of errors due to the following factors: 1. inaccuracies in the conductivity model; 2. neglect of ionospheric neutral winds; 3. inaccuracies in the method used in the KRM algorithm for representing earth currents.

The overall success of the blind test encourages us about the possibility of combining the KRM and RCM algorithms to study events. The KRM algorithm could provide high-time-resolution boundary ionospheric conditions for the RCM, which could then be used to study magnetospheric dynamics.

E. Region-1 currents in the Rice Convection Model

(Reference: Karty, 1983)

We report here on research in progress concerning the possibility that a large fraction of region-1 current connects, not to any kind of boundary layer, but to gradient-drift and curvature-drift currents that flow within closed flux tubes containing slowly drifting plasma.

Within the pure open model proposed by Dungey [1961], region-1 currents would flow almost entirely along the boundary between open and closed field lines, which is also the flow reversal, i.e., the boundary between antisunward-flowing and sunward-flowing flux tubes. Within the simple closed model, as proposed by Axford and Hines [1961], region-1 currents flow in a closed-field-line boundary layer that is estimated to be ~1 R_E thick and flows primarily antisunward. Combining the two models, as suggested by Crooker and others, we would expect the region-1 currents to flow mainly on antisunward-flowing field lines, or at the flow reversal.

Measurements made by the S3-2 and S3-3 spacecraft (Smiddy et al., 1980; Shuman et al., 1981; Mozer et al., 1979, 1980) give a quite different picture. Namely, most of the region-1 current frequently flows on sunward-convecting flux tubes, particularly on the night side and toward dusk. Frequently, most of the region-1 current occurs more than a degree equatorward of the electric-field reversal, i.e., well down into the sunward-convecting region. The following questions then arise: Can region-1 currents flow on slow-moving, sunward-convecting flux tubes? If so, how are the generated?

Normally, in our event simulations, the magnetic-field-aligned currents predicted by the model are in good agreement with observed region-2 currents (see, e.g., Figure 14 of Harel et al. [1981b]). Region-1 -sense currents do not occur, except temporarily in very brief disturbed periods. On the other hand, our previous simulations have also made an important simplifying assumption, namely that all plasma-sheet flux tubes drifting into the modeling region from the magnetotail have intrinsically identical plasma populations.

Janice Karty has investigated the possibility that we can get region-1-sense current in our modeling region, if we appropriately relax our tailward boundary condition. These region-1 currents connect to gradient-curvature-drift currents in the magnetotail, and on the flanks of the magnetosphere.

Some conclusions reached are the following:

1. We get region-1 currents generated on sunward-convecting plasma-sheet flux tubes if we install, as a back boundary condition, a depleted channel of lower-density flux tubes somewhere near the center of the magnetotail. A sample computed Birkeland current pattern is shown in Figure 15, a result of a preliminary computer run.
2. Earthward flow tends to be faster inside the depleted channel than outside.
3. A depleted channel near the center of the magnetotail, with flowing plasma inside, would be stable against interchange instability.

The depleted-channel idea resembles the classic tail-current-interruption picture for the expansion phase of a magnetospheric substorm — an idea that has been discussed by many people (see Figure 16). However, we have developed and modified it in a number of ways:

1. We envisage a depleted channel existing most of the time in the interior of the magnetotail, not just during substorm expansions, because nightside

region-1 currents are often be observed to flow on sunward-convecting flux tubes in periods other than substorm expansion phases. However, the depletion may be modest (perhaps less than a factor of 2) except during substorms.

2. We have performed detailed stability analyses, and also numerical simulations aimed at computing self-consistent electric field and current configurations, including the depleted channel.

F. Computer Simulation of the Magnetic Storm of March 22, 1979

We report here on the progress of our study of the magnetic-storm event of March 22, 1979. This event was chosen as the principal focus of Coordinated Data Analysis Workshop 6. In this large cooperative effort, data have been reduced and analyzed from a remarkably large number of spacecraft and ground stations. Specifically, good data are available from the solar wind (IMP-J and ISEE-3), the plasma sheet (ISEE-1 and 2) and the geosynchronous-orbit region (SCATHA, GEOS-2, and others). Excellent particle-precipitation data are available from DMSP and other polar-orbiting spacecraft.

Because of the excellent data coverage for March 22, 1979, we have decided to use it as the experimental basis of what we hope will be a definitive theoretical study of ring-current injection. We are focusing on the simple question: What physical conditions govern ring-current injection? We are now attempting to answer the question within the context of the physics that is included in our model, i.e., without parallel electric fields, neutral winds, particle loss by particle precipitation and charge exchange, energetic-ion flow up from the ionosphere. These computer runs were made partly at the instigation, and with the participation of George Siscoe.

We present here some results of a series of six runs:

Run D: Run with nominal ionospheric conductivity model (based on the empirical model of Spiro et al. [1982] and preliminary AE index), nominal magnetic field model provided by G.-H. Voigt and based on observed solar-wind ram pressure and Dst, and boundary-condition plasma sheet density and temperature chosen to represent pre-substorm conditions observed at ISEE-2 [as provided by G. Paschmann, private communication].

Run F: Same as run D, but with plasma-sheet pressure decreased by a factor of 2, same temperature.

Run H: Same as run D, but with plasma-sheet temperature increased by a factor of about 2.4. Particle pressure is the same as for run D.

Run J: Same as run D, but with constant magnetic-field configuration, i.e., no compression at the time of the sudden commencement, no post-SSC expansions or compressions due to changes in solar-wind ρV^2, no inner-magnetospheric inflation due to development of the ring current.

Run L: Same as run J, but with double the nominal ionospheric conductivity.

Figure 17 shows universal-time plots of the principal input parameters for the March 22, 1979 event. The AE-index is used to choose a conductivity model with the appropriate degree of auroral enhancement. The magnetopause standoff distance, calculated from observed solar-wind ρV^2, is an input to the magnetic field model; the Dst index governs ring-current strength in the magnetic field model. The polar-boundary potential drop, which is estimated from the observed interplanetary magnetic field using a formula from Reiff et al. [1981], is an essential boundary condition for our electric-field calculation.

Figure 18 compares our predicted electric fields for the location of the Saint Santin radar with electric fields observed on March 22, 1979. Agreement is encouraging, and suggests that our model treats the shielding process reasonably realistically.

Energetics

Figure 19 shows time-integrated global Joule heatng and ring-current energy plotted against universal time, for the nominal run D, and for run J (same as run D, but using a constant, uncompressed magnetic-field model). For the nominal run D, total Joule heating was about 1.46 times ring current energy. Eliminating the compression of the magnetosphere (and other changes in the magnetic field model) does not change the Joule heating significantly, but reduces the ring current energy by a factor of 0.6. Thus for run J, Joule heating is about 2.4 times ring-current energy. This result is consistent with results of earlier simulations. Joule heating was about 2-3 times ring current energy for our simulations of the September 19, 1976 substorm, which involved no compression. Joule heating was about 0.5 times ring current energy for our simulations of the July 29, 1977 magnetic storm, which involved a massive compression. (The magnetopause came inside geosynchronous orbit.)

The conclusion is clear: Within the physics included in our model, compression of the magnetosphere plays an important role in ring-current injection.

Figure 20 shows the effect, on ring current energy, of changes in the plasma boundary condition of our calculation. (Ring-current energy is here defined as the total particle energy in our modeling region.) Halving the plasma-sheet pressure, but keeping the temperature the same, decreases the final ring-current energy by approximately a factor of 0.75. (If the electric-field configuration remained the same in the two cases, the change would be a factor of 0.5.) However, the decreased plasma-sheet density decreased the degree of shielding, allowing particles of a given energy to come closer to the Earth. (More evidence of this effect will be displayed later.) Increasing the plasma sheet temperature by a factor of 2.4 but keeping plasma-sheet pressure constant decreased ring-current energy by about 12%. Raising the plasma-sheet temperature decreased the low-energy particle population in the plasma sheet, and it is the low-energy part of the plasma-sheet ion population that is injected deep into the magnetosphere.

Figure 21 shows the effect of plasma-sheet changes on Joule heating. Reductions in shielding efficiency, and deeper penetration of plasma-sheet-particles into the magnetosphere, makes the auroral zone thicker, effectively. The potential drop, which is the same in each case, is spread over a greater latitudinal range, and the integral over the ionosphere of $\Sigma_p \tilde{E}^2$ becomes smaller.

Figure 22 shows the effect of ionospheric conductivity on ring-current injection. Doubling the conductivity increases the ring-current energy by a factor of about 1.4, in the case where the magnetic field model is held constant (so that ring-current injection is strictly a convection effect). Increasing conductivity decreases the shielding efficiency, allowing particles to be injected deeper into the magnetosphere.

Figure 23 shows the actual ring-current energy for March 22, 1979, as estimated from the observed Dst index. Specifically, we assume

$$\Delta B = -\frac{2}{3} B_o (U_{ring}/U_m)$$

where ΔB = northward magnetic field perturbation at the Earth's surface near the equator, B_o = surface field at the equator = 31000 γ, U_{ring} = ring current

energy, and U_m = magnetic energy in the Earth's dipole field above the surface $\approx 8 \times 10^{17}$ J (see Cummings and Dessler, 1967). The values for Dst were supplied by Olson and Pfitzer [private communication, 1982]. They were based on the observed Dst for March 22, 1979, but were corrected for the effects of Chapman-Ferraro currents, as estimated from the solar-wind ρV^2. Comparing Figure 23 with Figure 20, we see that the ring-current energies deduced from observations are smaller than those predicted theoretically, for nominal values of the input parameters. We suspect that most of this discrepancy results from particle loss by precipitation and charge exchange, processes that are not included in the present version of the model.

Particle arrival times at SCATHA. Figure 24 displays low-energy ion fluxes observed by SCATHA [Strangeway and Johnson, 1983]. The times when apparently fresh ions of various energies arrived at SCATHA are shown in Figure 25.

Figures 26-30 show computed inner edges for equatorially mirroring particles that started at 10 R_E geocentric distance at 0400 UT. (10 R_E approximately coincides with the initial inner edge of the plasma sheet.) Some conclusions from Figures 24-30 are the following:

1. For our nominal run (run D, Figure 26), particles arrive at SCATHA in the model 1-2 hours later than they actually arrived at the spacecraft (Figure 24).
2. Reducing the plasma sheet pressure by a factor of 2 (run F, Figure 27) makes the shielding less efficient and allows low-energy ions to penetrate closer to the Earth. Predicted particle arrival times now are close to the observed ones. (This suggests that particle loss would also allow particles to penetrate deeper.)
3. Increasing the plasma-sheet temperature (as in run H, Figure 28) reduces the number of low-energy ions, and allows them to penetrate closer to the Earth. The arrival time for 10 keV ions was again close to the observed time.
4. For the case where the magnetic field is not compressed in the sudden commencement (run J, Figure 27), low-energy ions do not penetrate as close to the Earth. Predicted arrival of 10 keV ions is about 3 hours later than observed.
5. Increasing ionospheric conductivity by a factor of two (run L, Figure 30) reduces the shielding and causes particles to arrive at SCATHA earlier.

We have also made a rough comparison between our predicted flux levels and the observed fluxes (Figure 24). Our predicted fluxes are based on adiabatic convection and compression of plasma-sheet flux tubes. At our model boundary, the plasma-sheet distribution function is set equal to a Maxwellian, with temperature chosen to match pre-substorm observations at ISEE-2. At 10 keV, the predicted and observed fluxes approximately agree. Of course, the model Maxwellian distribution implies that the differential flux is proportional to energy E, for $E << kT$, and the observed fluxes clearly are not like that. The large observed ion fluxes at low energies may, of course, have been injected from the ionosphere within the modeling region. Our predicted 20 keV ion fluxes are higher than those observed.

In summary, we have now performed a fairly complete theoretical study of the physics of ring-current injection, within the physics that is included in our model. Ring-current development is mainly a convection phenomenon, but magnetospheric compression plays a very important role. Dependence on ionospheric conductivity and plasma-sheet boundary conditions have been investigated.

III. RECAPITULATION OF THE WORK EFFORT

This section recapitulates, in approximately chronological order, the individual steps in the contracted research, as mentioned in the quarterly reports. The items mentioned below mainly concern programming and data acquisition and display. The various reports on the work, for the scientific community, are listed separately in Section V. Scientific conclusions and results were summarized in Section II.

Second Quarter

1. Moshe Harel, Bob Spiro, and Dick Wolf ran the program for the period 0415-0900 UT in the main phase of the July 29, 1977 magnetic storm. The computed Dst agrees well with observations.
2. Moshe Harel prepared a tape of our program and sent it to Mike Heinemann of Boston College, for running on machines at AFGL and/or Boston College.
3. Janice Karty improved our model by extending it to include the poleward part of the ionosphere (see Section IIA).

Third Quarter

4. Moshe Harel, Dick Wolf, Bob Spiro, and Mike Heinemann ran a series of computer experiments for the substorm-type event of 19 September 1976, with various modifications to input assumptions and numerical methods.

(a) Runs were made for several different magnetic field models prepared by Hannes Voigt. Different models give only slightly different electric-field configurations.

(b) We ran an experiment where we suddenly decreased the polar-cap potential drop and conductivity model at 1200 UT, two hours after the onset of the initial expansion phase. Ring current energy dropped sharply and Dst increased sharply, though neither recovered all the way back to their pre-substorm level. This partial recovery results from a temporary overshielding of low L values.

5. Mike Heinemann of Boston College spent two weeks at Rice learning about program details and participating in computer experiments. Moshe Harel at Rice cooperated with Dr. Heinemann to get our program functioning on the machine at Boston College.

Fourth Quarter

6. Moshe Harel, Dick Wolf, and Bob Spiro ran many computer experiments for the event of September 19, 1976 for the purpose of improving the numerical accuracy of program Version I (which allows an inner edge to cross a local-time grid line only once).

7. Collaborating with Moshe Harel, Mike Heinemannn successfully ran program Version II on the VAX machine at Boston College and, by telephone, on the ITEL AS/6 machine at Rice.

Fifth Quarter

8. Hannes Voigt and Dick Wolf constructed a series of force-balanced two-dimensional magnetotail models. They indicate that steady sunward convection and force balance are consistent in the magnetotail only if B_z in the equatorial plane decreases as you approach the Earth.

9. Dick Wolf and Yohsuke Kamide started work on a blind test of the KRM model (see Section IID).

10. Bob Spiro completed programming for computation and display of Birkeland currents for July 29, 1977 (see Section IIC).

Sixth Quarter

11. Papers dealing with the high-latitude extension of the model (Section IIA), magnetospheric current systems (Section IIB), and the July 29, 1977 event (Section IIC) were submitted to the Journal of Geophysical Research.

12. Bob Spiro and Dick Wolf did more analysis of our simulation of the July 29, 1977 event, and comparison with S3-3 data.

13. Hannes Voigt and Dick Wolf constructed and analyzed various magnetic field models, to understand the effect of the sudden commencement of July 29, 1977 on Birkeland current and electric-field patterns (see Section IIC).

Seventh Quarter

14. Papers on the July 29, 1977 storm and the high-latitude extension of our model were revised in response to referees' comments, and accepted for publication in the Journal of Geophysical Research.

15. Dick Wolf sent data to Kamide for the blind test of the KRM algorithm (see Section IID).

16. Janice Karty completed a first series of computer runs in which the population levels of plasma-sheet flux tubes drifting through the back boundary were assumed to depend on boundary position. These first results were tantalizing, but also showed the need for some programming refinements to improve numerical accuracy (later results summarized in Section IIE).

Eight Quarter

17. Camera-ready copy was prepared and submitted for the paper on the July 29, 1977 event and the high-latitude extension of the model. The paper on magnetospheric current systems was revised in response to referee comments, resubmitted, and accepted for publication in the Journal of Geophysical Research.

18. Preparations for CDAW 6.1 were begun. Pat Reiff collected data for the event of March 22, 1979. Bob Spiro wrote a new conductivity subroutine, which uses AE index and solar activity as input. He also estimated the polar-cap potential drop using IMP-8 data and a semi-empirical formula developed by Reiff et al. [1981]. Dick Wolf chose initial and boundary-condition plasma distributions using data from ISEE-2 and 3. Hannes Voigt produced a time sequence of magnetic-field models for the event, using measured solar-wind pressure as input. Bob Spiro wrote a particle-trace routine to follow tra-

jectories of particles of various magnetic moments through the event, using our computed electric fields and Voigt's time-dependent magnetic field model.

Ninth Quarter

19. Three computer simulations of the March 22, 1979 magnetic storm were performed before and during CDAW 6.1, by Bob Spiro, Moshe Harel, Dick Wolf, and Mike Heinemann. The model's predictions for the arrival of ions at SCATHA were compared with observations. Our predicted arrival times were all rather late. Computer experiments were performed to try to determine the cause of the discrepancy, without much success.

20. Work was completed on the blind test of the KRM method, with current and electric-field plots exchanged between Yohsuke Kamide and Dick Wolf.

21. Dick Wolf and Bob Spiro prepared a paper, "The Role of the Auroral Ionosphere in Magnetospheric Substorms," for publication in the Proceedings of Nobel Symposium No. 54. Camera-ready copy was submitted.

Tenth Quarter

22. Hannes Voigt modified his magnetic field model by moving the inner edge of his assumed ring current outward, in an effort to force agreement between his model and the observed magnetic field at SCATHA.

23. Bob Spiro modified our ionospheric conductivity model to make the equatorward edge of the auroral conductivity enhancement coincide with the computed equatorward edge of the plasma-sheet electrons.

24. A new simulation was run for the March 22, 1979 event, using the revised magnetic-field and conductivity model. Computed particle arrival times for SCATHA were in quite good agreement with observations.

25. Camera-ready copy of the paper on magnetospheric current systems was prepared and sent to the Journal of Geophysical Research.

26. An initial draft of the paper on the test of the KRM algorithm was prepared.

Eleventh Quarter

27. Bob Spiro wrote a program that evaluates the inertial-drift currents in our model plasma sheet. (We neglect these currents in computing self-consistent electric fields, but we need to check that this neglect is justified.) The essential result of calculating these currents for the September 19, 1976

event was that the strength of the inertial currents was $\sim 10^3$ A, only about 0.1% of the total region-2 current at the time.

28. In collaboration with George Siscoe, Bob Spiro and Dick Wolf ran several more computer experiments through the March 22, 1979 event to determine how the input parameters and boundary conditions affect ring current injection within the model. Results of this work are described in Section IIF.

29. As a result of discussions with George Siscoe and careful examination of the results of the computer experiments described above, Dick Wolf derived an energy theorem that should be satisfied by our runs, provided that the magnetic-field model is held constant. This theorem provides a much needed numerical-accuracy test of the program.

Twelfth Quarter and up to the Present

30. Bob Spiro and Dick Wolf attended CDAW 6.3 and, with help from Moshe Harel, performed a few more computer-experiment runs on the March 22, 1979 event. Predicted particle arrival times were compared with SCATHA results. Improved input information on plasma-sheet particle distributions was obtained from Götz Paschmann (ISEE-2 data). Bob Spiro compared predicted mid-latitude electric fields with observations from the Saint-Santin radar, made available by C. Mazaudier. (A comparison between the radar data and recent model results is shown in Figure 18.)

31. Dick Wolf and Moshe Harel did the programming necessary for computation of "theoretical Dst" for the March 22, 1979 event. These Dst predictions for each run were compared with the actual values.

32. Bob Spiro completed programming of the energy check derived earlier (item 29). Performing that energy check on various runs through the March 22, 1979 event indicated poor numerical accuracy, beginning in the recovery phase of the first substorm. This accuracy problem pertains to Version I of the program, which we had been using for the March 22, 1979 event. The energy test program was also applied to our simulation of the July 29, 1977 event, using Version II of the program (which entails a more detailed treatment of inner edge motions). In that case, the energy test came out satisfactorily.

33. Bob Spiro made a number of updates and improvements in Version II of the program, and applied it to the March 22, 1979 event. The energy test came out acceptable, although energy discrepancies of as much as 20% occasionally occur.

34. The computer experiments originally performed in collaboration with George Siscoe (item 28) have been rerun, using Version II of the program. Results of this series of runs are summarized in Section IIF.

35. The paper described as the blind test of the KRM algorithm has been submitted to the Journal of Geophysical Research.

IV. BUSINESS DATA

A. Contributing Scientists

Rice University

C.-K. Chen, Research Associate
G. M. Erickson, Graduate Student
M. Harel, Senior Research Associate
J. L. Karty, Graduate Student
G. Mantjoukis, Graduate Student
P. H. Reiff, Associate Research Scientist
R. W. Spiro, Senior Research Associate
G.-H. Voigt, Associate Research Scientist
R. A. Wolf, Professor

NOAA, Boulder

Y. Kamide

Boston College

M. A. Heinemann

UCLA

G. L. Siscoe

B. Previous and Related Contracts

F19628-77-C-0005	(10/01/76 – 02/01/80)
F19628-77-C-0012	(10/01/76 – 09/30/77)
F19628-78-C-0078	(10/01/77 – 09/30/78)
F19628-80-C-0009	(01/01/83 – 12/31/85)

C. Publications

Chen, C.-K., R. A. Wolf, M. Harel, and J. L. Karty, Theoretical magnetograms based on quantitative simulation of a magnetospheric substorm, J. Geophys. Res., 887, 6137, 1982.

Karty, J. L., C.-K. Chen, R. A. Wolf, M. Harel, and R. W. Spiro, Modeling of high latitude currents in a substorm, J. Geophys. Res., 87, 777, 1982.

R. A. Wolf et al., Computer simulation of inner magnetospheric dynamics for the magnetic storm of July 29, 1977, J. Geophys. Res., 87, 5949, 1982.

D. Papers Accepted for Publication

R. A. Wolf and R. W. Spiro, The role of the auroral ionosphere in magnetospheric substorms, to be published in the Proceedings of Nobel Symposium No. 54.

R. A. Wolf, The quasi-static (slow-flow) region of the magnetosphere, to be published in the Proceedings of the Solar-Terrestrial Theory Institute, Boston College.

E. Papers Submitted for Publication

R. A. Wolf and Y. Kamide, Inferring electric fields and currents from ground magnetometer data: A test with theoretically derived inputs, submitted to the Journal of Geophysical Research, 1983.

F. Papers Presented at Meetings

M. Harel, R. W. Spiro, R. A. Wolf, and P. H. Reiff, Dynamic storm-time model for July 29, 1977, invited paper presented at AGU meeting, Toronto, May 1980.

G. M. Erickson and R. A. Wolf, Is steady convection possible in the Earth's magnetotail?, Paper SM 34, Fall 1980 AGU meeting, San Francisco.

G.-H. Voigt, The shape and position of the plasma sheet in the Earth's magnetospheric tail, Paper SM 36, Fall 1980 AGU meeting, San Francisco.

M. Harel, R. A. Wolf, R. W. Spiro, and G.-H. Voigt, Computer experiments for the September 19, 1976 substorm, Paper SM 129, Fall 1980 AGU meeting, San Francisco.

C.-K. Chen, J. L. Karty, M. Harel, and R. A. Wolf, Theoretical magnetograms for the substorm event of September 19, 1976, Paper SM 130, Fall 1980 AGU meeting, San Francisco.

R. A. Wolf, C.-K. Chen, M. Harel, J. L. Karty, and R. W. Spiro, Substorm current systems and partial ring currents, Paper SM 131, Fall 1980 AGU meeting, San Francisco.

R. A. Wolf, Numerical simulations talk presented at the Radiation Belt Workshop, AFGL, January 26-27, 1981.

R. A. Wolf, Computer modeling of the inner magnetosphere lecture presented at U.S.-Japan Seminar on Wave-Particle Interactions, Kyoto, Japan, March, 1981.

R. A. Wolf, paper presented at the IMS Assessment Symposium, Goddard Space Flight Center, May 1981.

M. Harel, R. A. Wolf, C.-K. Chen, and R. W. Spiro, Computed Birkeland currents, paper SM17 presented at the Spring AGU meeting, Baltimore, MD, May, 1981.

M. Harel, R. A. Wolf, and R. W. Spiro, Modeling of magnetospheric convection for specific events, Paper 3Q.13, IAGA meeting, Edinburgh, Scotland, August, 1981.

J. L. Karty, Calculation of high-latitude currents for a substorm, paper SM127 presented at the Spring AGU meeting, Baltimore, MD, May, 1981.

G.-H. Voigt, A quantitative magnetospheric model with a self-consistent tail plasma sheet, Paper 3Q.08, IAGA meeting, Edinburgh, Scotland, August, 1981.

R. A. Wolf, R. W. Spiro, and M. Harel, Polar-cap electric fields, (presented by P. H. Reiff), Paper 3C.01, IAGA meeting, Edinburgh, Scotland, August, 1981.

R. A. Wolf, Magnetosphere-ionosphere interactions, Reporter Review, Topic III-1, IAGA meeting, Edinburgh, Scotland, August, 1981.

R. A. Wolf and R. W. Spiro, The role of the auroral ionosphere in magnetospheric substorms, invited lecture presented at Nobel Symposium No. 54, Kiruna, Sweden, March, 1982.

M. Harel, R. A. Wolf, R. W. Spiro, and G.-H. Voigt, Preliminary results from quantitative modeling of the March 22, 1979, magnetic storm, paper SM21-26 presented at the Spring AGU meeting, Philadelphia, PA, May, 1982.

Y. Kamide, R. A. Wolf, R. W. Spiro, and A. D. Richmond, Inferring electric fields and currents from ground-magnetometer data — A test with theoretically derived inputs, paper SM52B-7 presented at the Spring AGU meeting, Philadelphia, PA, May, 1982.

R. W. Spiro, G.-H. Voigt, R. A. Wolf, and M. Harel, Application of the Rice Convection Model to the magnetic storm of March 22, 1979, paper SM51-16 presented at the Spring AGU meeting, Philadelphia, PA, May, 1982.

P. H. Reiff and R. W. Spiro, Satellite studies of dynamical effects on electron precipitation morphology, paper SM12A-7 presented at the Spring AGU meeting, PA, May, 1982.

P. H. Reiff, The use and misuse of correlation analyses, lecture presented at the Solar-Terrestrial Theory Institute, Boston College, August, 1982.

R. A. Wolf, The quasi-static (slow-flow) region of the magnetosphere, lecture presented at the Solar-Terrestrial Theory Institute, Boston College, August, 1982.

G.-H. Voigt, paper presented at the Solar-Terrestrial Theory Institute, Boston College, August, 1982.

G.-H. Voigt, Theory of magnetospheric equilibrium configuration, paper presented at the First International School for Space Simulations, Kyoto, Japan, November, 1982.

R. A. Wolf, Computer modeling of inner-magnetospheric behavior during a magnetic storm, paper presented at the First International School for Space Simulations, Kyoto, Japan, November, 1982.

R. W. Spiro, Evaluation of Birkeland current due to acceleration drift in the inner magnetosphere, paper SM12A-12 presented at Fall AGU meeting, San Francisco, December 1982.

G. Travel Performed

(All of the trips listed below involved contract reserch, but most combined contract research with other business. Thus the contract bore only a fraction of the costs.)

R. A. Wolf visited the Air Force Geophysics Laboratory 8-10 April 1980, for extensive discussions with AFGL personnel concerning the logic and basis of the computer model and also concerning plans for work under the contract.

M. Harel attended the Spring 1980 AGU meeting in Toronto and presented and invited paper concerning our preliminary computer run for the magnetic storm of July. 29 1977.

R. A. Wolf visited the Air Force's Global Weather Central facility at Offett Field, Nebraska on September 29, 1980. The purpose of the visit was to discuss the way predictions are being made, possible future needs and the relevance of the Rice Convection Model to those needs.

C.-K. Chen, G. M. Erickson, M. Harel, J. L. Karty, R. W. Spiro, G.-H. Voigt, and R. A. Wolf attended the Fall 1980 AGU meeting, and presented several papers displaying results of contract research.

M. Harel and R. A. Wolf attended the Radiation-Belt Workshop at AFGL on January 26-27, 1981, and then spent about 1 1/2 days discussing contract plans with W. J. Burke and M. Heinemann.

G.-H. Voigt and R. A. Wolf visited AFGL on April 7, 1981 for discussions with AFGL visitors, including M. Abdalla, B. Coppi, and M. Heinemann, and AFGL personnel, including W. J. Burke, P. L. Rothwell, and R. Sagalyn.

R. A. Wolf participated in the U.S.-Japan Seminar on Wave Particle Interactions in Space Plasmas on March 16-21, 1981. This trip, which allowed helpful information exchanges with several Japanese scientists concerning magnetospheric modeling, was supported entirely from funds other than contract F19628-80-C-0009.

R. A. Wolf attended the IMS Assessment Symposium at Goddard Space Flight Center, May 21-23, 1981. He presented results from our simulation of the July 29, 1977 event and also served on a review panel.

M. Harel, J. L. Karty, P. H. Reiff, R. W. Spiro, G.-H. Voigt, and R. A. Wolf attended the Spring 1981 AGU meeting in Baltimore, May 25-29. Several papers on our computer simulations were presented, and we had many useful conversations concerning contract work.

P. H. Reiff, G.-H. Voigt, and R. A. Wolf attended the IAGA meeting in Edinburgh, Scotland in August, 1981. They presented several papers reporting

resultings of contract-supported research. Approximately $325 of Wolf's expenses were charged to contract F19628-80-C-0009.

P. H. Reiff attended the preparatory CDAW-6 Workshop (CDAW 6.0) in Palo Alto, December 3-5, 1981, to collect the input data required for the simulations of the March 22, 1979 event.

M. Harel, P. H. Reiff, R. W. Spiro, G.-H. Voigt, and R. A. Wolf attended the CDAW 6.1 Workshop at Goddard Space Flight Center, February 11-13, 1982.

R. A. Wolf attended Nobel Symposium No. 54, "Problems in High-Latitude Magnetospheric/Ionospheric Plasma Physics and Strategies for their Solution," in Kiruna, Sweden on March 22-25, 1982. He presented an invited paper on the role of the ionosphere in substorms. Trip expenses were not charged to this contract.

J. L. Karty, R. W. Spiro, and R. A. Wolf attended a SWAMP (South Association of Magnetospheric Physics) meeting in Dallas, April 2-3, 1982. The purpose of the meeting was to discuss various mangetospheric issues, many related to this contract. Results of testing the KRM method were presented and discussed.

R. W. Spiro, M. Harel, and G.-H. Voigt atended the Spring 1982 AGU meeting in Philadelphia and gave poster and oral presentations of grant-supported work.

P. H. Reiff, R. W. Spiro, G.-H. Voigt, and R. A. Wolf attended the Solar-Terrestrial Theory Institute, which was held at Boston College, August 9-27, 1982. Reiff gave lectures on analysis of spacecraft data; Voigt gave a paper on his magnetic-field calculations; and Wolf lectured about the theoretical basis of the convection model and about model results. A small part of the attendant travel costs were borne by this contract.

R. W. Spiro and R. A. Wolf participated in CDAW 6.3, held at Goddard Space Flight Center, October 19-23, 1982.

G.-H. Voigt and R. A. Wolf traveled to Kyoto, Japan, to participate in the First International School for Space Simulations, held November 1-12, 1982. Both Voigt and Wolf gave invited lectures concerning magnetospheric simulations. Travel expenses were not charged to this contract.

R. W. Spiro attended the Fall 1982 AGU meeting in San Francisco, and presented a paper.

H. Fiscal Information

All of the $307,000 allotted for the contract has been spent. The work is completed.

I. Final Cumulative Cost Data

Labor Elements	Amount Planned	Actual
Principal Investigator (R. A. Wolf)...	$ 27,570	$ 32,856
Co-Investigators..... (M. Harel and P. H. Reiff)	44,478	18,200
Other Staff and Students.....	70,116	90,952
TOTAL LABOR.....	$142,164	$142,008
Expense		
International Travel.....	$ 500	$ 326
Domestic Travel.....	10,125	9,820
Computing.....	44,262	35,628
Fringe Benefits.....	16,766	17,574
Other Expenses.....	10,727	19,207
TOTAL EXPENSES.....	$ 82,380	$ 82,555
Equipment.....	$ 0	$ 0
Overhead.....	$ 82,456	$ 82,437
GRAND TOTAL.....	$307,000	$307,000

V. REFERENCES

Akasofu, S.-I., The solar-wind-magnetosphere energy coupling and magnetospheric disturbances, Planet. Space Sci., 28, 495, 1980.

Atkinson, G., The current system of geomagnetic bays, J. Geophys. Res., 72, 6063, 1967.

Axford, W. I., and C. O. Hines, A unifying theory of high-latitude geophysical phenomena and geomagnetic storms, Can. J. Phys., 39, 1433, 1961.

Boström, R., Ionosphere-magnetosphere coupling, in Magnetospheric Physics, edited by B. M. McCormac, p. 45, D. Reidel, Dordrecht, Netherlands, 1974.

Chen, C.-K., R. A. Wolf, M. Harel, and J. L. Karty, Theoretical magnetograms based on quantitative simulation of magnetospheric substorm, J. Geophys. Res., 87, 6137, 1982.

Clauer, C. R., and R. L. McPherron, The relative importance of the interplanetary electric field and magnetospheric substorms on partial ring current development, J. Geophys. Res., 85, 6747, 1980.

Crooker, N. U., and R. L. McPherron, On the distinction between the auroral electrojet and partial ring current systems, J. Geophys. Res., 77, 6886, 1972.

Crooker, N. U., and G. L. Siscoe, A study of geomagnetic disturbance field asymmetry, Radio Sci., 6, 495, 1971.

Crooker, N. U., and G. L. Siscoe, Birkeland currents as the cause of the low-latitude asymmetric disturbance field, J. Geophys. Res., 86, 11,201, 1981.

Cummings, W. D., and A. J. Dessler, Field-aligned currents in the magnetosphere, J. Geophys. Res., 72, 1007, 1967.

Dungey, J. W., Interplanetary magnetic field and the auroral zones, Phys. Res. Lett., 6, 47, 1961.

Fennell, J. F., R. G. Johnson, D. T. Young, R. B. Torbert, and T. E. Moore, Plasma and electric field boundaries at high and low altitudes on July 29, 1977, J. Geophys. Res., 87, 5933, 1982.

Fukushima, N., and Y. Kamide, Partial ring current models for worldwide geomagnetic disturbances, Rev. Geophys. Space Phys., 11, 795, 1973.

Garrett, H. B., A. J. Dessler, and T. W. Hill, Influence of solar wind variability on geomagnetic activity, J. Geophys. Res., 79, 4603, 1974.

Greenwald, R. A., Electric fields in the ionosphere and magnetosphere, Space Sci. Rev., in press, 1983.

Harel, M., and R. A. Wolf, Convection, in Physics of Solar-Planetary Environments, Vol. II, edited by D. J. Williams, p. 617, AGU, Washington, D.C., 1976.

Harel, M., R. A. Wolf, P. H. Reiff, R. W. Spiro, W. J. Burke, F. J. Rich, and M. Smiddy, Quantitative simulation of a magnetopheric substorm, 1. Model logic and overview, J. Geophys. Res., 86, 2217, 1981a.

Harel, M., R. A. Wolf, R. W. Spiro, P. H. Reiff, C.-K. Chen, W. J. Burke, F. J. Rich, and M. Smiddy, Quantitative simulation of a magnetospheric substorm, 2. Comparison with observations, J. Geophys. Res., 86, 2242, 1981b.

Hughes, T. J., and G. Rostoker, Current flow in the magnetosphere and ionosphere during periods of moderate activity, J. Geophys. Res., 82, 2271, 1977.

Hughes, T. J., and G. Rostoker, A comprehensive model current system for high-latitude magnetic activity, 1, The steady state system, Geophys. J. R. Astron. Soc., 58, 525, 1979.

Iijima, T., and T. A. Potemra, Large-scale characteristics of field-aligned currents associated with substorms, J. Geophys. Res., 83, 599, 1978.

Jaggi, R. K., and R. A. Wolf, Self-consistent calculation of the motion of a sheet of ions in the magnetosphere, J. Geophys. Res., 78, 2852, 1973.

Kamide, Y., and N. Fukushima, Positive geomagnetic bays in evening high latitudes and their possible connection with partial ring current, Rep. Ionos. Space Res. Jpn., 26, 79, 1972.

Kamide, Y., A. D. Richmond, and S. Matsushita, Estimation of ionospheric electric fields, ionospheric currents, and field-aligned currents from ground magnetic records, J. Geophys. Res., 86, 801, 1981.

Karty, J. L., The interaction of horizontal ionospheric and region one Birkeland currents, M.S. thesis, Rice University, Houston, TX, 1981.

Karty, J. L., High latitude field aligned currents, Ph.D. thesis, Rice University, Houston, TX, April, 1983.

Karty, J. L., C.-K. Chen, R. A. Wolf, M. Harel, and R. W. Spiro, Modeling of high-latitude currents in a substorm, J. Geophys. Res., 87, 777, 1982.

Karty, J. L., R. A. Wolf, and R. W. Spiro, Region one Birkeland currents connecting to sunward convecting flux tubes, submitted for publication in the Proceedings of the Chapman Symposium on Magnetospheric Currents, held in Irvington, VA, 1983.

Lyons, L. R., and D. J. Williams, A source for the geomagnetic storm main phase ring current, J. Geophys. Res., 85, 523, 1980.

McIlwain, C. E., Bouncing clusters of ions at seven earth radii (abstract), EOS Trans. AGU, 57, 307, 1976.

McPherron, R. L., C. T. Russell, and M. P. Aubry, Satellite studies of magnetospheric substorm on August 15, 1968, 9, Phenomenological model for substorms, J. Geophys. Res., 78, 3131, 1973.

Mishin, V. M., A. D. Bazarzhapov, and G. B. Shpynev, Electric fields and currents in the Earth's magnetosphere, in Dynamics of the Magnetosphere, edited by S.-I. Akasofu, pp. 249, D. Reidel, Hingham, Mass., 1980.

Mozer, F. S., C. A. Cattell, M. Temerin, R. B. Torbert, S. Von Glinski, M. Woldroff, and J. Wygant, The dc and ac electric field, plasma density, plasma temperature, and field-aligned current experiments on the S3-3 satellite, J. Geophys. Res., 84, 5875, 1979.

Mozer, F. S., C. A. Cattell, M. K. Hudson, R. L. Lysak, M. Temerin, and R. B. Torbert, Satellite measurements and theories of low altitude auroral particle acceleration, Space Sci. Rev., 27, 155, 1980.

Murayama, T., T. Aoki, H. Nakai, and K. Hakamada, Empirical formula to relate the auroral electrojet intensity with interplanetary parameters, Planet. Space Sci., 28, 803, 1980.

Rees, M. H., Scientific results of the U.S. IMS ground-based program, Rev. Geophys. Space Phys., 20, 654, 1982.

Reiff, P. H., R. W. Spiro, and T. W. Hill, Dependence of polar-cap potential drop on interplanetary parameters, J. Geophys. Res., 86, 7639, 1981.

Shelley, E. G., R. D. Sharp, and R. G. Johnson, Satellite observations of an ionospheric acceleration mechanism, Geophys. Res. Lett., 3, 654, 1976.

Shuman, B. M., R. P. Vancour, M. Smiddy, N. A. Saflekos, and F. J. Rich, Field-aligned current, convective electric field, and auroral particle measurements during a major magnetic storm, J. Geophys. Res., 86, 5561, 1981.

Siscoe, G. L., Magnetospheric inferences from low-latitude disturbance-field asymmetries, paper presented at the Workshop on the Geomagnetic Field, U.S. Air Force Geophysics Laboratory, Bedford, Mass., April, 1979.

Smiddy, M., W. J. Burke, M. C. Kelley, N. A. Saflekos, M. S. Gussenhoven, D. A. Hardy, and F. J. Rich, Effects of high-latitude conductivity on observed convection electric fields and Birkeland currents, J. Geophys. Res., 85, 6811, 1980.

Spiro, R. W., P. H. Reiff, and L. J. Maher, Jr., Precipitating electron energy flux and auroral zone conductances: An empirical model, J. Geophys. Res., 87, 8215, 1982.

Strangeway, B. J., and R. G. Johnson, Mass composition of substorm-related energetic ion dispersion events, J. Geophys. Res., 88, 2057, 1983.

Voigt, G.-H., A mathematical magnetospheric field model with independent physical parameters, Planet. Space Sci., 29, 1, 1981.

Wolf, R. A., Effects of ionospheric conductivity on convective flow of plasma in the magnetosphere, J. Geophys. Res., 75, 4677, 1970.

Wolf, R. A., and Y. Kamide, Inferring electric fields and currents from ground magnetometer data: A test with theoretically derived inputs, submitted to J. Geophys. Res., 1983.

Wolf, R. A., M. Harel, R. W. Spiro, G.-H. Voigt, P. H. Reiff, and C.-K. Chen, Computer simulation of inner magnetospheric dynamics for the magnetic storm of July 29, 1977, J. Geophys. Res., 87, 5949, 1982.

VI. FIGURE CAPTIONS AND FIGURES

Fig. 1. Ionospheric total current density. The two highest latitude "circles" of arrows are at the poleward and equatorward boundaries of the high-latitude band (from Karty et al. [1982]).

Fig. 2. Joule heating per unit ψ (both hemispheres) as a function of local time showing contributions from both the high and low latitude models. The open circles designate calculations from the high-latitude band. Results from the lower latitude computer simulation are indicated by a solid line, with no symbols or label attached. The uppermost curve is the sum of calculations from both the high latitude model and lower latitude simulation (from Karty et al. [1982]). (UT = 1100.)

Fig. 3. The top panel shows ring current energy and integrated (total) Joule heating as functions of universal time through the event. The bottom panel shows Joule heating (both hemispheres) as a function of universal time through the modeled event. Total Joule heating rates from the high-latitude band are indicated by crosses. Joule heating rates for the region equatorward of the equatorward edge of region 1 currents, are indicated by a solid line, with no symbols or label attached. The topmost curve is the sum of the other two curves, i.e., total Joule heating calculated in both the high-latitude band and the lower latitude computer simulation region (from Karty et al. [1982]).

Fig. 4. (a) A double current system to account for the substorm disturbance field at the Earth's surface [Crooker and McPherron, 1972]. (b) A substorm current system based on our computer simulation of magnetic disturbance. Dashed curves indicate that net Birkeland currents flow down from the magnetosphere on the day side, up to the magnetosphere on the night side. The current system denoted by the thin curve, which connects R1 Birkeland current, ionospheric north-south current, R2 Birkeland current and partial ring current, causes most of the magnetic perturbation observed from polar orbiting satellites, but causes a modest ground magnetic disturbance (from Chen et al. [1982]).

Fig. 5. The shaded area in the top three panels shows the asymmetry in low latitude ΔB_x caused by total, ionospheric, ring, and Birkeland currents, respectively. The bottom panel shows the decomposition of asymmetry caused by Birkeland currents; the region 1 asymmetry is much larger than region 2 asymmetry (from Chen et al. [1982]).

Fig. 6. (a) Computed Birkeland current per unit local time per hemisphere for 1050 UT. Upward current out of the ionosphere is positive. R1 and R2 represent region 1 and region 2 Birkeland currents, respectively. "R1 + R2" refers to net Birkeland current. (b) A sketch of three-dimensional connection of net Birkeland currents and ionospheric currents based on our computer simulation results for 1050 UT (from Chen et al. [1982]).

Fig. 7. Model electric-equipotential patterns for four universal times on July 29, 1977. The magnetospheric equatorial plane is shown, with the sun to the left. Displayed equipotentials are 6 kV apart. Corotation electric fields are not included in the display. The model sudden commencement occurred at 0300 UT. The symbol δ represents a positive infinitesimal, so the top two diagrams pertain to just before (diagram a) and just after the

sudden commencement (diagram b). Note that the sudden commencement disrupted shielding, which was then gradually reestablished (diagrams c and d) (from Wolf et al. [1982]).

Fig. 8. Birkeland current patterns, viewed from above the north pole. Regions where $|j_\parallel| > 0.01\ \mu A/m^2$ are shown. Dotted regions indicate upward current, solid black regions downward current. (a) Observational summary for Iijima and Potemra [1978], displayed here for reference. (b) Theoretical pattern for 0300-δ UT, just before sudden commencement. (c) Theoretical pattern for 0100 UT, half an hour after SSC. (d) Theoretical pattern for 0120 UT, 50 minutes past SSC. (e) Theoretical pattern for 0300 UT. Note the temporary disruption of the pattern by the sudden commencement (from Wolf et al. [1982]).

Fig. 9. Disruption of shielding and region 2 currents during a sudden magnetospheric compression. Curves with arrows indicate gradient/curvature drift currents, which flow along curves of constant flux tube volume $\int ds/B$. The top diagram shows the pre-compression situation, with positive charges on the dusk side inner edge, and negative charges on the dawnside inner edge; this tends to shield the low L region from the convection electric field. The shielding is disrupted in the sudden compression (bottom diagram) (from Wolf et al. [1982]).

Fig. 10. Computed inner edge for one species of plasma-sheet electrons, for five times during the early main phase. These electrons have energy invariant $\lambda = 3900\ eV\ (R_E/\gamma)^{2/3}$, which corresponds to approximately 8 keV at L = 10, 32 keV at L = 6. Note the eastward-drifting tongue of gradient/curvature drifting particles (from Wolf et al. [1982]).

Fig. 11. Comparison of observed and predicted Dst index. The zero level of the theoretical curve was chosen arbitrarily. The model sudden commencement occurred at 0030 UT, and a partial re-expansion occurred at 0430 UT (observed Dst values were provided by M. Sugiura through the National Space Science Data Center) (from Wolf et al. [1982]).

Fig. 12. Comparison of ionospheric currents computed from theoretical magnetograms by the KRM algorithm and the ionospheric currents used to compute the theoretical magnetograms (from Wolf and Kamide [1983]).

Fig. 13. Comparison of horizontal $\underset{\sim}{E} \times \underset{\sim}{B}$-drift velocities computed from the Rice source-model (left side) and from theoretical magnetograms using the KRM algorithm (right side) (from Wolf and Kamide [1983]).

Fig. 14. Comparison of equipotentials computed from the Rice source-model (left side) and from theoretical magnetograms using the KRM algorithm (right side). Plotted equipotentials are 5 kV apart in the top diagrams, 7 kV apart in the bottom diagrams. Curve H is the boundary of the polar cap, i.e., the region of zero conductivity in the RCM (from Wolf and Kamide [1983]).

Fig. 15. Global pattern of Birkeland currents, for UT = 1040 (from Karty et al. [1983]).

Fig. 16. Substorm currents caused by magnetotail current interruption. Top panel: The sun is to the left. The view is the noon-midnight meridian plane. Bottom panel: The sun is to the left. The view is looking down on the north geomagnetic pole and equatorial plane. Field-aligned currents and remnants of the "old" neutral current sheet are shown (from Boström [1974]).

Fig. 17. Key input parameters for simulation of the March 22, 1979 magnetic storm. The three panels show polar-boundary potential drop (from IMF data), AE index (used in conductivity model), and magnetopause standoff distances (from solar-wind ρV^2).

Fig. 18. Comparison of predicted and observed ionospheric plasma flow at Saint-Santin. Top panel shows north-south flow, while bottom panel shows east-west flow, Saint-Santin.

Fig. 19. Effect of magnetic-field compression on ring-current energy and Joule heating. Diagram (a) shows ring current energy and Joule heating for our nominal run (run D), which included a "realistic" magnetic field model, including a compression at the time of the sudden commencement. Diagram (b) shows the same parameters for run J, in which there was no compression. (The pre-storm, uncompressed magnetic-field model was used throughout the event.)

Fig. 20. Effect of the plasma-sheet boundary condition on ring-current injection. The two plots curves pertain to run D ("nominal") and run F ("half p"), and run H ("high T").

Fig. 21. Effects of the plasma-sheet boundary condition on Joule heating. The labels "nominal," "half p," and "high T" refer to runs D, F, and H, respectively.

Fig. 22. Effect of conductivity on ring-current energy. The curve labeled "doubled Σ" gives results for run L. The unlabeled curve is for run J. Run L is the same as run J, except that the ionospheric conductivity was doubled everywhere in the ionosphere.

Fig. 23. Ring current energy, as estimated from observed Dst.

Fig. 24. Three dimensional plot of the differential number flux for both protons and oxygen on March 22, 1979, as observed by SCATHA. The data have been plotted on a linear scale as indicated by the labels on the leftmost axis in each plot. Note that the flux scales are different for each species. The spectra are shown as a function of energy and universal time (UT). In addition, the local time (LT) and L shell (L) are given (from Strangeway and Johnson [1983]).

Fig. 25. Observed ion arrival times at SCATHA on March 22, 1979. Thin lines correspond to 90° pitch angle particles with thick lines corresponding to 30° ± 15° particles. Mass species are as indicated by the legend in the uper right corner of the figure. As a guide to the uncertainty in the measurements, the energy channel numbers corresponding to the energies are also given (from Strangeway and Johnson [1983]).

Fig. 26. Computed plasma-sheet inner edges as functions of time for our nominal run (run D). All the particles started on a 10 R_E circle at 0400 UT (4.33 hr before the SSC). The small circle represents the position of the SCATHA spacecraft. (a) Inner edge for equatorially mirroring particles with $\mu = 0$; (b) $\mu = 65$ eV/γ ($\approx$ 10 keV at SCATHA); (c) $\mu = 130$ eV/γ ($\approx$ 20 keV at SCATHA); (d) $\mu = 260$ eV/γ ($\approx$ 40 keV at SCATHA).

Fig. 27. Same as Figure 26, but for run F, which had plasma-sheet particle densities decreased a factor of 2.

Fig. 28. Same as Figure 26b, but for run H, which had plasma-sheet temperature increased by a factor of 2.4.

Fig. 29. Same as Figure 26b, but for run J, which assumed no magnetospheric compression. The magnetic field model was held in its pre-storm configuration for all times.

Fig. 30. Same as Figure 29, but for run L, which involved doubled ionospheric conductivity.

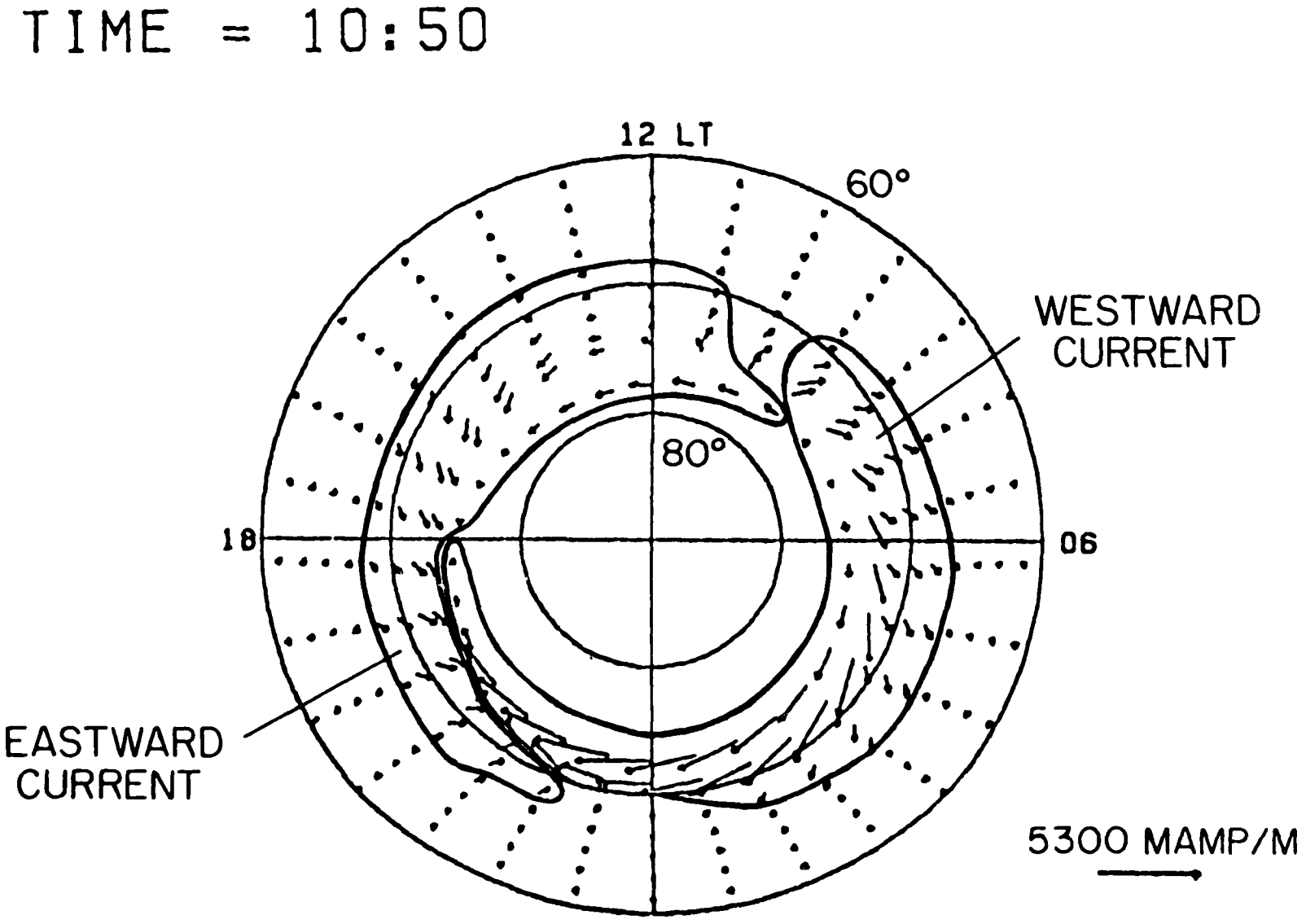
TIME = 10:50
12 LT
60°
80°
18
06
WESTWARD
CURRENT
EASTWARD
CURRENT
5300 MAMP/M

Figure 1

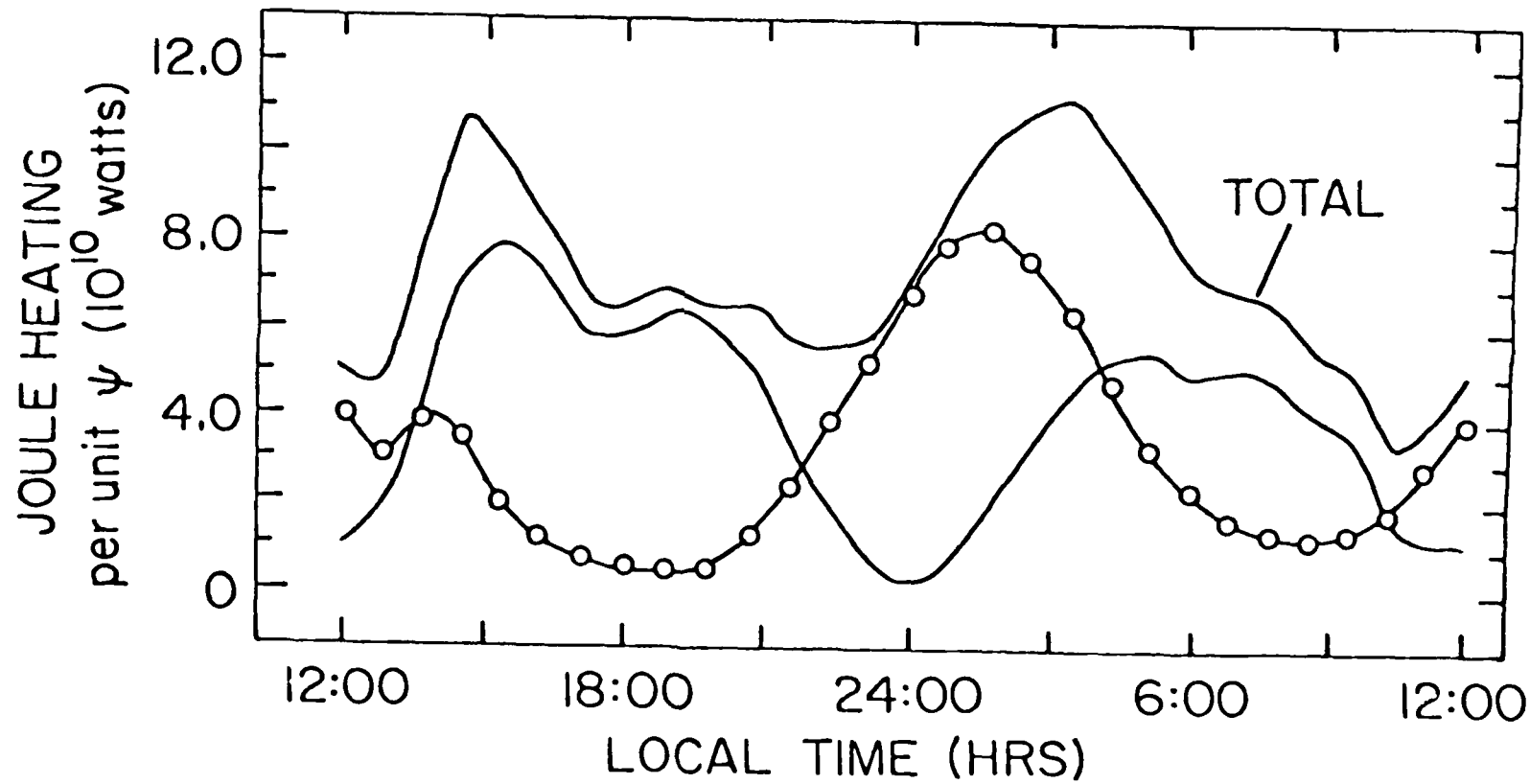
JOULE HEATING
per unit ψ (10^10 watts)
12.0
8.0
4.0
0
TOTAL
12:00
18:00
24:00
6:00
12:00
LOCAL TIME (HRS)

Figure 2

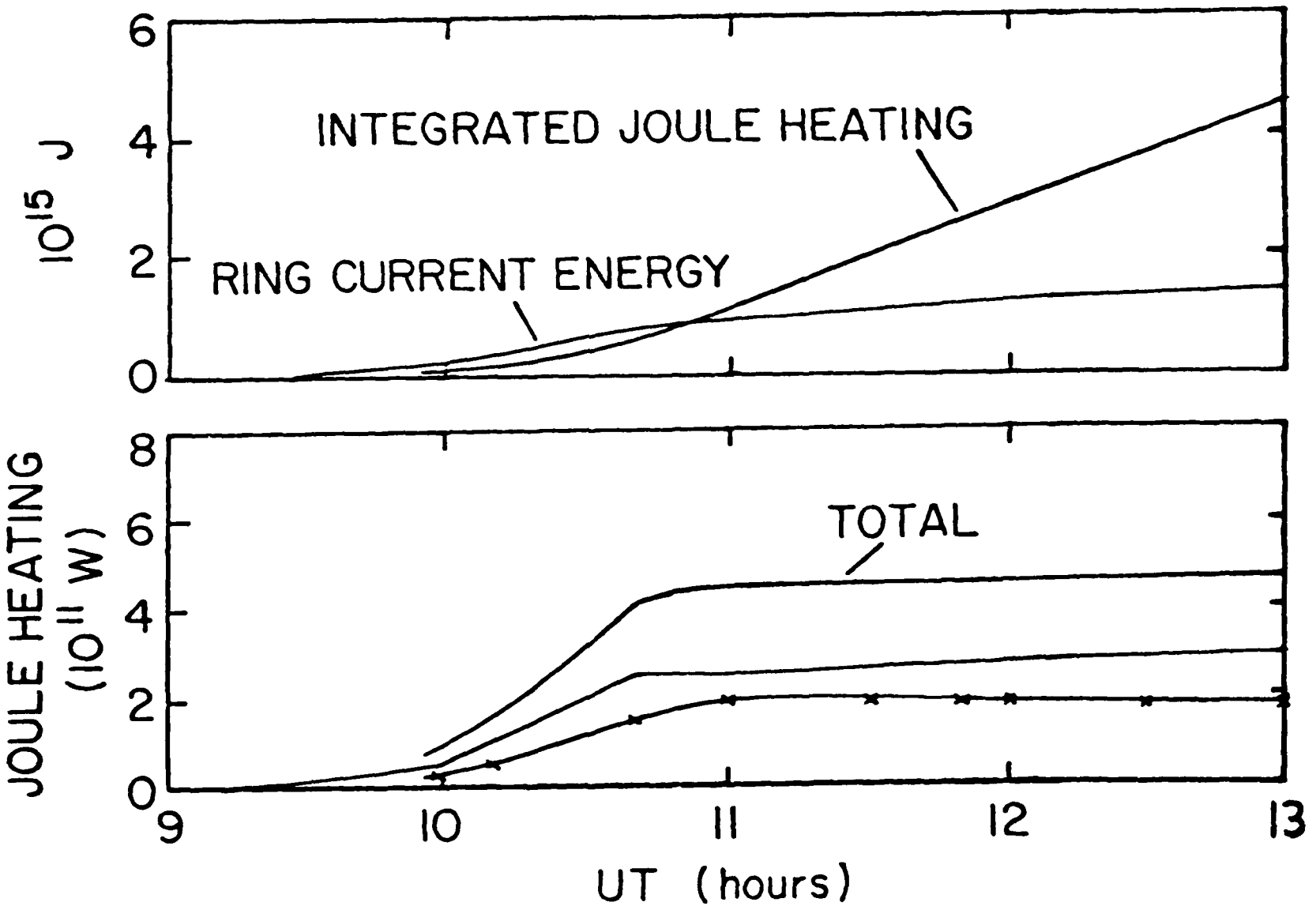
6
4
2
0
10^{15} J
INTEGRATED JOULE HEATING
RING CURRENT ENERGY
8
6
4
2
0
JOULE HEATING
(10^{11} W)
TOTAL
9
10
11
12
13
UT (hours)

Figure 3

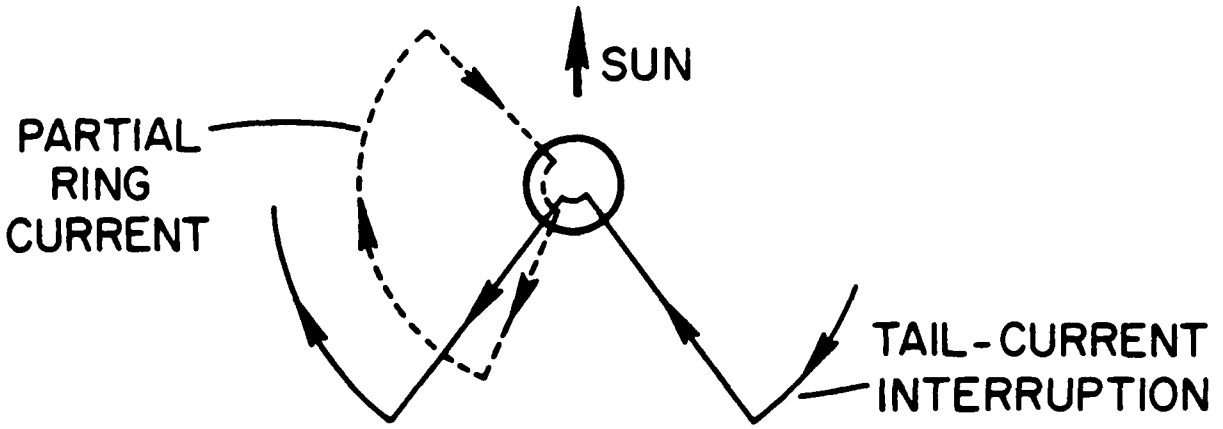
SUN
PARTIAL
RING
CURRENT
TAIL-CURRENT
INTERRUPTION

(a)

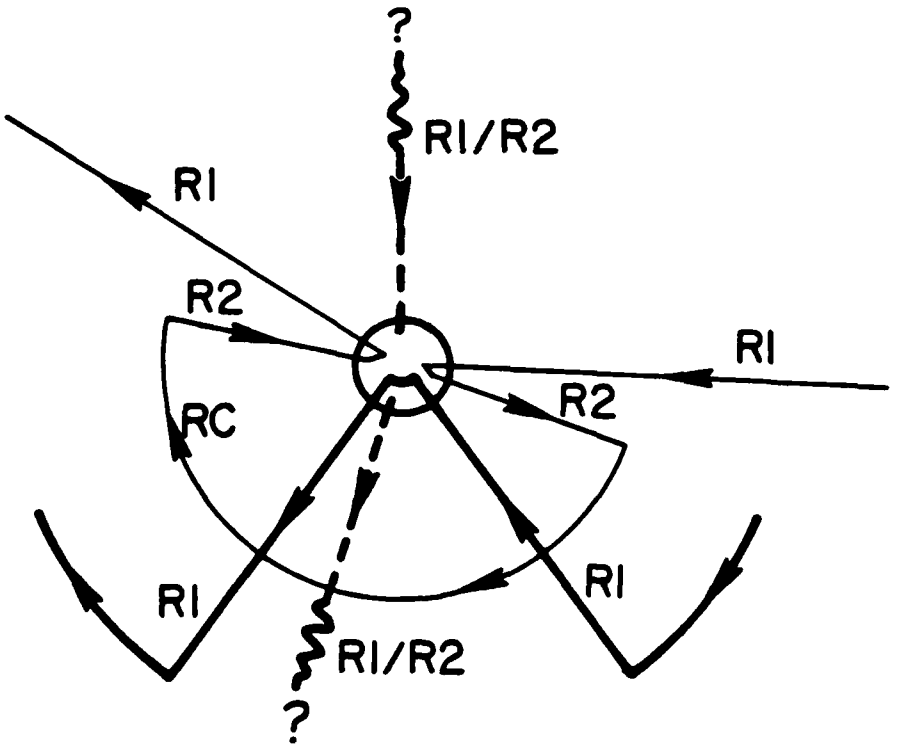
?
RI/R2
RI
R2
RI
RC
R2
RI
RI
RI/R2
?

(b)

Figure 4

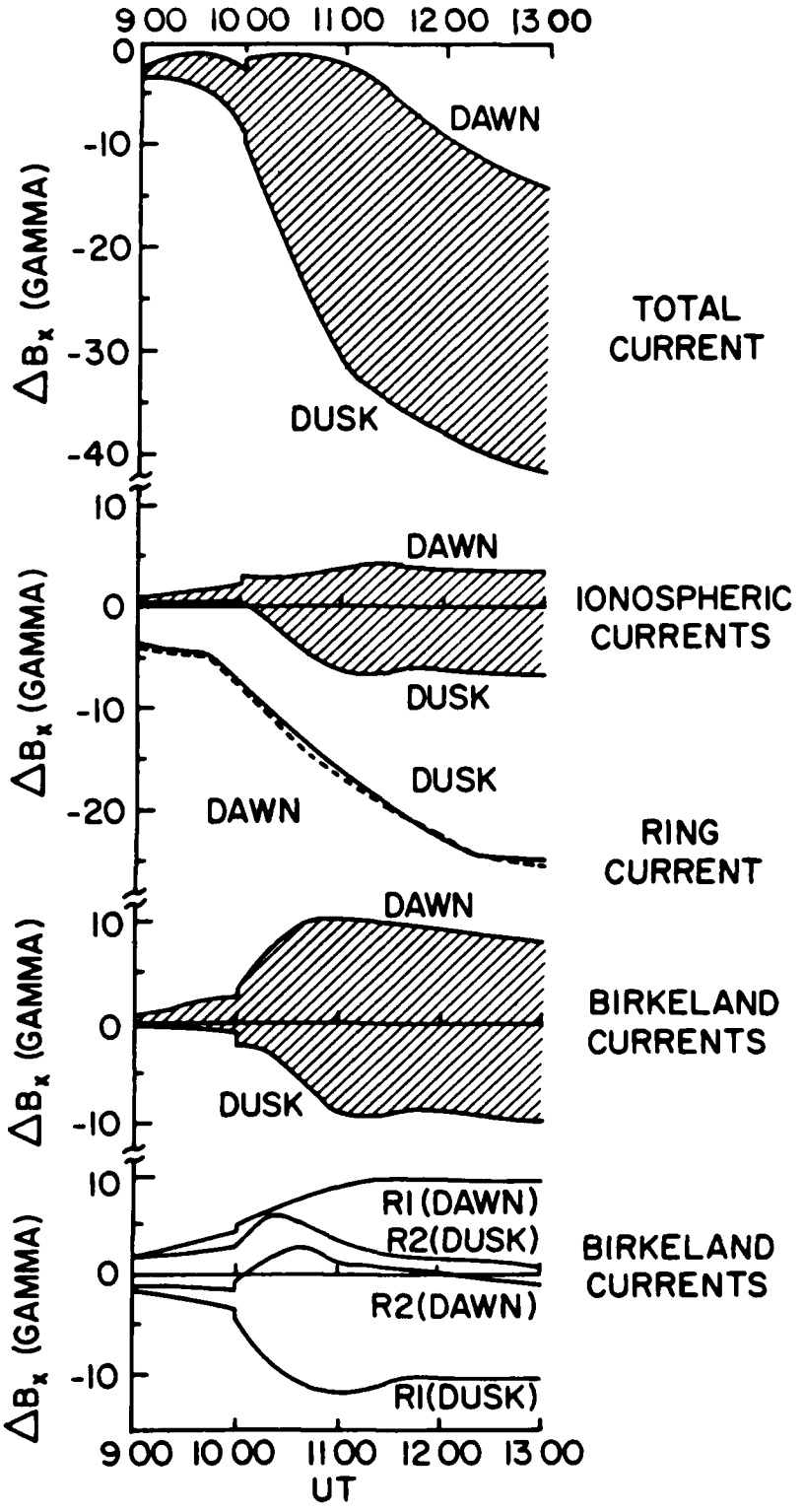
9 00 10 00 11 00 12 00 13 00
0
-10
-20
-30
-40
ΔBx (GAMMA)
DAWN
DUSK
TOTAL CURRENT
10
0
-10
-20
DAWN
DUSK
DUSK
DAWN
IONOSPHERIC CURRENTS
RING CURRENT
10
0
-10
DAWN
DUSK
BIRKELAND CURRENTS
10
0
-10
RI (DAWN)
R2(DUSK)
R2(DAWN)
RI(DUSK)
BIRKELAND CURRENTS
9 00 10 00 11 00 12 00 13 00
UT

Figure 5

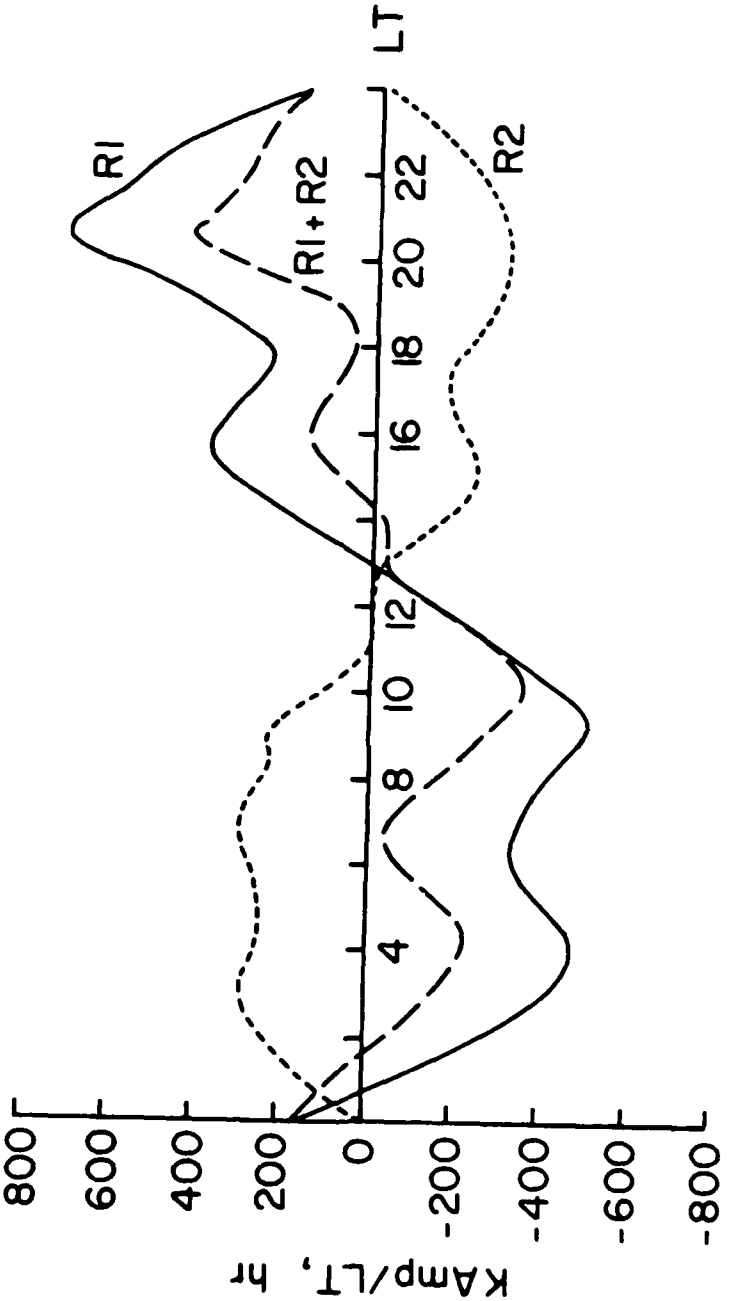
LT
R1
R1+R2
R2
0
4
8
10
12
16
18
20
22
800
600
400
200
0
-200
-400
-600
-800
kAmp/LT, hr

Figure 6a

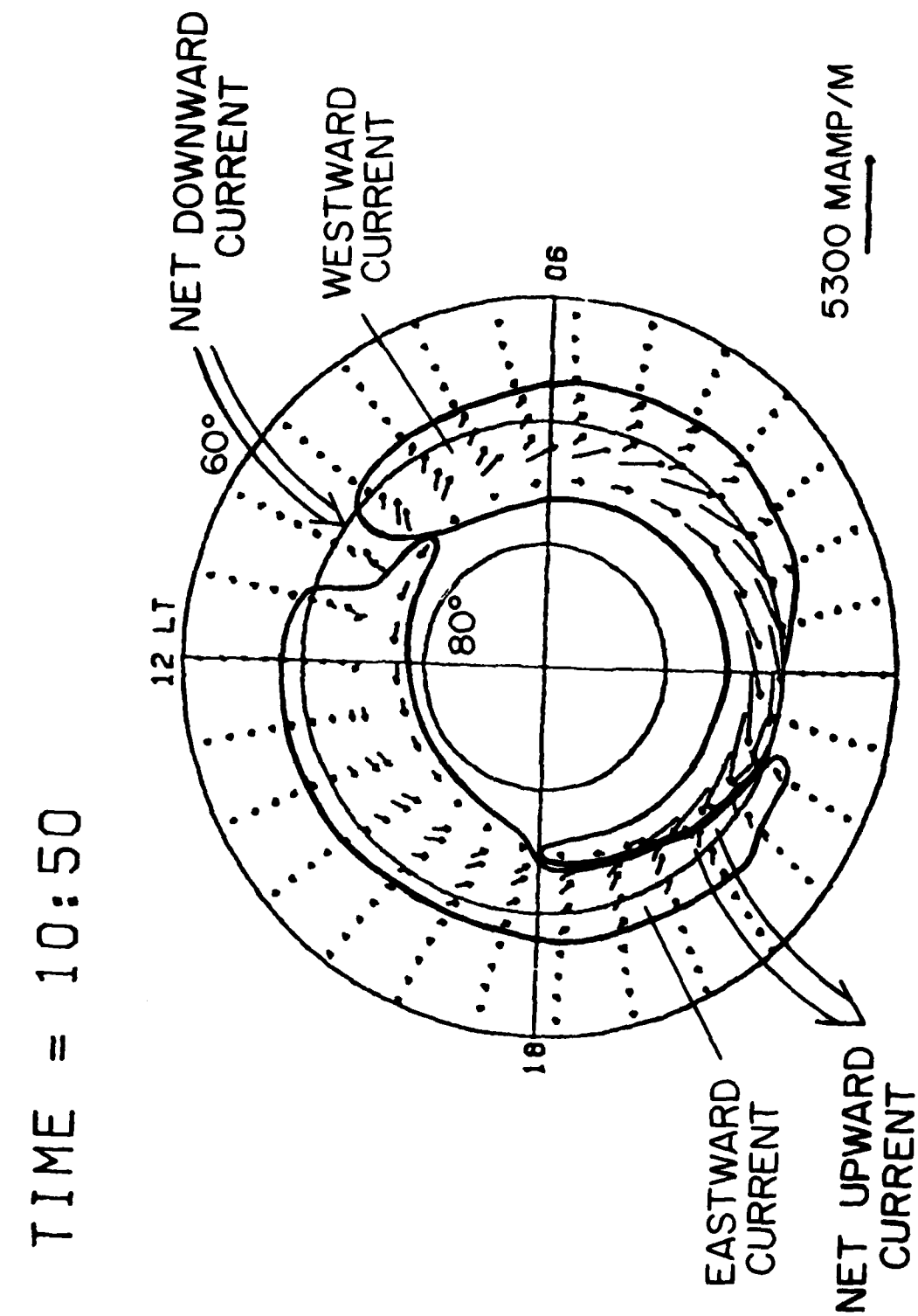
TIME = 10:50
NET DOWNWARD CURRENT
WESTWARD CURRENT
5300 MAMP/M
60°
80°
12 LT
06
18
EASTWARD CURRENT
NET UPWARD CURRENT

Figure 6b

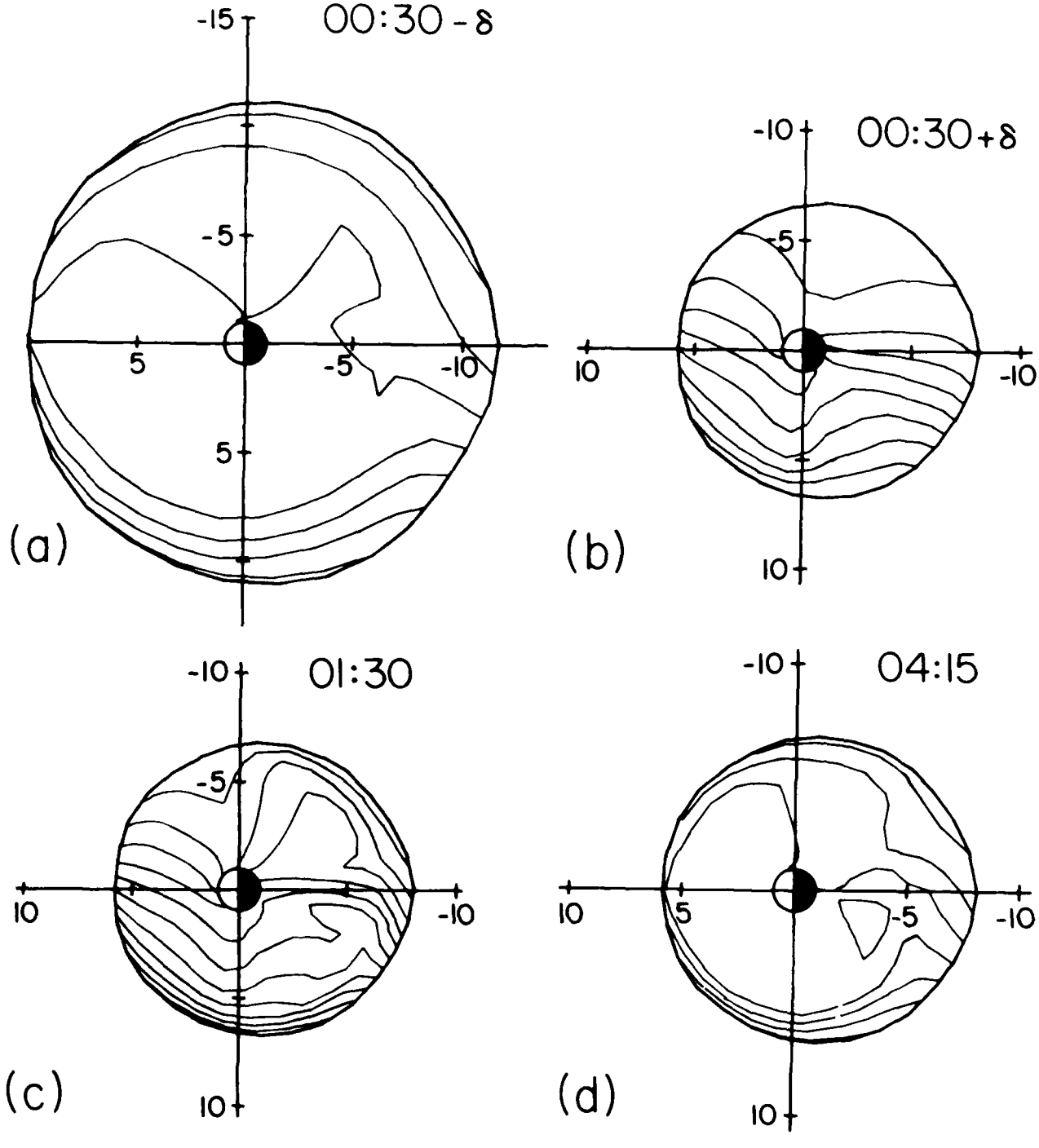
00:30 - δ
-15
-5
5
-5
-10
5
(a)
00:30 + δ
-10
-5
10
-10
10
(b)
01:30
-10
-5
10
-10
10
(c)
04:15
-10
10
5
-5
-10
10
(d)

Figure 7

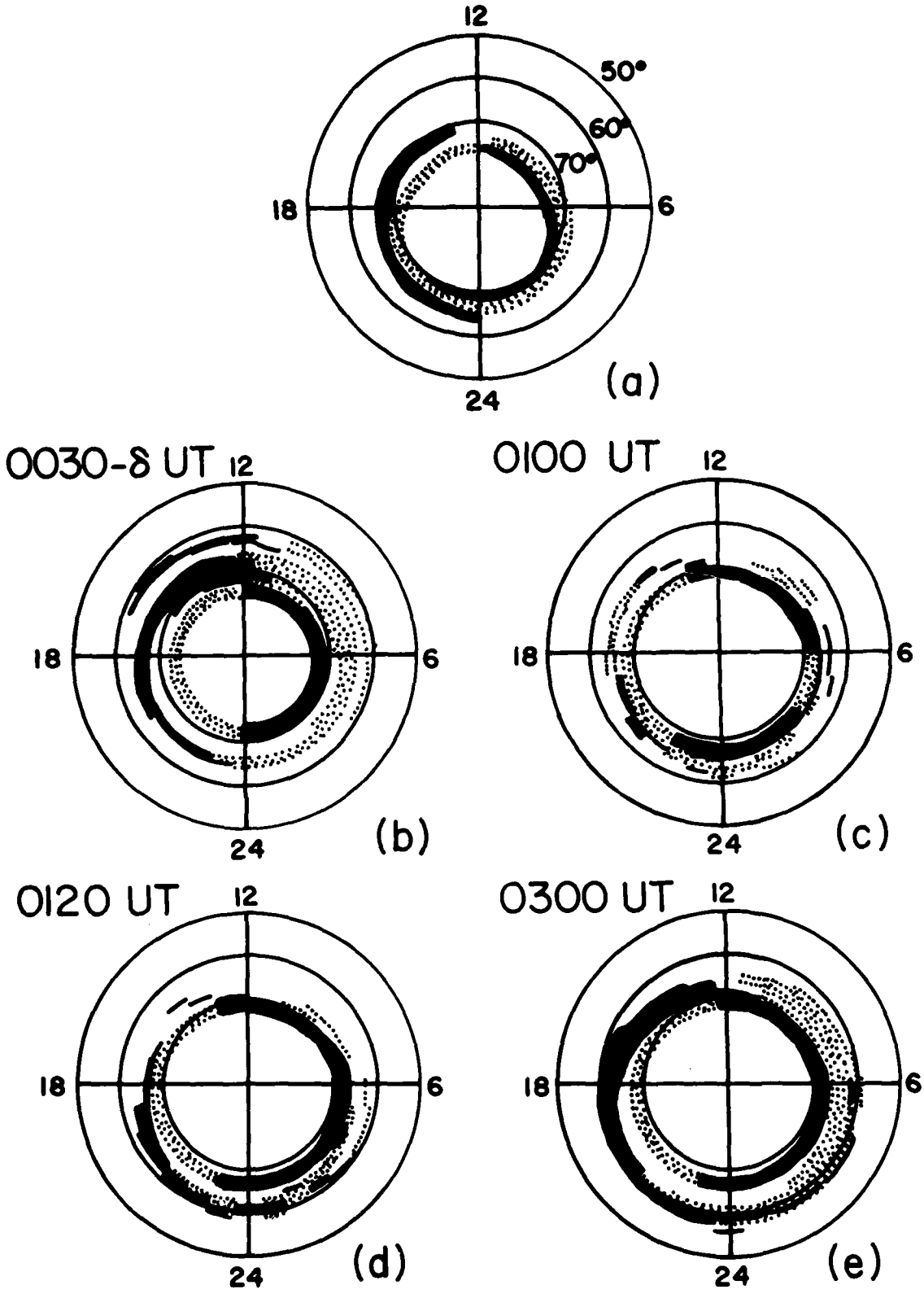
12
50°
60°
70°
18
6
24
(a)
0030-δ UT
12
18
6
24
(b)
0100 UT
12
18
6
24
(c)
0120 UT
12
18
6
24
(d)
0300 UT
12
18
6
24
(e)

Figure 8

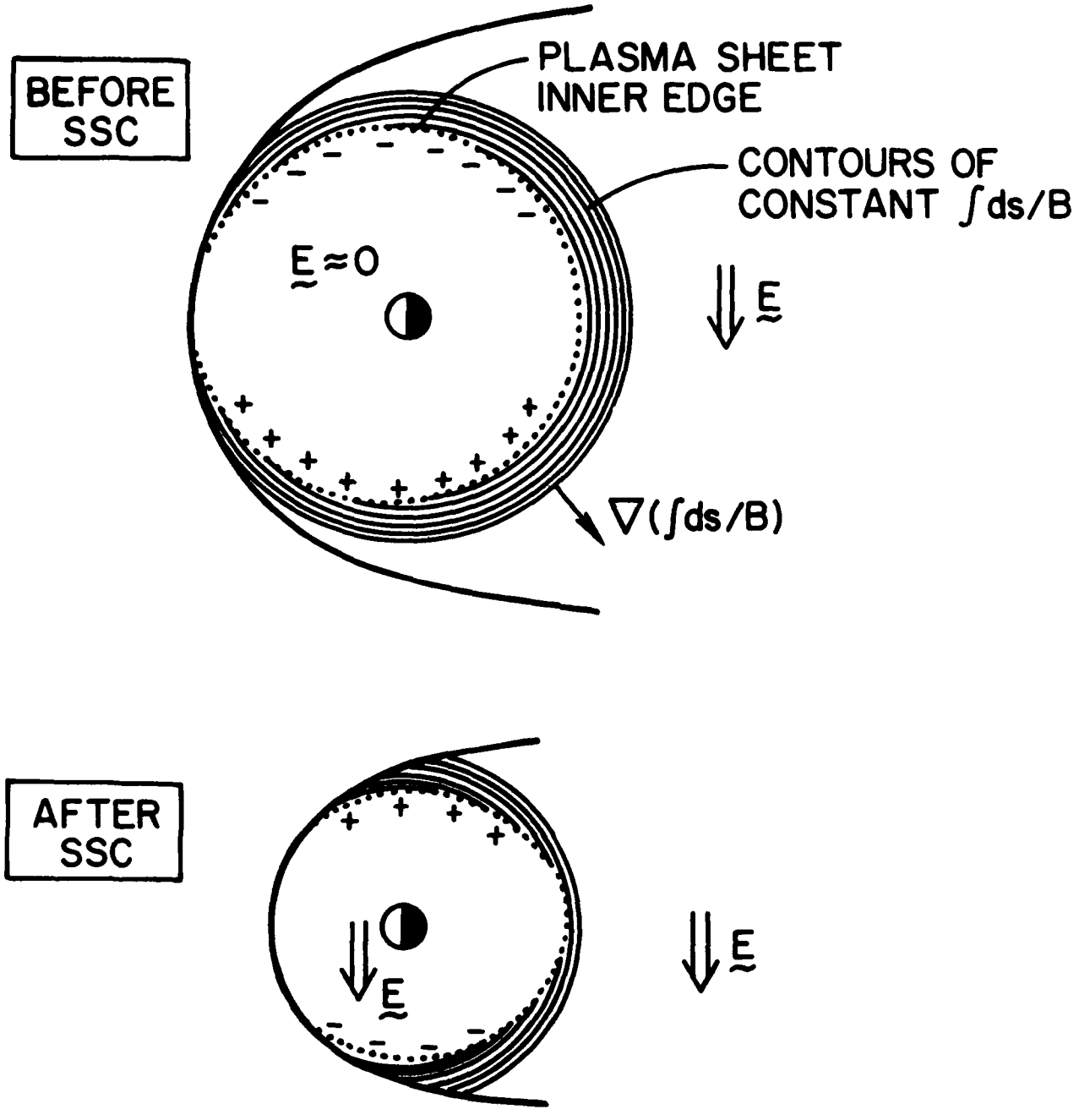
BEFORE SSC
PLASMA SHEET INNER EDGE
CONTOURS OF CONSTANT ∫ds/B
E ≈ 0
E
∇(∫ds/B)
AFTER SSC
E
E

Figure 9

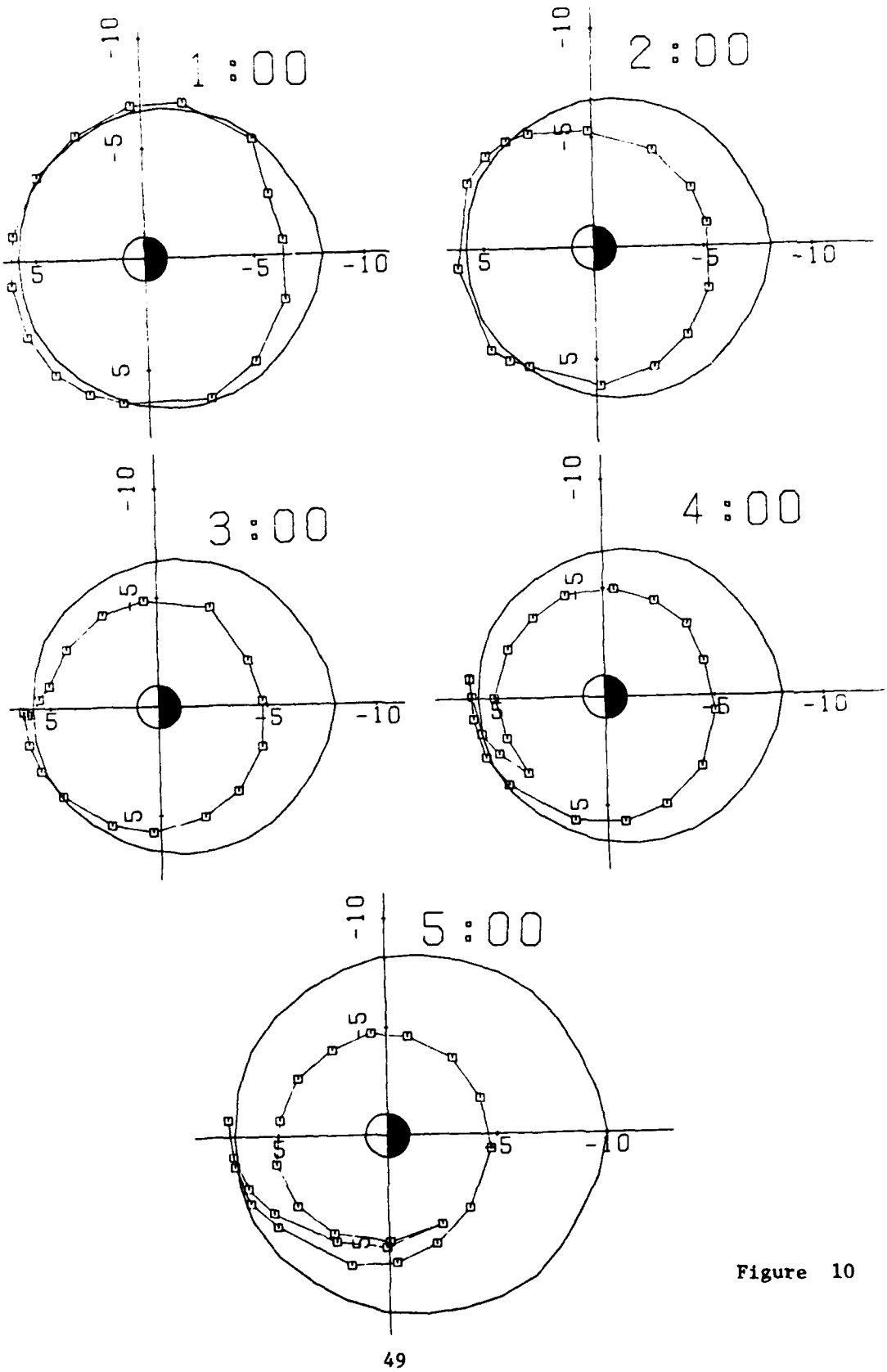

Figure 10

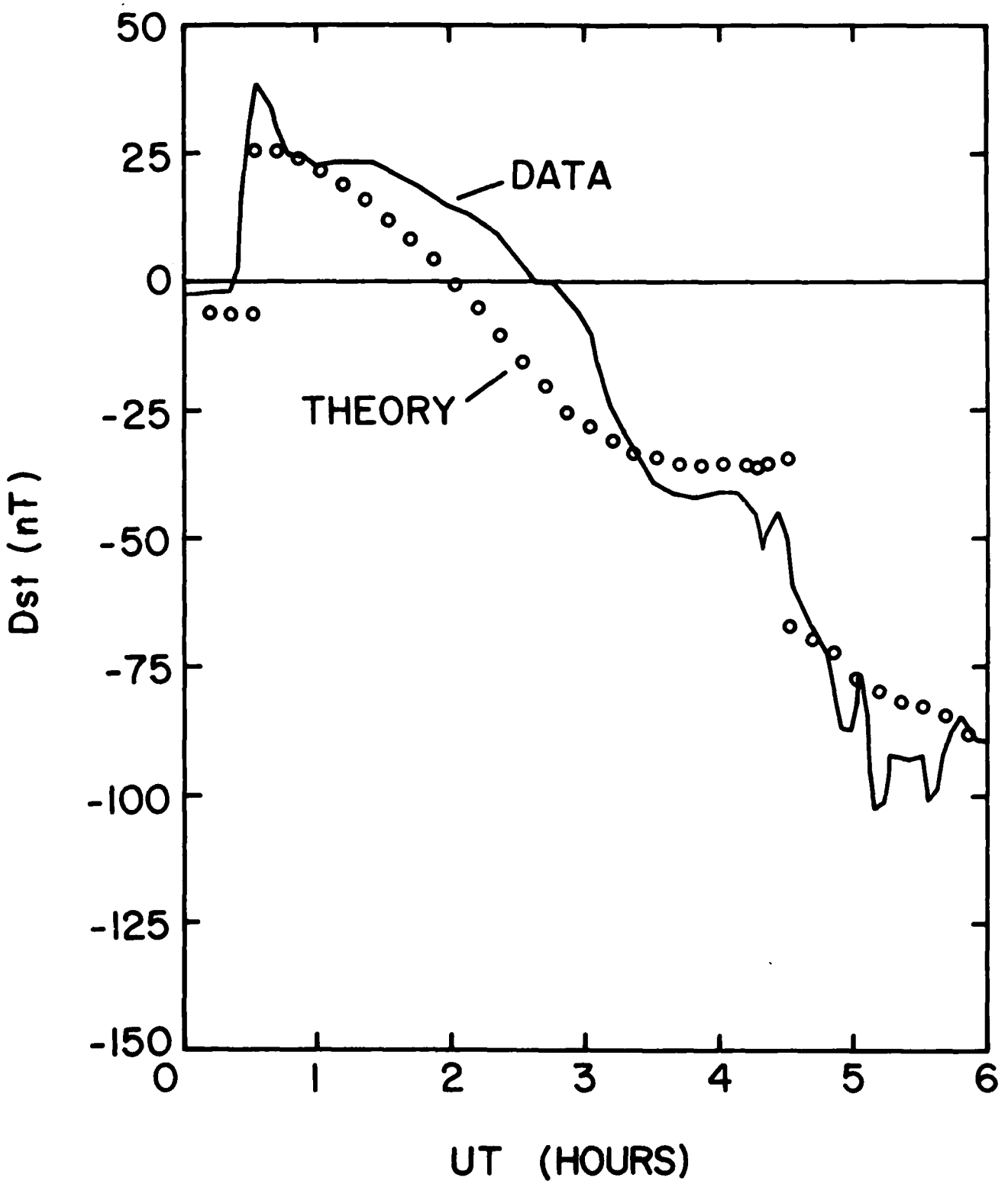

Figure 11

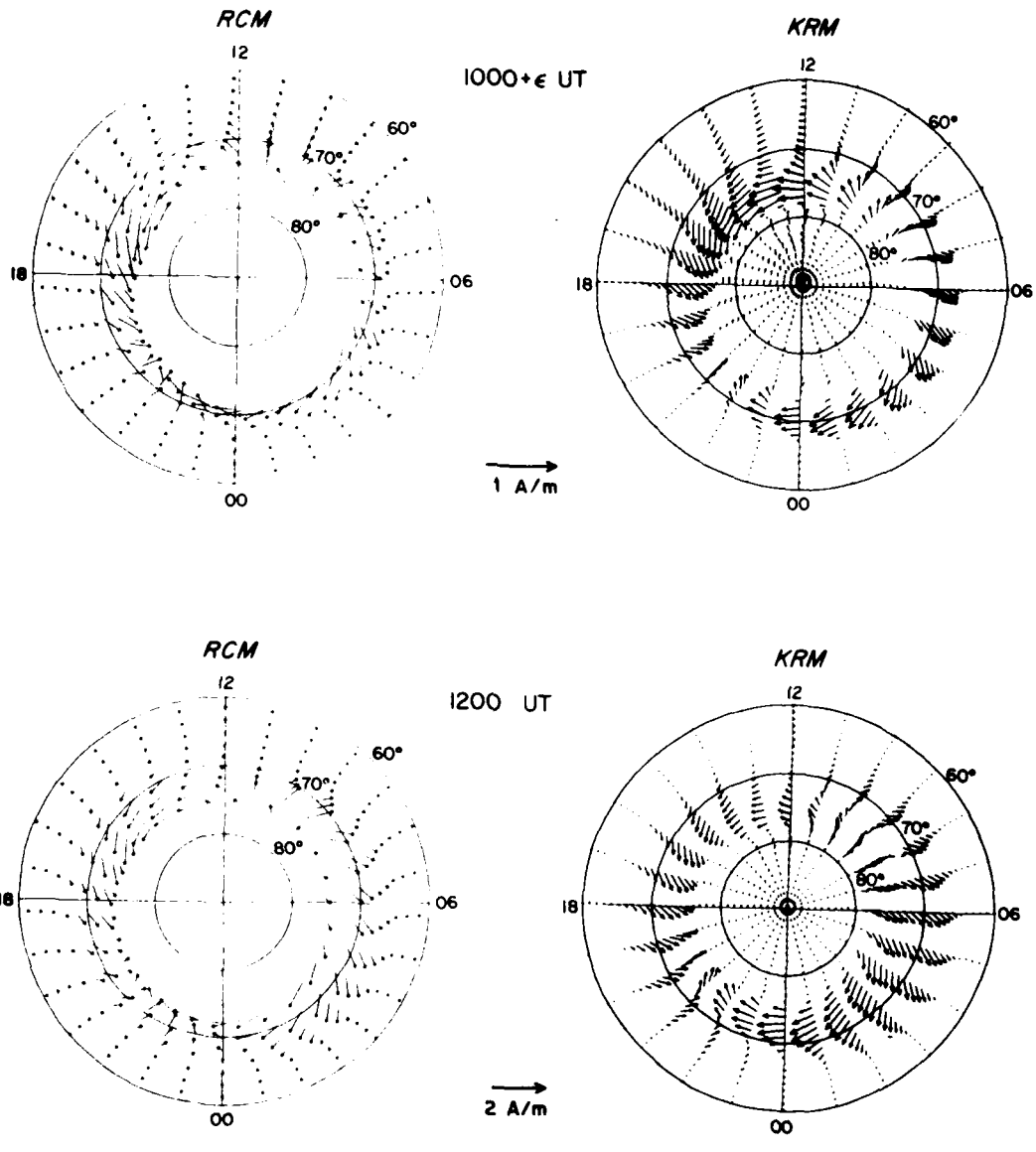
IONOSPHERIC CURRENT VECTORS
RCM
KRM
1000+ϵ UT
1200 UT
12
60°
70°
80°
18
06
00
1 A/m
2 A/m

Figure 12

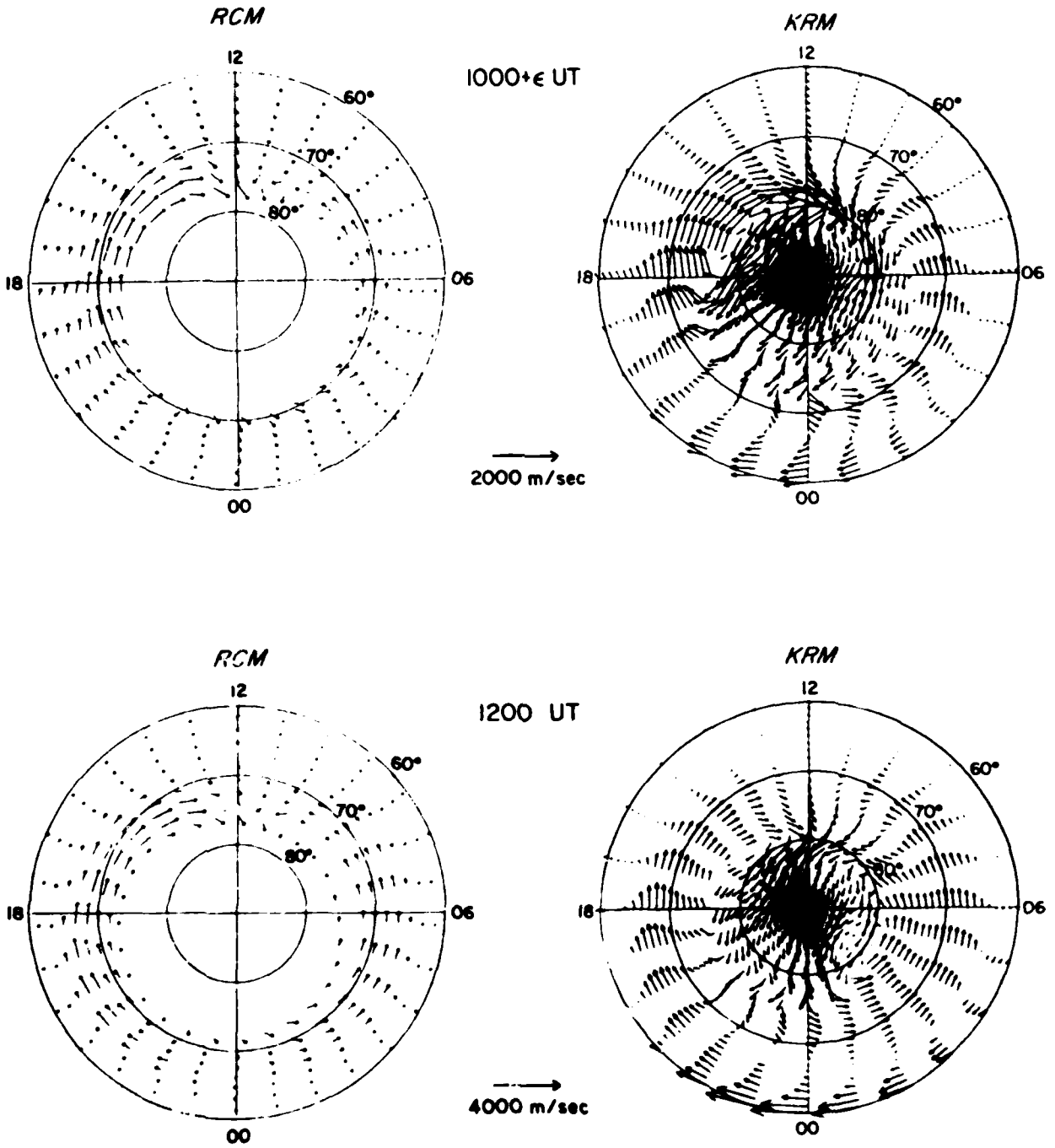
FLOW VELOCITIES
RCM
KRM
1000+ϵ UT
12
60°
70°
80°
18
06
00
2000 m/sec
RCM
KRM
1200 UT
12
60°
70°
80°
18
06
00
4000 m/sec

Figure 13

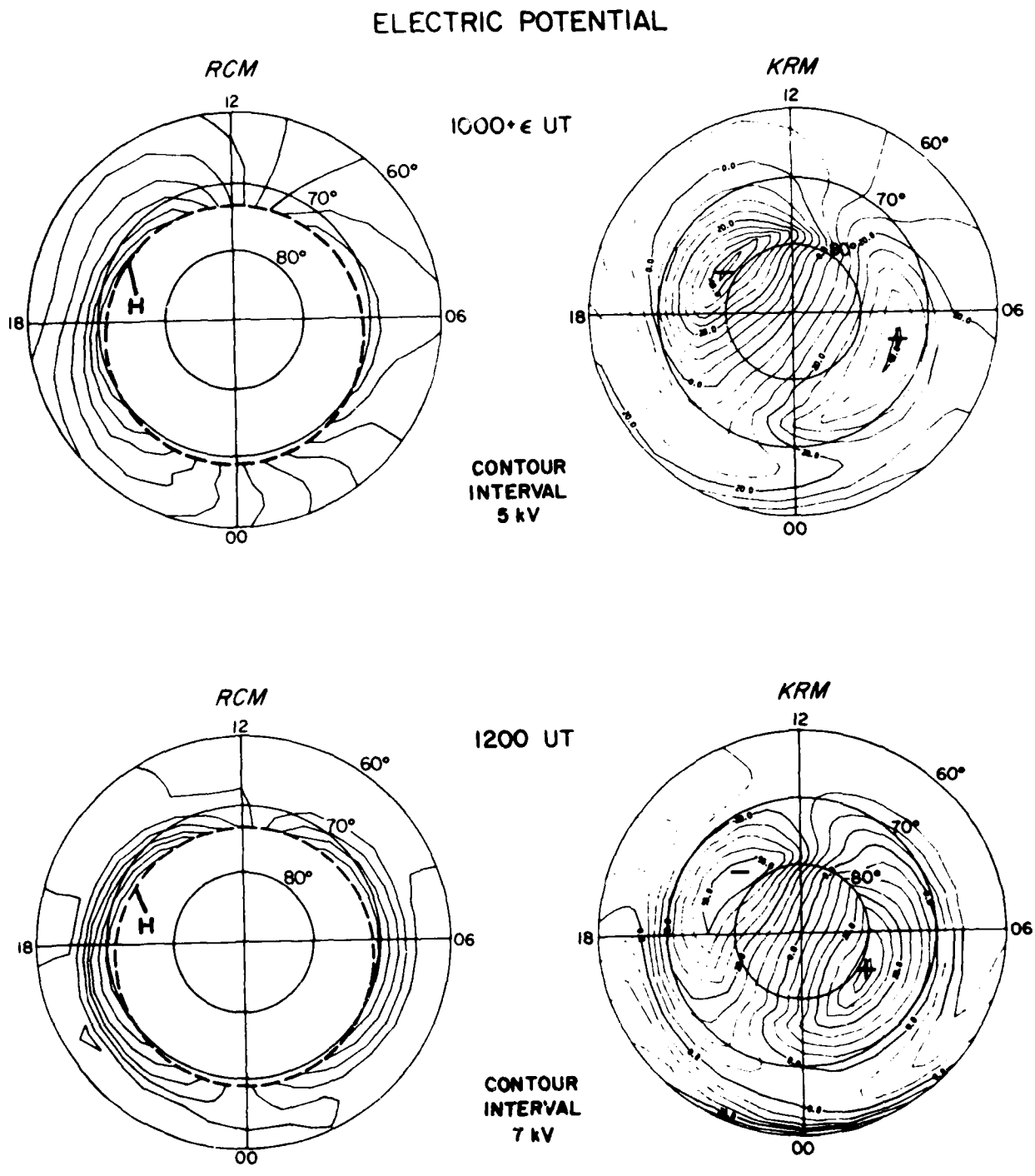
ELECTRIC POTENTIAL
RCM
KRM
1000+ϵ UT
1200 UT
12
60°
70°
80°
18
06
00
H
CONTOUR
INTERVAL
5 kV
CONTOUR
INTERVAL
7 kV

Figure 14

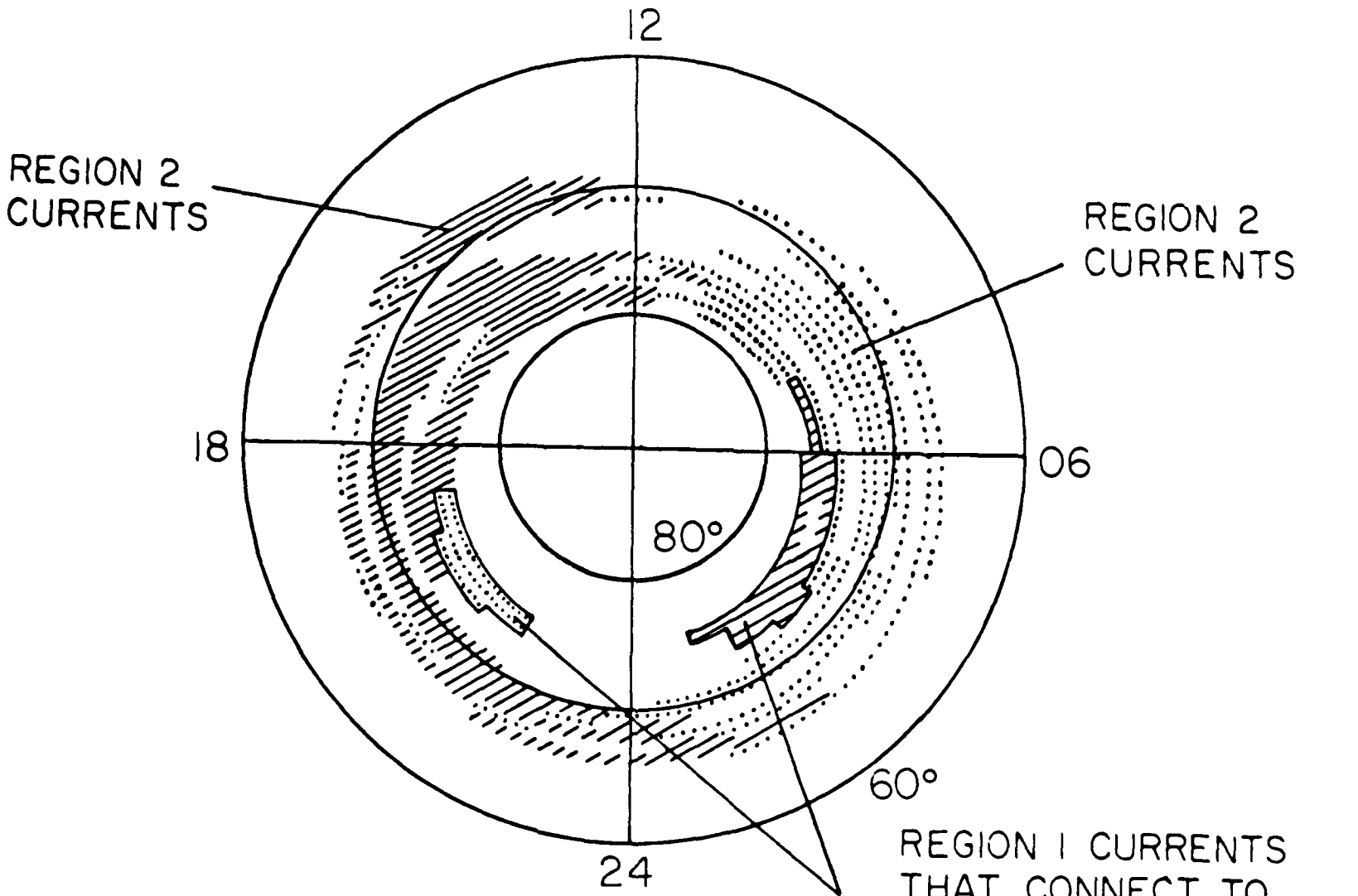
12
REGION 2
CURRENTS
REGION 2
CURRENTS
18
06
80°
60°
24
REGION I CURRENTS
THAT CONNECT TO
GRADIENT/CURVATURE-
DRIFT CURRENTS IN
THE PLASMA SHEET
CURRENTS INTO IONOSPHERE
CURRENTS OUT OF IONOSPHERE

Figure 15

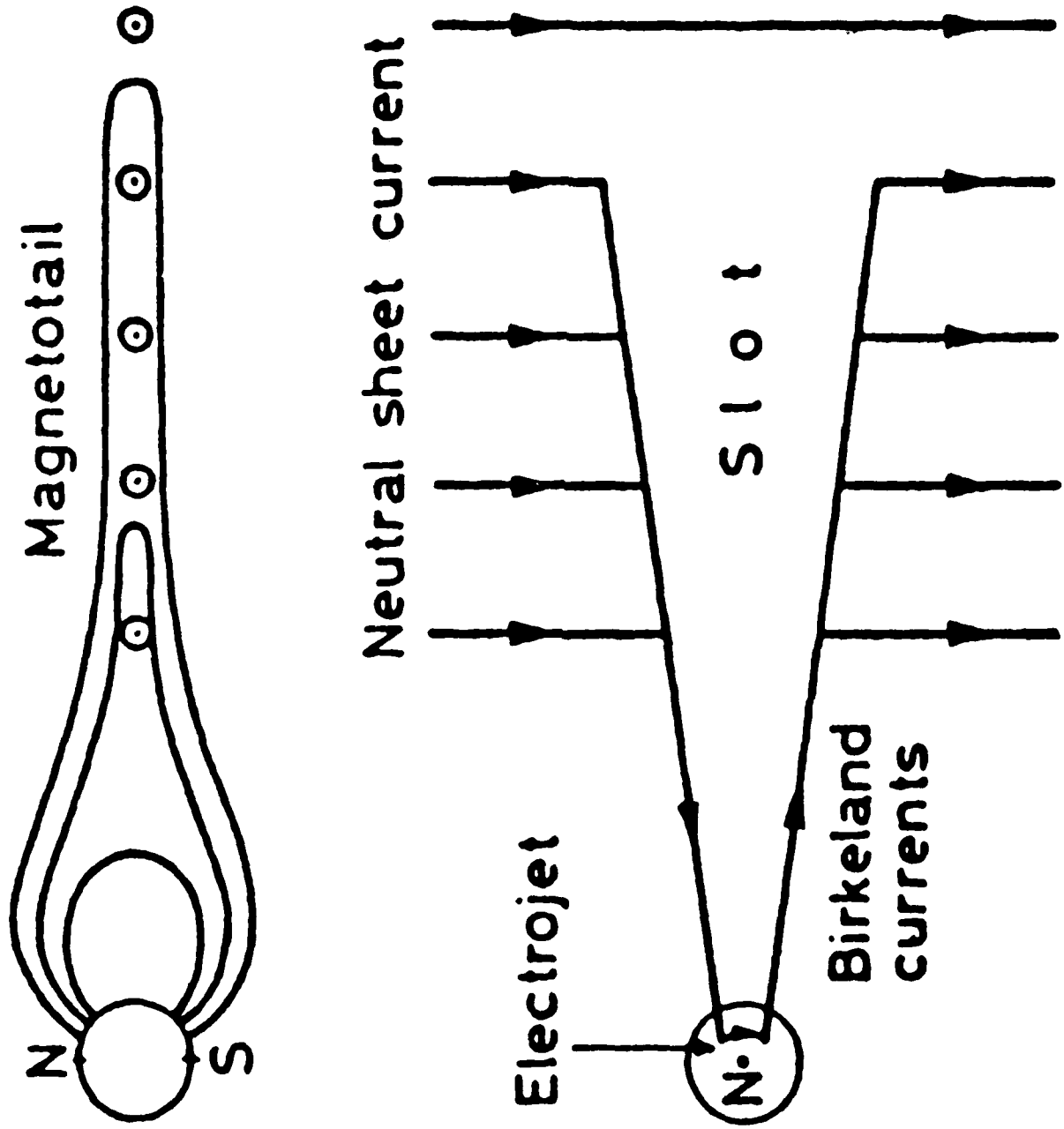
Magnetotail
N
S
Neutral sheet current
Slot
Electrojet
Birkeland currents

Figure 16

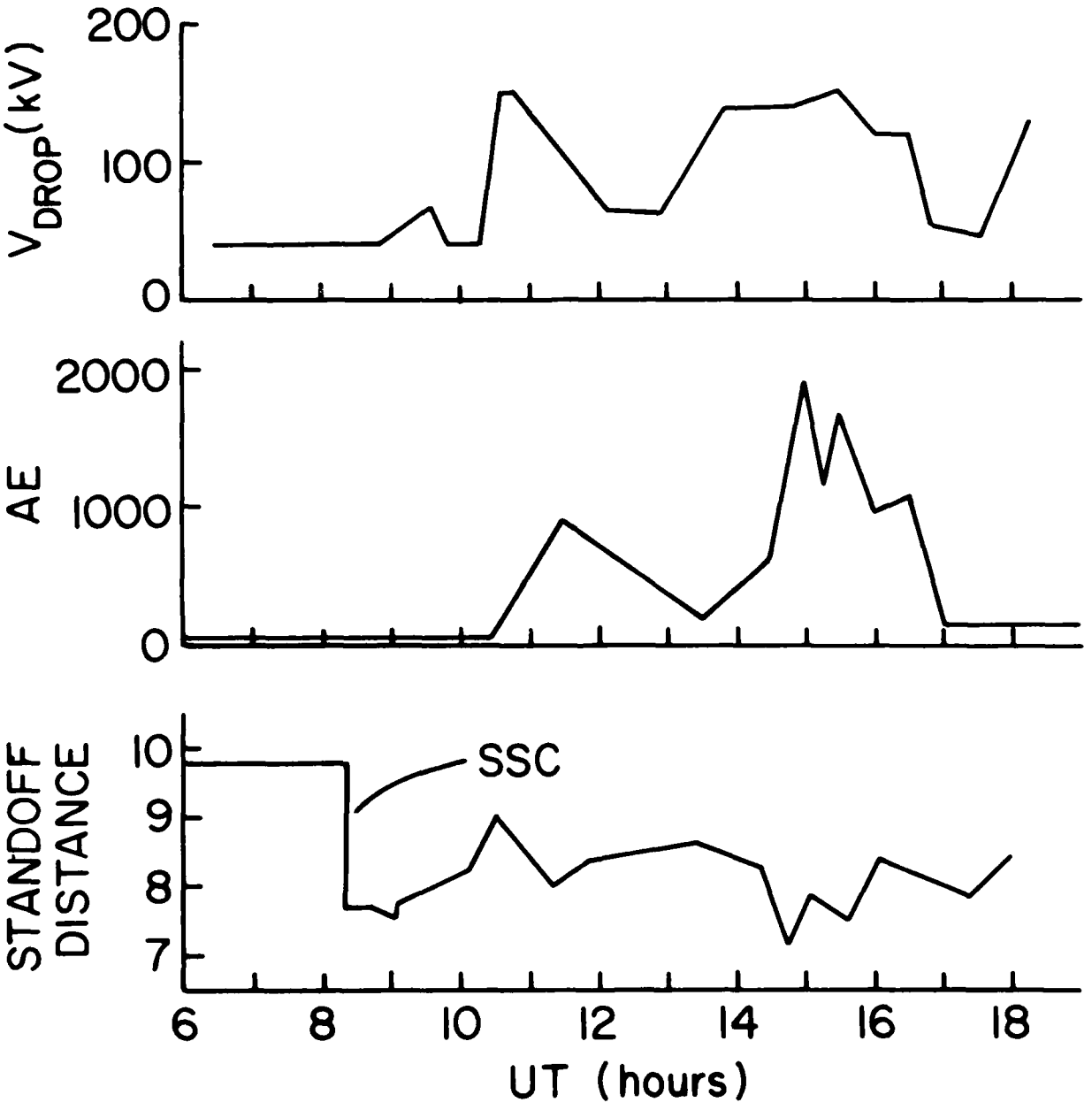
200
100
0
V_{DROP}(kV)
2000
1000
0
AE
10
9
8
7
STANDOFF DISTANCE
SSC
6
8
10
12
14
16
18
UT (hours)

Figure 17

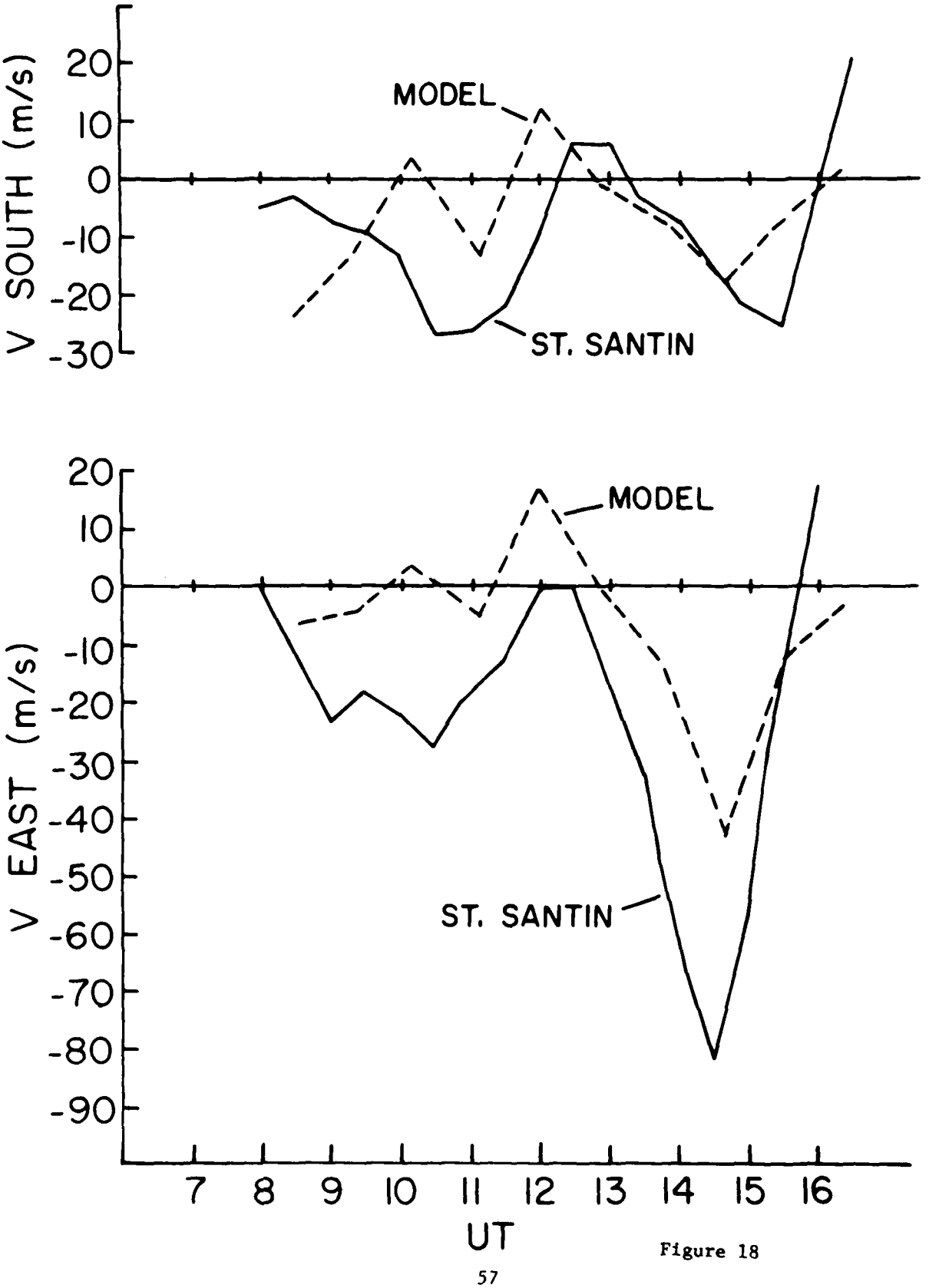
V SOUTH (m/s)
20
10
0
-10
-20
-30
MODEL
ST. SANTIN
V EAST (m/s)
20
10
0
-10
-20
-30
-40
-50
-60
-70
-80
-90
MODEL
ST. SANTIN
7
8
9
10
11
12
13
14
15
16
UT

Figure 18

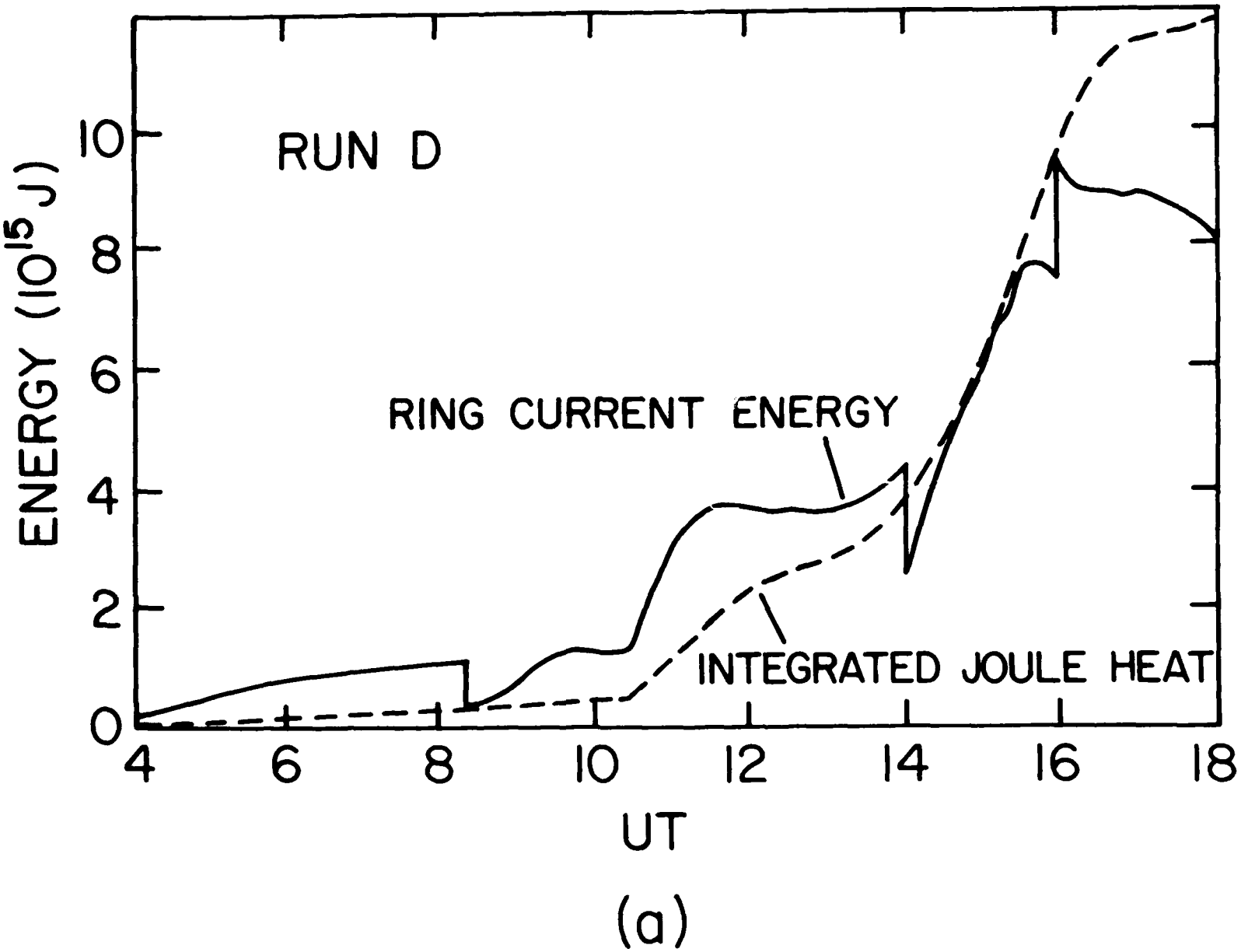
RUN D
ENERGY (10^{15} J)
RING CURRENT ENERGY
INTEGRATED JOULE HEAT
0
2
4
6
8
10
4
6
8
10
12
14
16
18
UT
(a)

Figure 19a

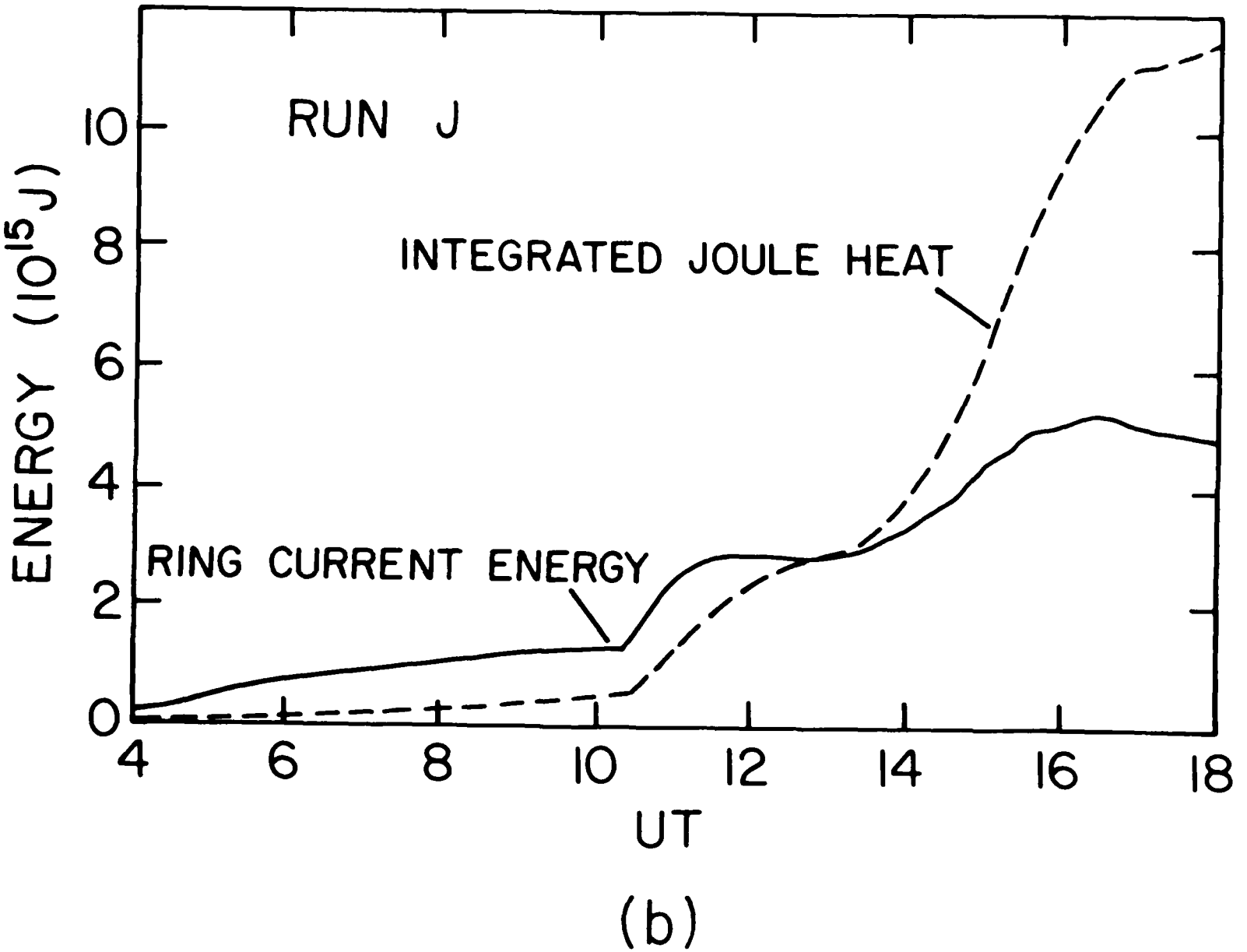
RUN J
INTEGRATED JOULE HEAT
RING CURRENT ENERGY
ENERGY (10^{15} J)
0
2
4
6
8
10
4
6
8
10
12
14
16
18
UT

(b)

Figure 19b

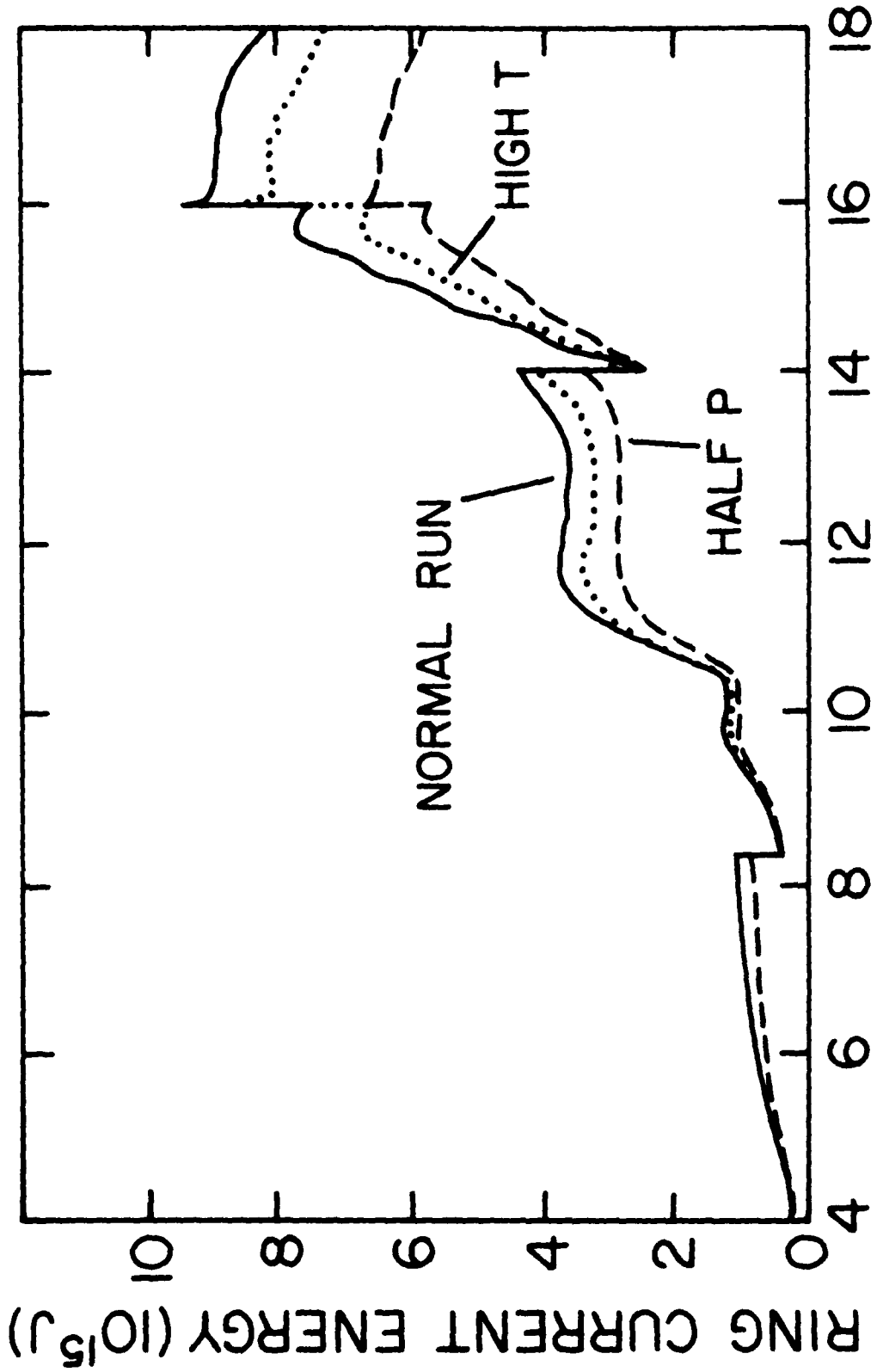
RING CURRENT ENERGY (10^{15} J)
0
2
4
6
8
10
4
6
8
10
12
14
16
18
UT
NORMAL RUN
HIGH T
HALF P

Figure 20

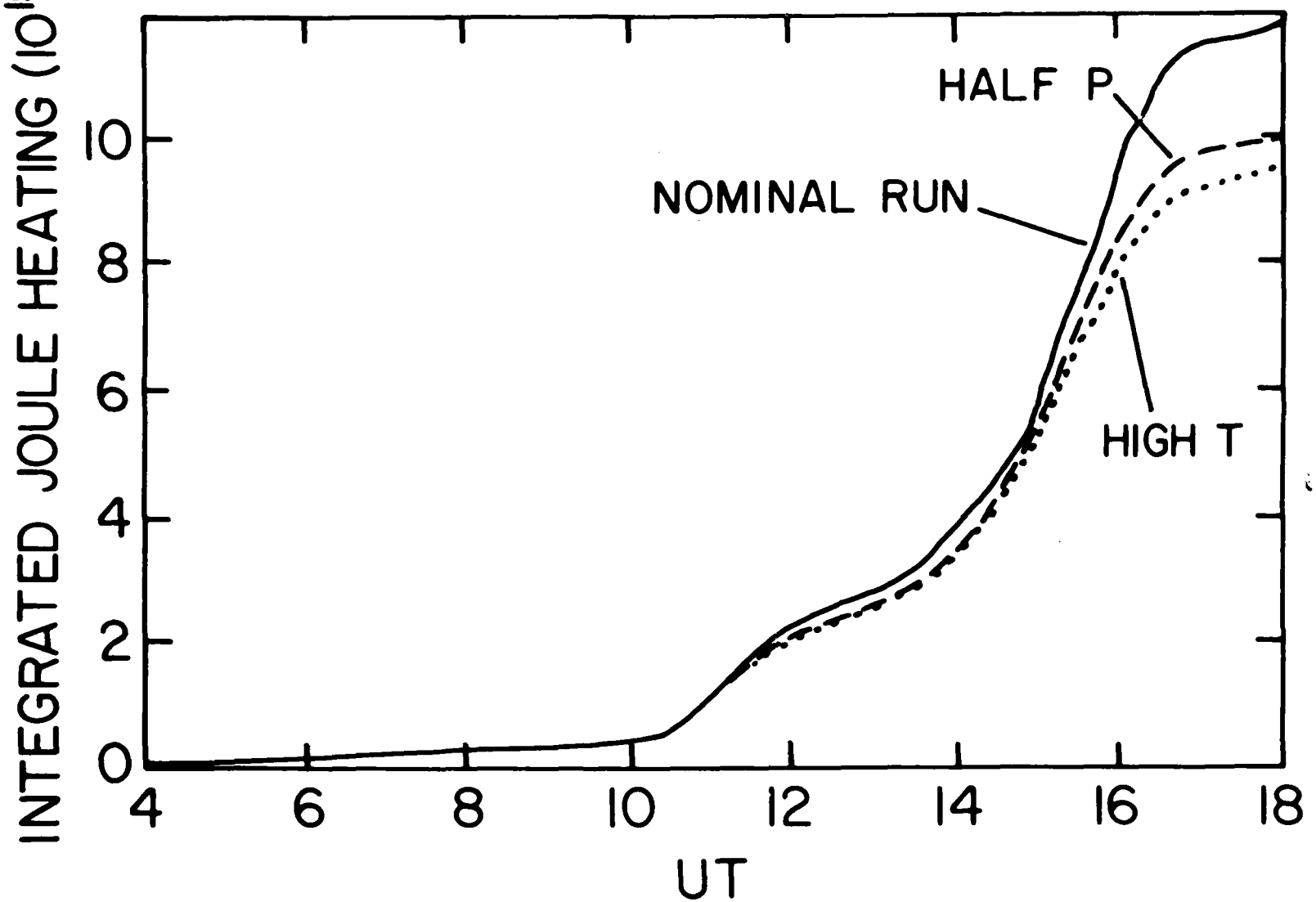
INTEGRATED JOULE HEATING (10^{15}J)
0
2
4
6
8
10
4
6
8
10
12
14
16
18
UT
HALF P
NOMINAL RUN
HIGH T

Figure 21

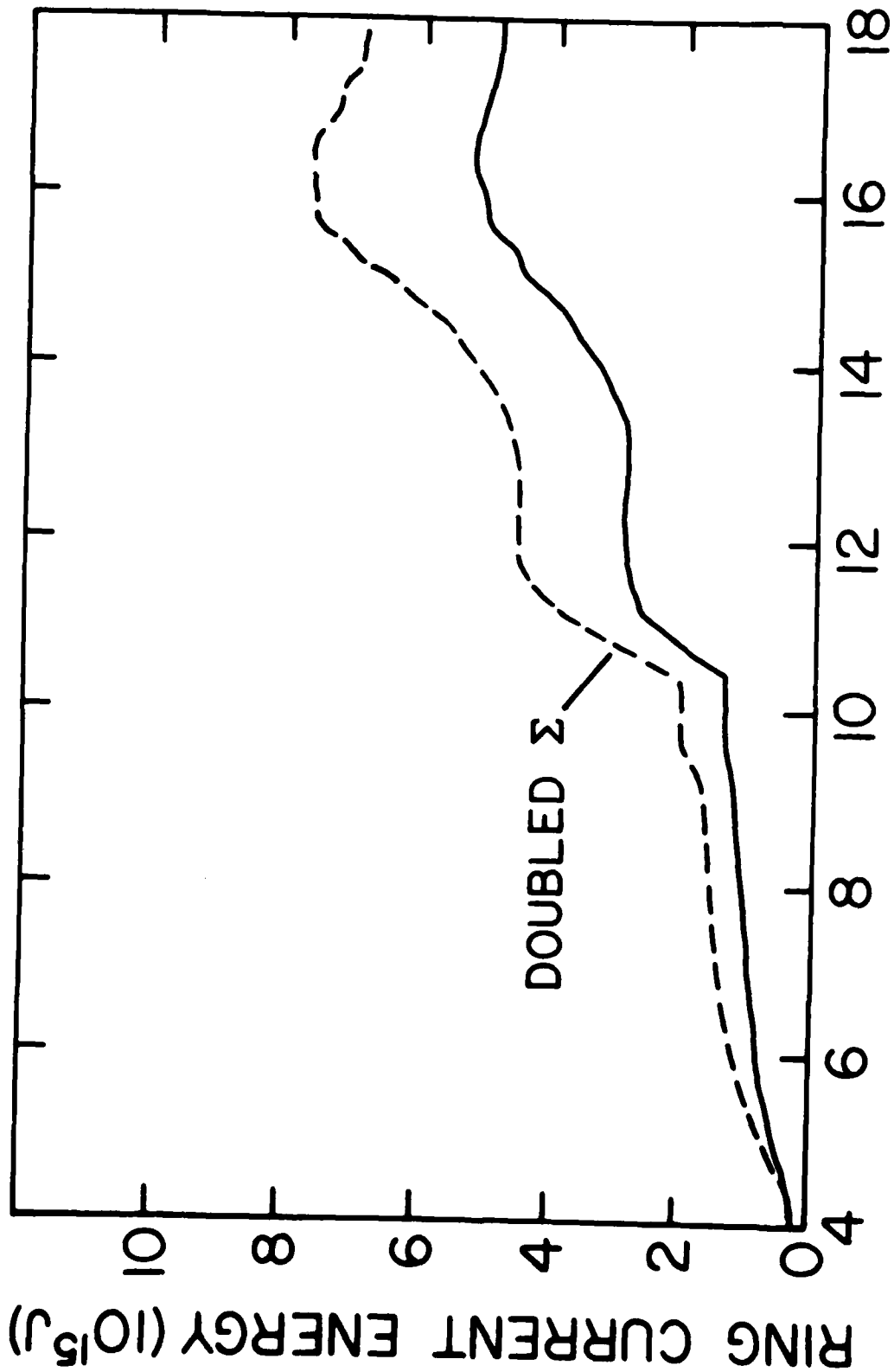
RING CURRENT ENERGY (10^{15} J)
0
2
4
6
8
10
4
6
8
10
12
14
16
18
UT
DOUBLED Σ

Figure 22

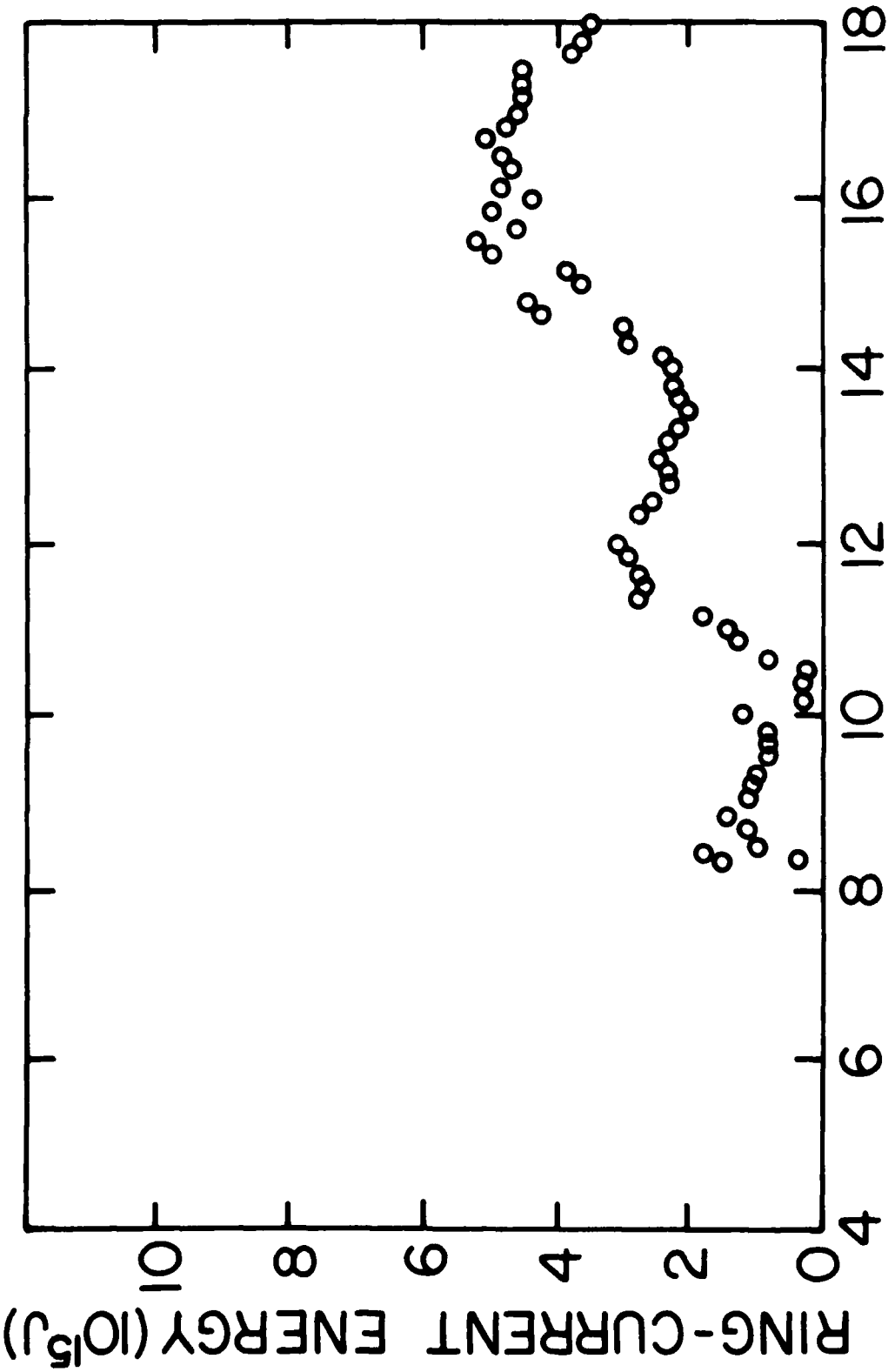

Figure 23

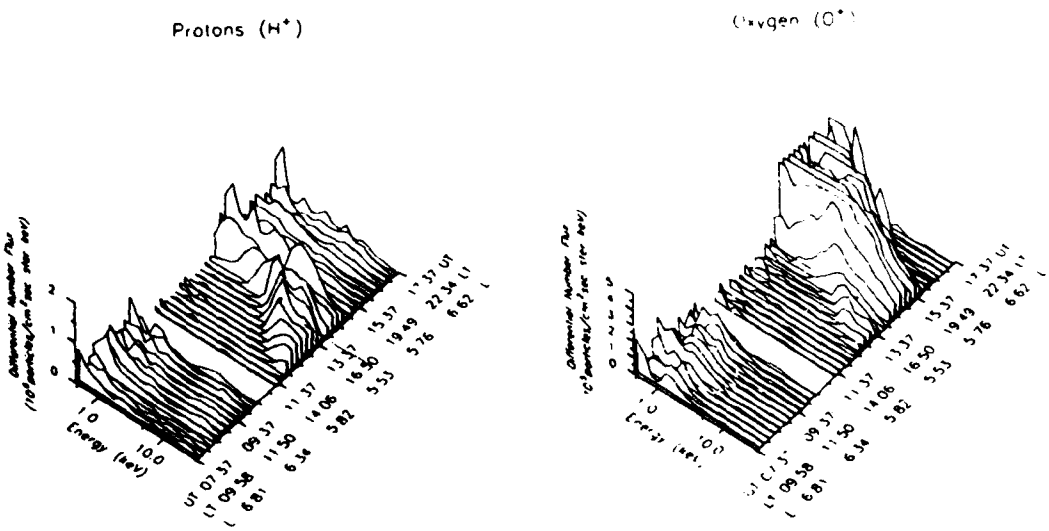

Figure 24

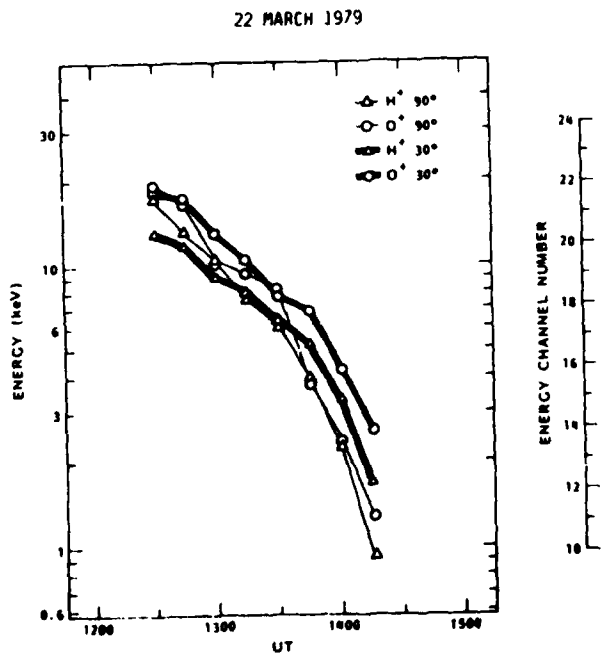

Figure 25

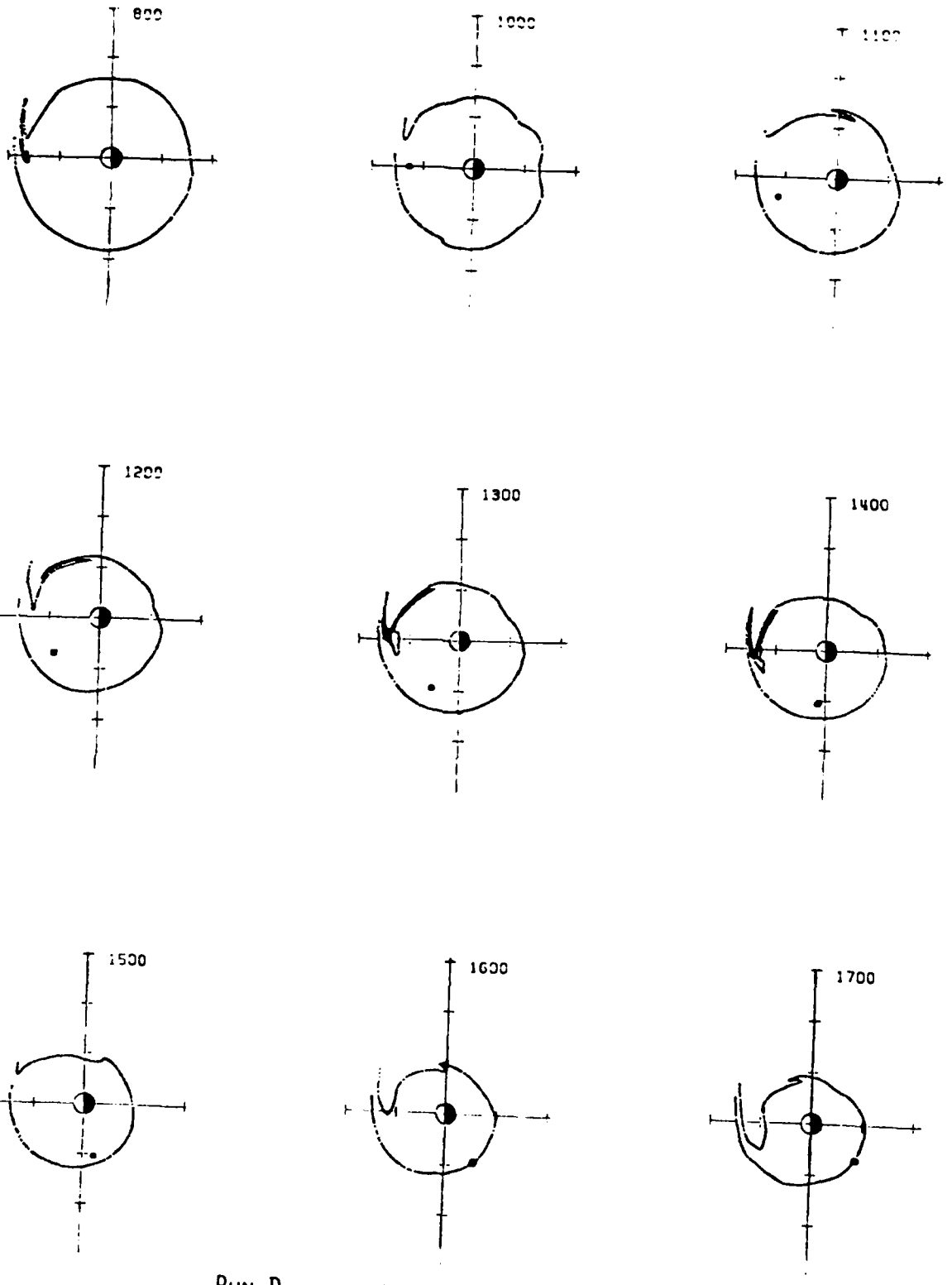

RUN D Figure 26a MU=0

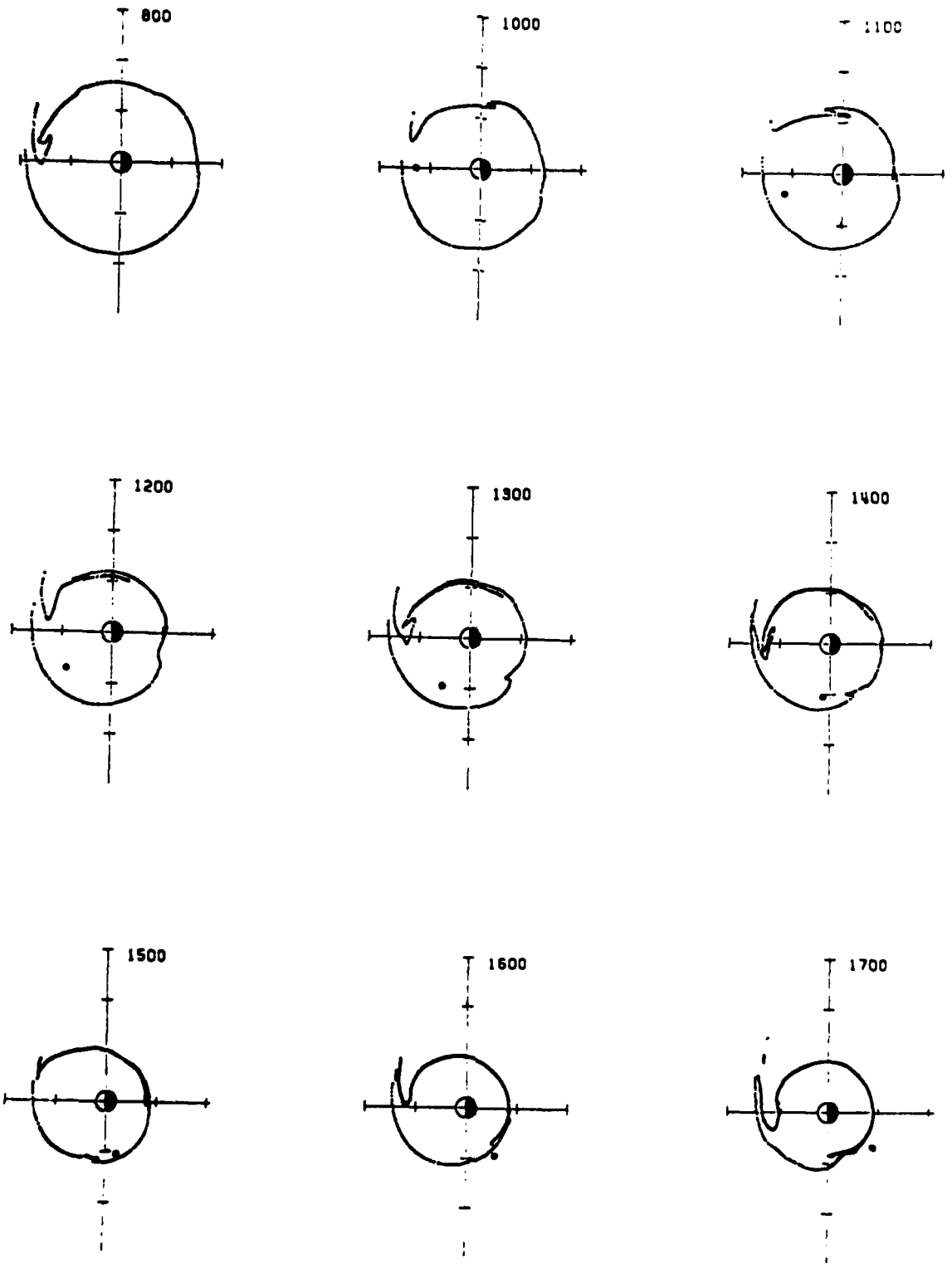

RUN D Figure 26b MU=65

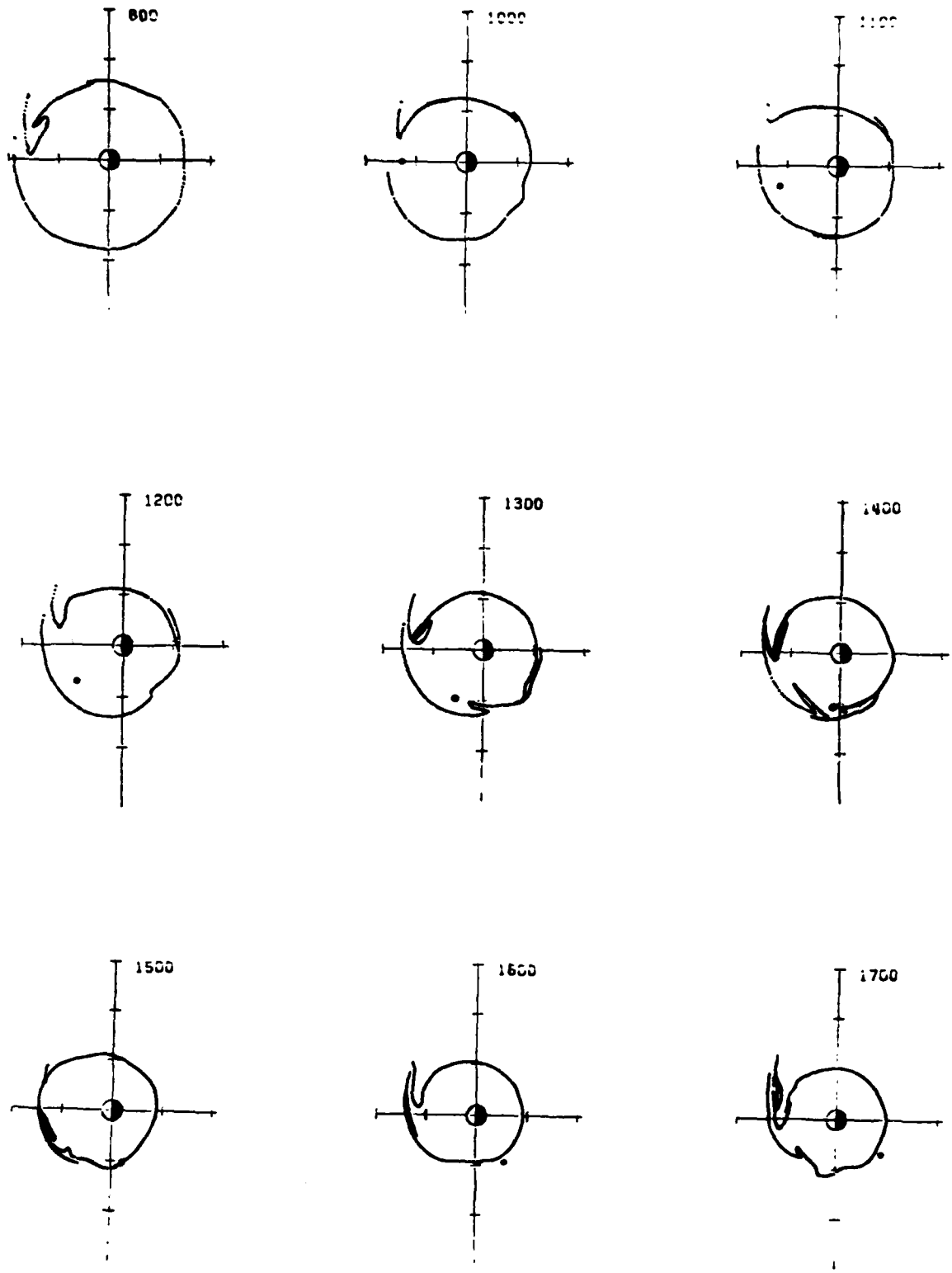

RUN D Figure 26c MU=130

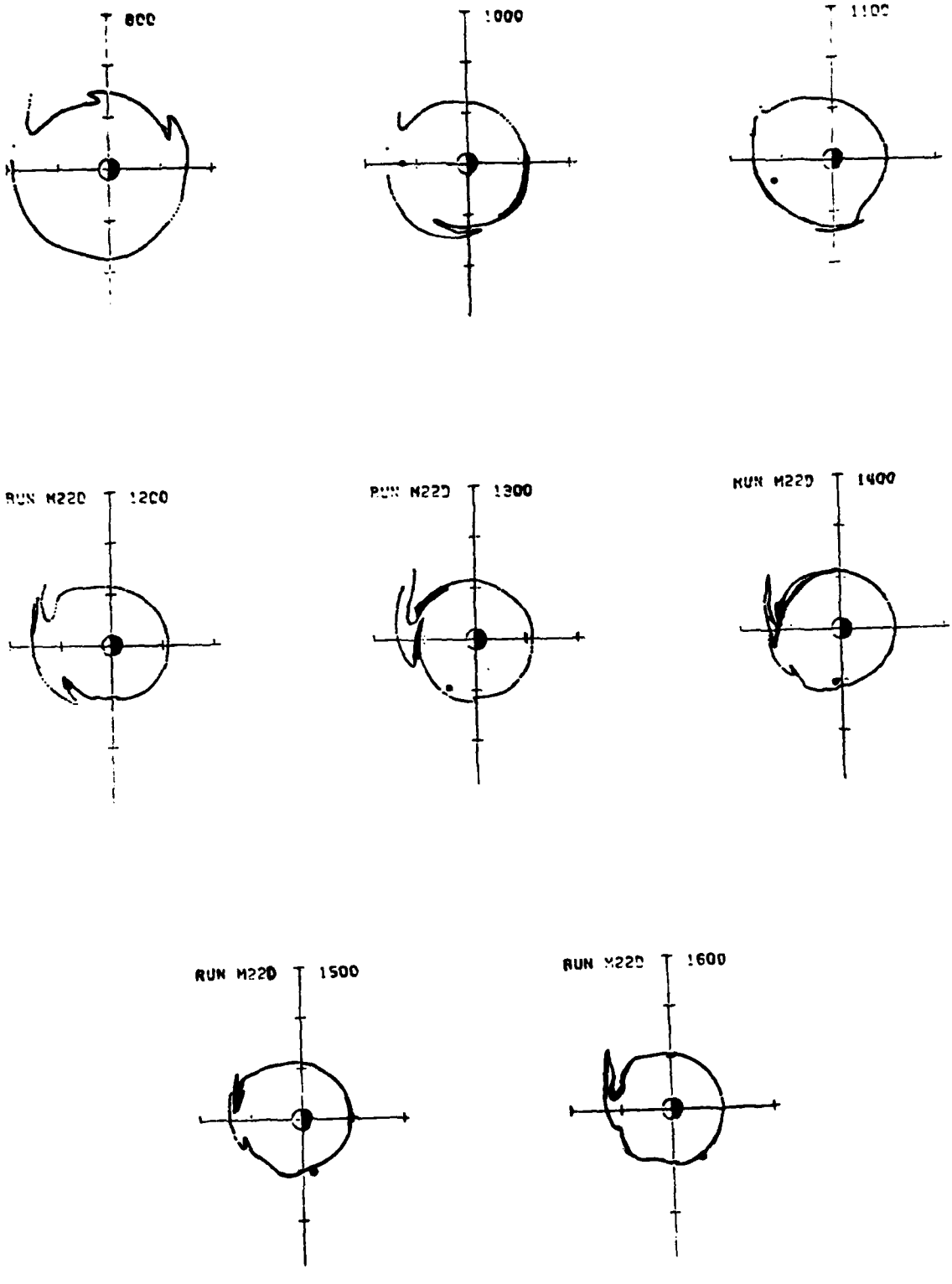

RUN D Figure 26d Mu=260

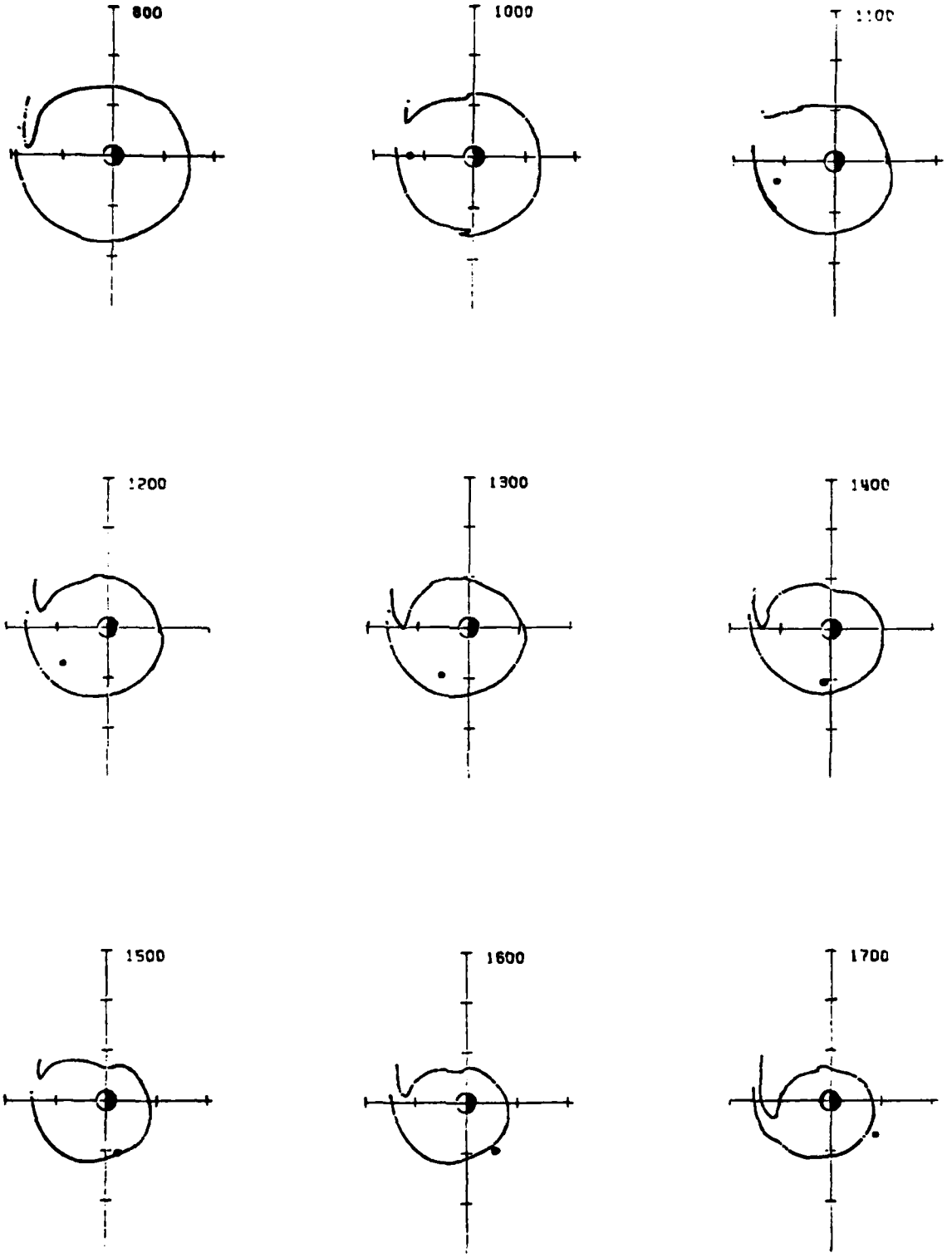

RUN F Figure 27a MU=0

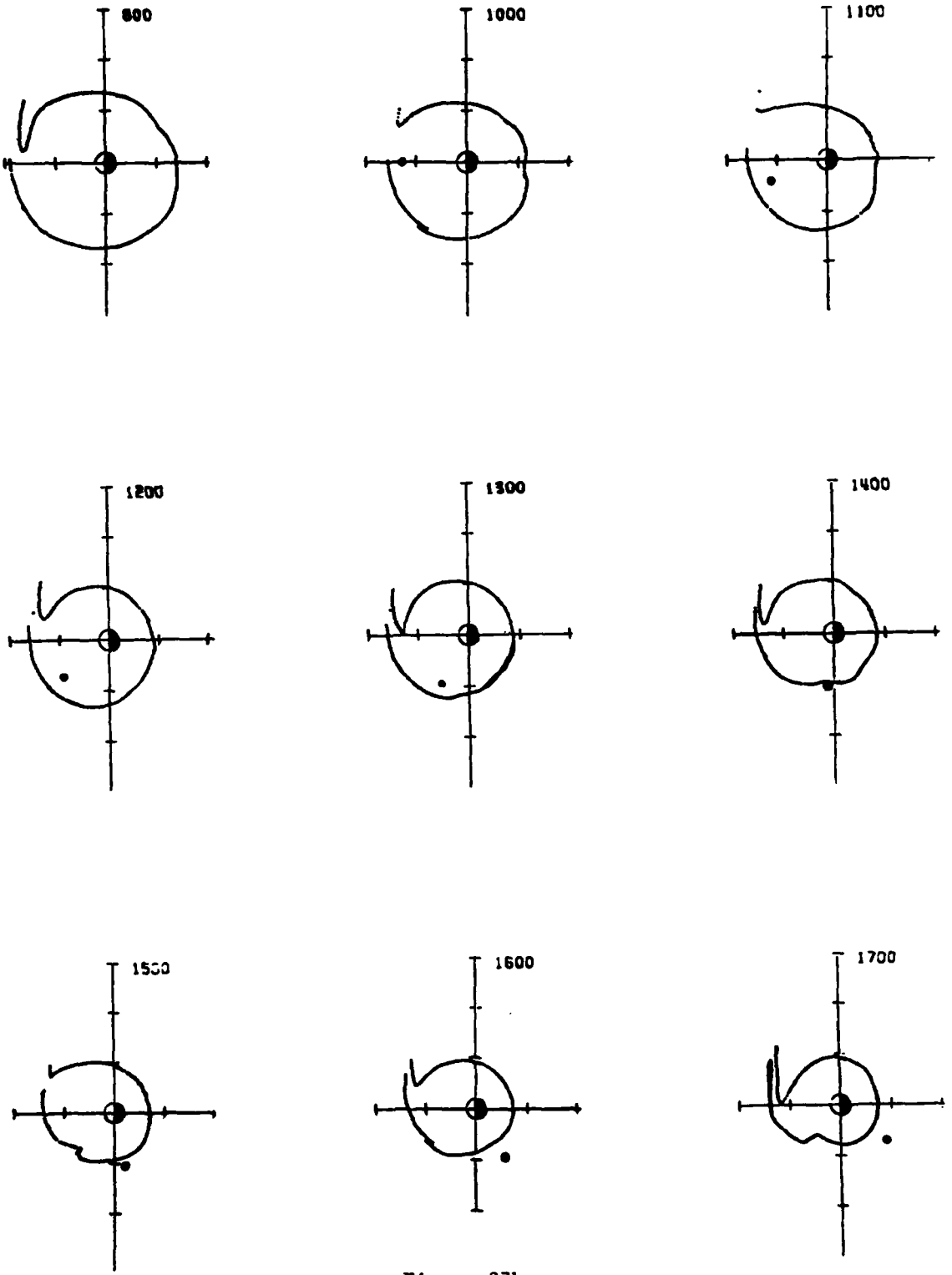

RUN F Figure 27b MU=65

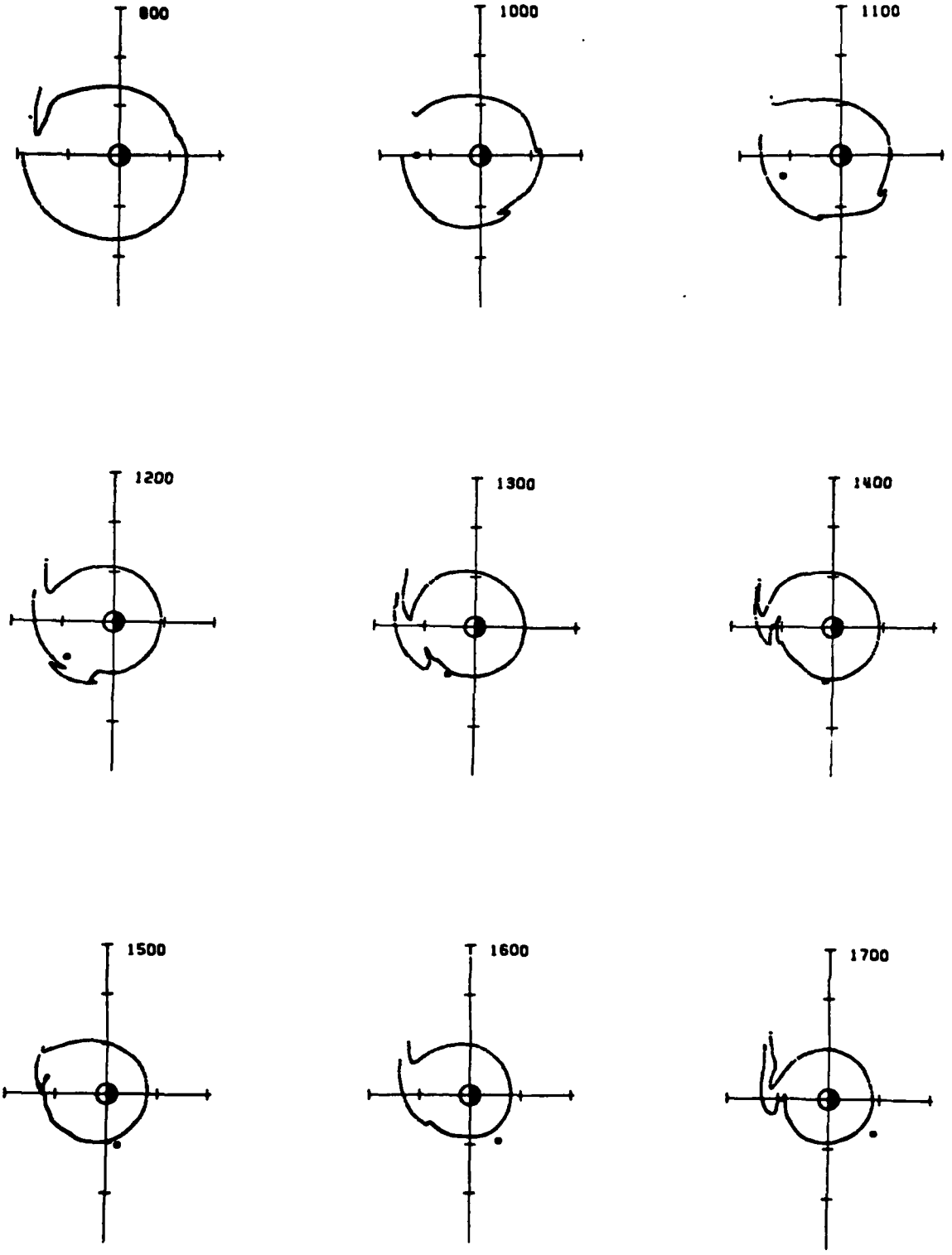

RUN F Figure 27c MU=130

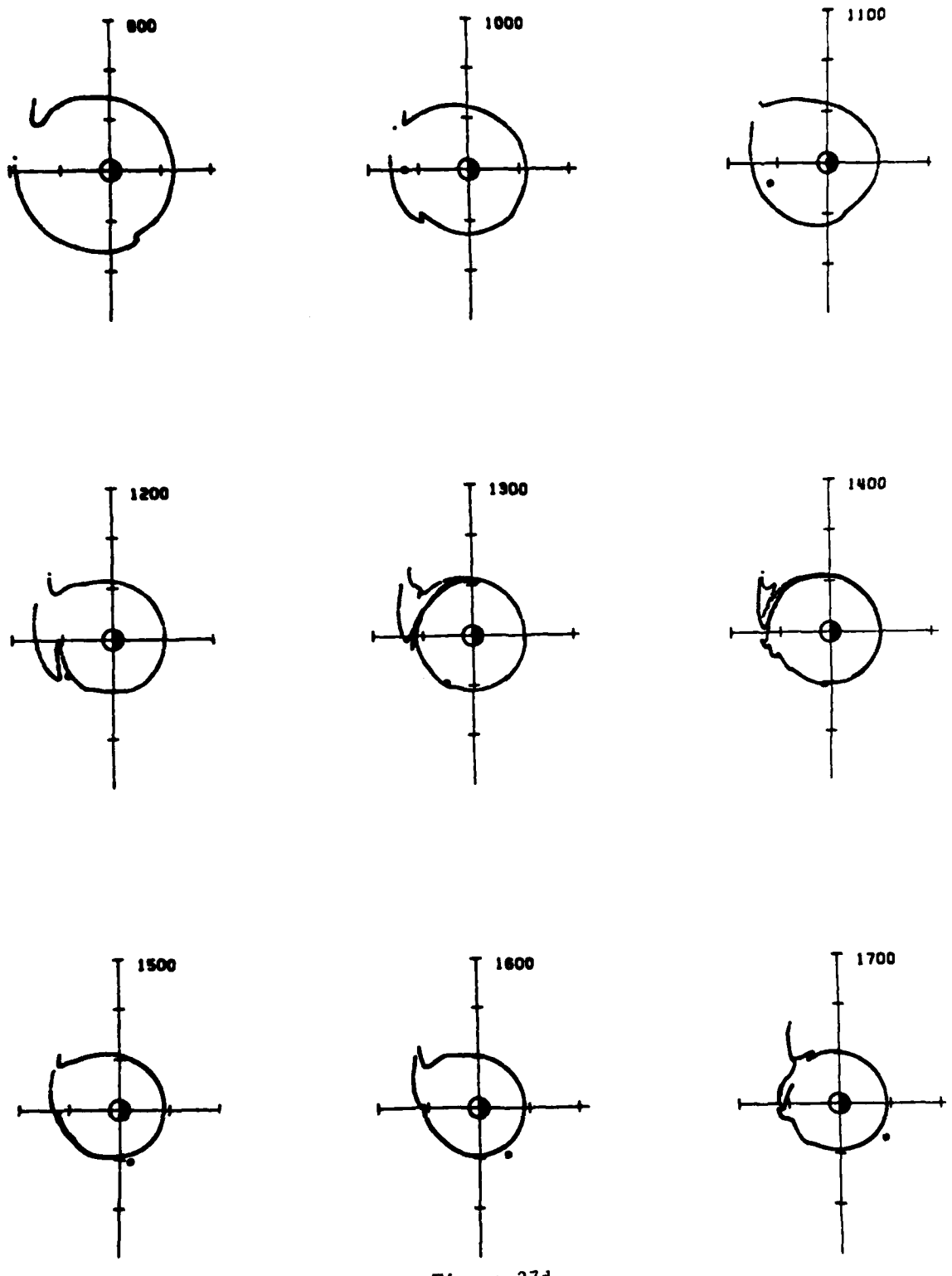

RUN F Figure 27d MU=260

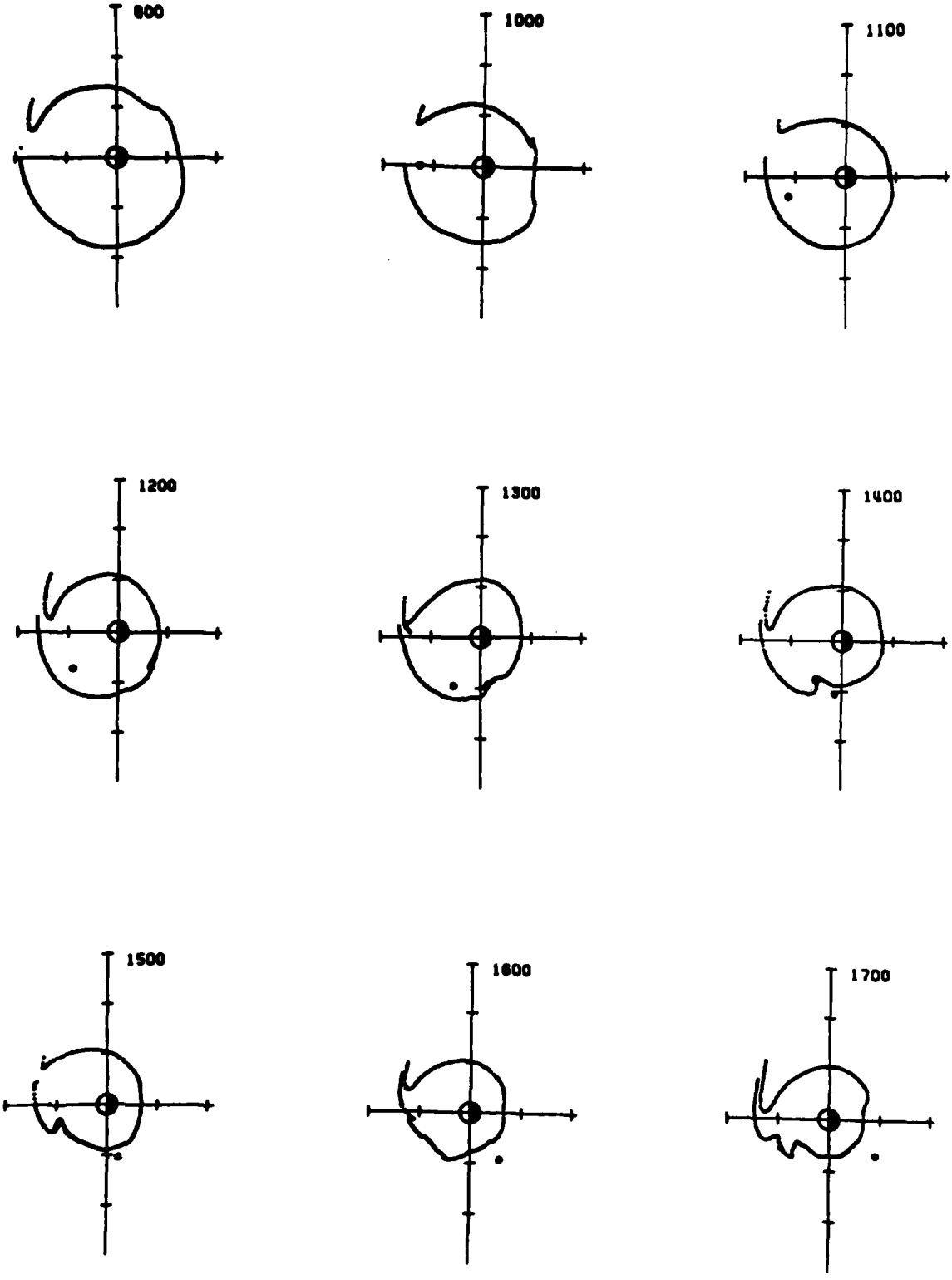

RUN H Figure 28 MU=65

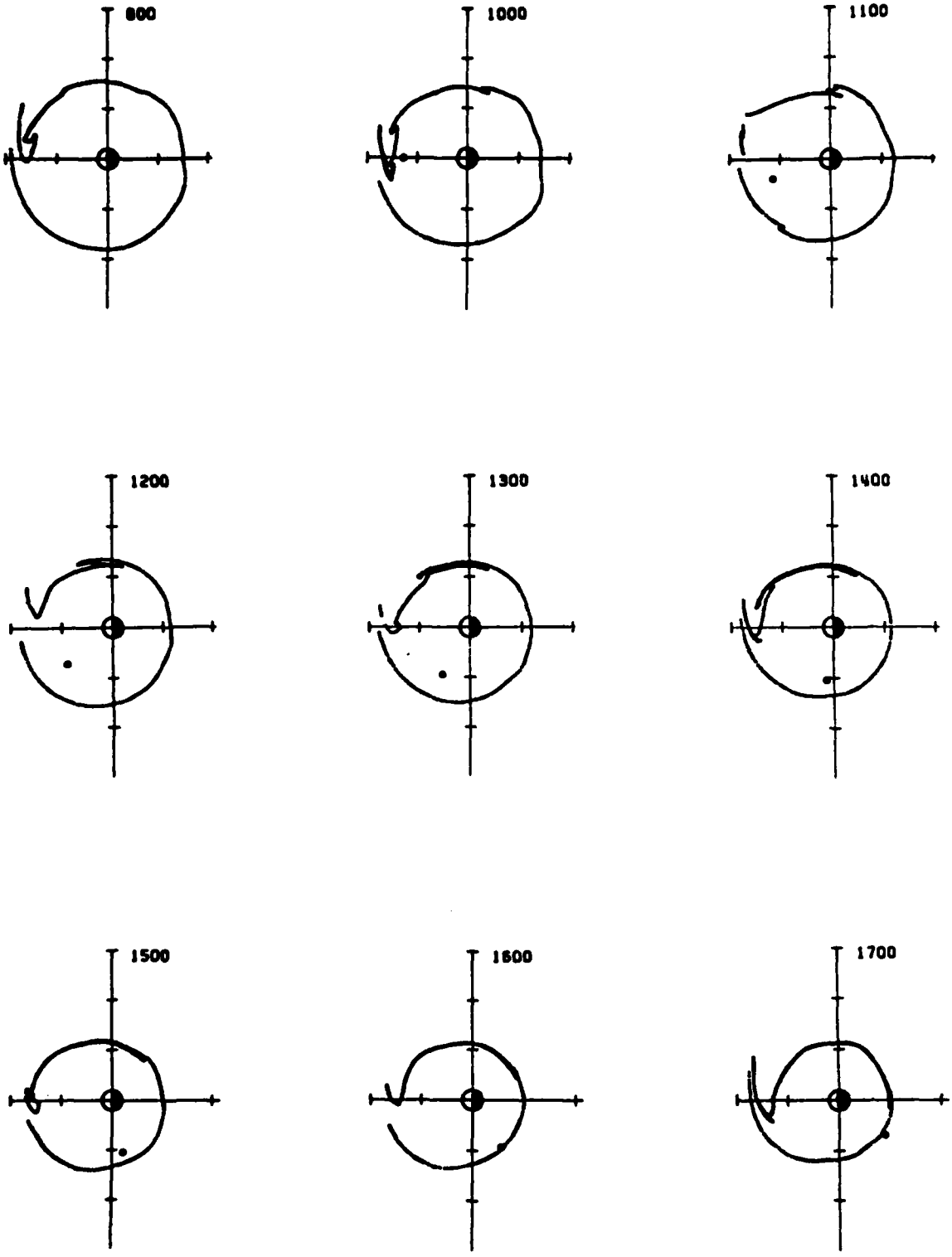

RUN J Figure 29 MU=65

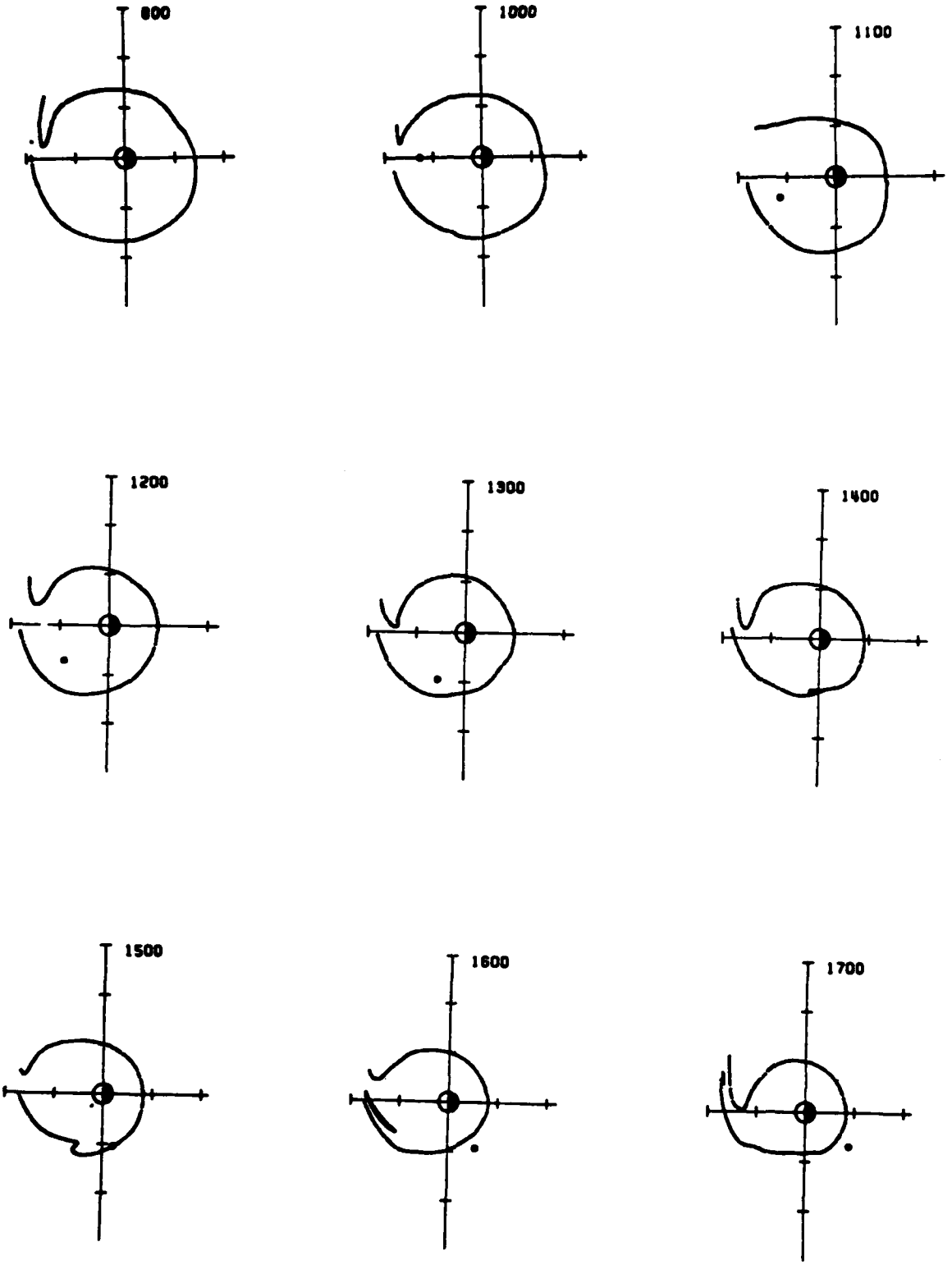

RUN L Figure 30 MU=65

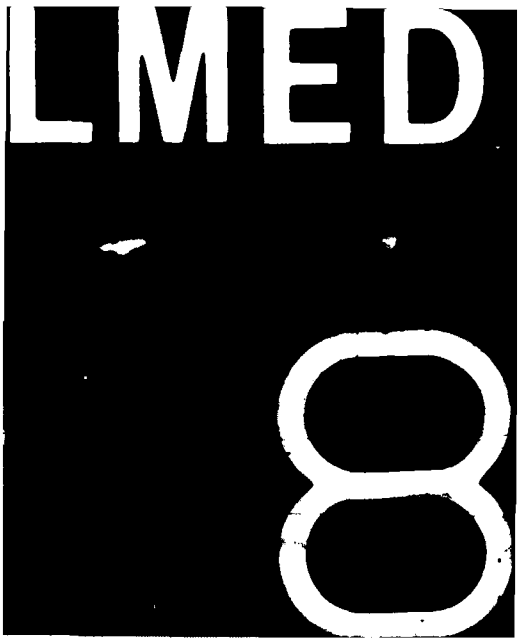
LMED
8